2002-09

Performance of IEEE 802.11a wireless LAN standard over frequency-selective, slow, ricean fading channels

Kao, Chi-Han

Monterey California. Naval Postgraduate School

NAVAL POSTGRADUATE SCHOOL
Monterey, California

THESIS

PERFORMANCE OF THE *IEEE 802.11a* WIRELESS LAN STANDARD OVER FREQUENCY-SELECTIVE, SLOW, RICEAN FADING CHANNELS

by

Chi-han Kao

September 2002

Thesis Advisor:	R. Clark Robertson
Second Reader:	Roberto Cristi

Approved for public release; distribution is unlimited.

THIS PAGE INTENTIONALLY LEFT BLANK

REPORT DOCUMENTATION PAGE			Form Approved OMB No. 0704-0188
Public reporting burden for this collection of information is estimated to average 1 hour per response, including the time for reviewing instruction, searching existing data sources, gathering and maintaining the data needed, and completing and reviewing the collection of information. Send comments regarding this burden estimate or any other aspect of this collection of information, including suggestions for reducing this burden, to Washington headquarters Services, Directorate for Information Operations and Reports, 1215 Jefferson Davis Highway, Suite 1204, Arlington, VA 22202-4302, and to the Office of Management and Budget, Paperwork Reduction Project (0704-0188) Washington DC 20503.			
1. AGENCY USE ONLY ***(Leave blank)***	**2. REPORT DATE** September 2002	**3. REPORT TYPE AND DATES COVERED** Master's Thesis	
4. TITLE AND SUBTITLE: Title (Mix case letters) Performance of *IEEE 802.11a* Wireless LAN Standard over Frequency-Selective, Slow, Ricean Fading Channels			**5. FUNDING NUMBERS**
6. AUTHOR(S) **Kao, Chi-han**			
7. PERFORMING ORGANIZATION NAME(S) AND ADDRESS(ES) Naval Postgraduate School Monterey, CA 93943-5000			**8. PERFORMING ORGANIZATION REPORT NUMBER**
9. SPONSORING /MONITORING AGENCY NAME(S) AND ADDRESS(ES) N/A			**10. SPONSORING/MONITORING AGENCY REPORT NUMBER**
11. SUPPLEMENTARY NOTES The views expressed in this thesis are those of the author and do not reflect the official policy or position of the Department of Defense or the U.S. Government.			
12a. DISTRIBUTION / AVAILABILITY STATEMENT Approved for public release; distribution is unlimited.			**12b. DISTRIBUTION CODE**

13. ABSTRACT ***(maximum 200 words)***

With the rapidly growing demand for more reliable and higher data rate wireless communications, the *Institute of the Electrical and Electronics Engineers (IEEE) 802.11* working group approved a standard for 5 GHz band, wireless local area networks (WLAN) in 1999. This standard, *IEEE 802.11a*, supports data rates from 6 up to 54 Mbps, and uses orthogonal frequency division multiplexing (OFDM) for transmission in indoor wireless environments. This thesis examines the performance of the *IEEE 802.11a* standard for different combinations of sub-carrier modulation type and code rate and determines the signal-to-noise ratio required to obtain a probability of bit error P_b of 10^{-5}. The channel is modeled as a *frequency-selective, slow, Ricean fading channel* with additive white Gaussian noise (AWGN). Contrary to expectations, for the combinations of sub-carrier modulation type and code rate utilized by the *IEEE 802.11a* standard, some of the higher data rate combinations outperform some of the lower data rate combinations. On the other hand, the results also show significant coding gain when applying *convolutional coding* with *Viterbi decoding*, and hence highlight the importance of forward error correction (FEC) coding to the performance of wireless communications systems.

14. SUBJECT TERMS *IEEE 802.11a* standard, WLAN, OFDM, BPSK, QPSK, QAM, probability of bit error, frequency-selective fading, flat fading, fast fading, slow fading, Ricean fading, Rayleigh fading, Viterbi algorithm, convolutional code, hard-decision decoding, soft-decision decoding, coding gain.	**15. NUMBER OF PAGES** 115
	16. PRICE CODE

17. SECURITY CLASSIFICATION OF REPORT	**18. SECURITY CLASSIFICATION OF THIS PAGE**	**19. SECURITY CLASSIFICATION OF ABSTRACT**	**20. LIMITATION OF ABSTRACT**
Unclassified	Unclassified	Unclassified	UL

NSN 7540-01-280-5500

Standard Form 298 (Rev. 2-89)
Prescribed by ANSI Std. 239-18

THIS PAGE INTENTIONALLY LEFT BLANK

Approved for public release; distribution is unlimited

PERFORMANCE OF THE *IEEE 802.11a* WIRELESS LAN STANDARD OVER FREQUENCY-SELECTIVE, SLOW, RICEAN FADING CHANNELS

Chi-han Kao
Lieutenant Commander, Taiwan Navy
B.S., Chinese Naval Academy, 1989

Submitted in partial fulfillment of the
requirements for the degree of

MASTER OF SCIENCE IN ELECTRICAL ENGINEERING

from the

NAVAL POSTGRADUATE SCHOOL
September 2002

Author: Chi-han Kao

Approved by: R. Clark Robertson
Thesis Advisor

Roberto Cristi
Second Reader

John Powers
Chairman, Department of Electrical and Computer Engineering

THIS PAGE INTENTIONALLY LEFT BLANK

ABSTRACT

With the rapidly growing demand for more reliable and higher data rate wireless communications, the *Institute of the Electrical and Electronics Engineers (IEEE) 802.11* working group approved a standard for 5-GHz band, wireless local area networks (WLAN) in 1999. This standard, *IEEE 802.11a*, supports data rates from 6 up to 54 Mbps and uses orthogonal frequency division multiplexing (OFDM) for transmission in indoor wireless environments. This thesis examines the performance of the *IEEE 802.11a* standard for different combinations of sub-carrier modulation type and code rate and determines the signal-to-noise ratio required to obtain a probability of bit error P_b of 10^{-5}. The channel is modeled as a *frequency-selective, slow, Ricean fading channel* with additive white Gaussian noise (AWGN). Contrary to expectations, for the combinations of sub-carrier modulation type and code rate utilized by the *IEEE 802.11a* standard, some of the higher data rate combinations outperform some of the lower data rate combinations. On the other hand, the results also show significant coding gain when applying *convolutional coding* with *Viterbi decoding*, and hence highlight the importance of forward error correction (FEC) coding to the performance of wireless communications systems.

THIS PAGE INTENTIONALLY LEFT BLANK

TABLE OF CONTENTS

LIST OF FIGURES

THIS PAGE INTENTIONALLY LEFT BLANK

LIST OF TABLES

THIS PAGE INTENTIONALLY LEFT BLANK

ACKNOWLEDGMENTS

First and foremost I am grateful to my beautiful wife, Tanyi, and wonderful daughter, Jenny, for the sacrifices they made in support of my completing this thesis.

Secondly I would like to thank my thesis advisors, Dr. Clark Robertson and Dr. Roberto Cristi, for their endless hours of help, suggestions, ideas and advise during the development of this thesis.

Thanks go out as well to LT Gell Tiger L. Pittman III, USN, and LT Patrick A. Count, USN, for introducing me OFDM.

Finally in appreciation of CDR Jim Hill, previous Code 35 Curriculum Officer and Eva Anderson, Code 35 Education Specialist, and LCDR Peter Duke, my best friend, for their assistance through my tour at the Naval Postgraduate School.

THIS PAGE INTENTIONALLY LEFT BLANK

EXECUTIVE SUMMARY

The objective of this thesis is to analyze the performance of the *IEEE 802.11a* WLAN standard over frequency-selective, slow, Ricean fading channels. Prior to the analysis, we discuss the issues of multipath fading and introduce four different types of small-scale fading: *frequency-selective* fading, *flat* fading, *fast* fading, and *slow* fading. We then introduce the physical layers of the *IEEE 802.11a* WLAN standard, the fundamentals of OFDM, and the reasons that *IEEE 802.11a* adopted OFDM for transmission.

In order to perform the analysis, we derived analytic expressions for all sub-carrier modulations used in *IEEE 802.11a*: BPSK, QPSK, 16QAM, and 64QAM. Actually, only two expressions are required, one for BPSK and one for square QAM, since QPSK and BPSK have the same probability of bit error and both 16QAM and 64QAM are square QAM. After the derivation, we show that two analytic expressions yield accurate results when compared to the exact results for both Rayleigh and Ricean fading channels. Further, we assume the channel coherence bandwidth is such that we have 48 independent sub-carriers for large office buildings and 24 independent sub-carriers for small office buildings. In turn, we consider the performance of *IEEE 802.11a* over both a pure Rayleigh fading channel and over a composite Rayleigh/Ricean fading with either 48 or 24 independent sub-carriers.

Next, we evaluate the performance of uncoded *IEEE 802.11a* over Ricean fading channels so that we can obtain the coding gain later by comparing these results to those with FEC coding. As expected, the performance of uncoded BPSK/QPSK modulated OFDM is better than uncoded 16QAM and 64QAM; however, even BPSK/QPSK does not yield performance acceptable for wireless communications.

After the evaluation of uncoded *IEEE 802.11a*, we examine the performance of *IEEE 802.11a* with FEC coding, where convolutional encoding and Viterbi decoding are applied. The effect of Viterbi hard decision decoding (HDD) is analyzed for BPSK, QPSK, 16QAM, and 64QAM, while the effect of Viterbi soft decision decoding (SDD) is analyzed for BPSK and QPSK only due to the difficulty of analyzing the probability of bit error for SDD of a binary code transmitted with non-binary modulation.

For the performance of *IEEE 802.11a* with HDD, as expected, the signal-to-noise ratios required for a pure Rayleigh fading channel are more than for a composite Rayleigh/Ricean fading channel, in the range of four to seven dB for $P_b = 10^{-5}$. Also as expected, for a specific modulation type, regardless of the channel conditions considered, as the code rate increases, the signal-to-noise ratio required to achieve a fixed probability of bit error increases. Moreover, the coding gains for all sub-channel modulations range from 21 to 30 dB. Contrary to expectations, however, the signal-to-noise ratio required to achieve a specific P_b does not monotonically decrease with decreasing bit rate. This phenomenon is observed whether the channel is modeled as a pure Rayleigh fading channel or as a composite Rayleigh/Ricean fading channel.

For the performance of *IEEE 802.11a* with SDD for BPSK/QPSK with code rate $r = 1/2$, SDD improves performance by about 2.5 dB over HDD in AWGN and by about 3.3 dB over a composite Rayleigh/Ricean fading channel. For BPSK/QPSK with code rate $r = 3/4$, SDD improves performance by about 5.5 dB over HDD in a composite Rayleigh/Ricean fading channel.

From an examination of the performance difference between 48 and 24 independent sub-carriers, we conclude that the performance difference decreases as more powerful coding technique are used.

I. INTRODUCTION

A. OBJECTIVE

With the rapidly growing demand for more reliable and higher data rates in wireless communications, the *IEEE 802.11* working group approved a standard for a 5 GHz band wireless local area network (WLAN) in 1999. This standard, *IEEE 802.11a*, supports a variable bit rate from 6 up to 54 Mbps and selects orthogonal frequency division multiplexing (OFDM) for transmission in indoor wireless environments. With OFDM as specified by the *IEEE 802.11a* standard, the data signal is divided among 48 separate sub-carriers. For each of the sub-carriers, OFDM uses either phase-shift keying (BPSK/QPSK) or M-ary quadrature amplitude modulation (16 and 64QAM) to modulate the digital signal depending on the selected data rate of transmission. Higher data rates are achieved by combining a high-order sub-carrier modulation with a high rate convolutional code, while lower data rates are obtained by lowering either the sub-carrier modulation order or the code rate or both. Logically, the expectation is that lower data rates result in a continually more robust wireless communication system; that is, the target performance level for the system can be maintained as the received signal-to-noise ratio goes down simply by reducing the bit rate (since both lower-order sub-carrier modulation and lower code rates are more robust). In this thesis, this assumption was investigated for the *IEEE 802.11a* WLAN standard. The channel was modeled as a frequency-selective, slow, Ricean fading channel with additive white Gaussian noise (AWGN); although, each sub-channel was modeled as flat due to OFDM. Another objective of this thesis was to investigate performance when applying forward error correction (FEC) channel coding using both hard decision decoding (HDD) and soft decision decoding (SDD) in conjunction with the Viterbi algorithm. However, due to the difficulty of analyzing the probability of bit error for SDD of a binary code transmitted with non-binary modulation, SDD with MQAM modulation will not be considered in this thesis.

B. RELATED RESEARCH

After the European Telecommunication Standards Institute Broadband Radio Access Networks (ETSI BRAN) in Europe and the Multimedia Mobile Access Communications (MMAC) in Japan followed the *IEEE* decision, OFDM became a single worldwide physical layer standard for WLAN in the 5-GHz band. Therefore, many studies focus on the performance of OFDM for different combinations of fading channels, such as frequency-nonselective, fast, Rayleigh and Ricean fading channels [1] and [2], frequency-selective, Rayleigh fading channels [3], and frequency-selective, slow, Nakagami channels [4]. Unlike the above referenced work, this thesis investigates the performance of the *IEEE 802.11a* standard over frequency-selective, slow, Ricean fading channels. In this thesis, we derive analytic expressions for the probability of bit error for BPSK/QPSK, 16QAM and 64QAM in Ricean fading channels. To the best knowledge of the author, these results have not been previously published. Further, in addition to 48 independent sub-carriers, this thesis will also examine performance with 24 independent sub-carriers. The reason for investigating 24 independent sub-carriers will be explained in Chapter IV.

C. THESIS ORGANIZATION

After the introduction, the thesis is organized into five remaining chapters. The most important issue in wireless communications, *multipath fading* (since it determines system performance and the data rate for transmission) is discussed in Chapter II. In this thesis, even though the channel is modeled as a frequency-selective, slow, Ricean fading channel, a thorough discussion of small scale fading is still given because a complete understanding of this phenomenon is essential. The *IEEE 802.11a* standard for WLAN Medium Access Control (MAC) and Physical Layer (PHY) specifications [5] is introduced in Chapter III, and why *IEEE* selected OFDM is explained. Moreover, some important OFDM concepts such as *orthogonality* and *multicarrier* techniques and the major OFDM parameters, as well as OFDM signal processing are also covered in Chapter III. The performance of OFDM without FEC coding in AWGN and Ricean fading channels is examined in Chapter IV. The analysis begins with the sub-carrier modulation

schemes utilized in *IEEE 802.11a* standard, which are BPSK, QPSK, 16QAM, and 64QAM and then advances to composite OFDM modulation. Analytic expressions are derived for the probability of bit error for BPSK/QPSK and square MQAM in this chapter. OFDM performance with FEC coding and Viterbi hard decision decoding (HDD) with BPSK, QPSK, 16QAM, and 64QAM is examined in Chapter V, but Viterbi soft decision decoding (SDD) is only considered with BPSK and QPSK. The results will be compared to those of Chapter IV in order to find the coding gain. Finally, this thesis concludes with Chapter VI and a brief review of the results obtained in the previous chapters, followed by recommendations for further research.

THIS PAGE INTENTIONALLY LEFT BLANK

II. MULTIPATH FADING CHANNELS

Unlike satellite communications, many wireless communications channels do not have a line-of-sight (LOS) transmission path. Instead, a signal can travel from transmitter to receiver over many reflective paths. This phenomenon is referred to as *multipath propagation*. Due to multipath, a signal will arrive at receiver multiple times with different amplitudes, phases, and arrival times, giving rise to the terminology *multipath fading*. This chapter begins with a discussion of the two main types of fading effects and their characteristics and then focuses on the small-scale fading. The last part of this chapter introduces Rayleigh and Ricean fading.

A. FADING CHANNELS

On wireless communications channels, the effect of multipath fading on the received signal amplitude is broken into two components; *large-scale fading* and *small-scale fading*, as shown in Figure 1.

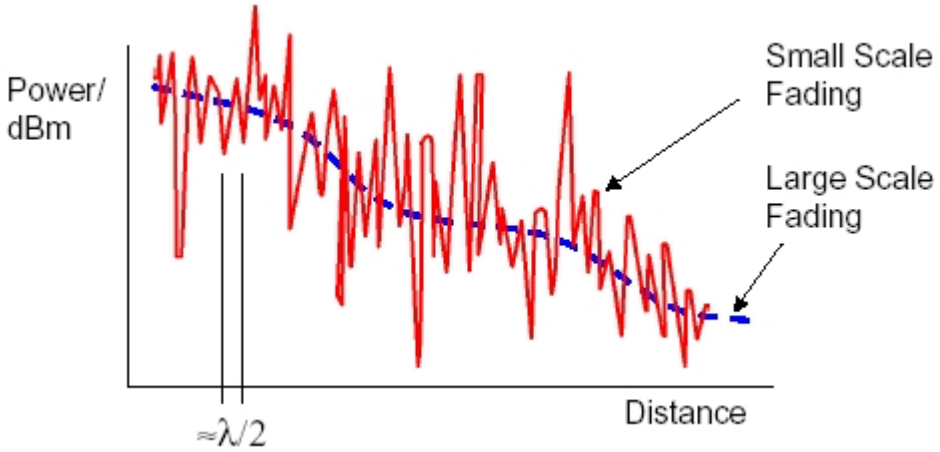

Figure 1. Large and small scale fading [From Ref. 6]

Large-scale fading represents the average received signal power attenuation or the path loss over large transmitter-to-receiver (T-R) separation distances, usually hundreds or

thousands of meters. Small scale fading refers to the dramatic fluctuation in signal amplitude over very small changes in T-R distance (as small as a half-wavelength) or over a short duration (in the range of fractions of a second to several seconds). All indoor wireless communication system will experience small-scale fading. This thesis will focus on the effects of small-scale fading since *IEEE 802.11a* is intended for WLAN transmission in indoor environment.

B. SMALL-SCALE FADING

There are two mechanisms that contribute to small-scale fading: *time spreading of the signal* due to multipath and *time variance of the channel* due to motion. The *time spreading of the signal* leads to either *frequency-selective fading* or *flat fading,* while the *time variance of the channel* leads to either *fast fading* or *slow fading*.

1. Time-Spreading Mechanism Due To Multipath

As mentioned above, time dispersion will cause the transmitted signal to undergo either frequency-selective fading or flat fading. Two related parameters that characterize the time spreading mechanism need to be addressed, the *coherence bandwidth* and *maximum excess delay*.

Coherence bandwidth B_c is a statistical measure of the range of frequencies over which the channel can be considered non-distorting (equal gain and linear phase). In other words, the coherence bandwidth represents the range of frequencies over which signal's frequency components are strongly amplitude correlated. It is shown in [7] that B_c and T_m are reciprocally related by

$$B_c \approx \frac{1}{T_m} \tag{2.1}$$

where T_m is the maximum excess delay, or the time difference of arrival between the first and last received signal components. The maximum excess delay is defined in terms of

the multipath intensity profile (MIP), illustrated in Figure 2, where the average received power $S(\tau)$ varies as a function of time delay τ.

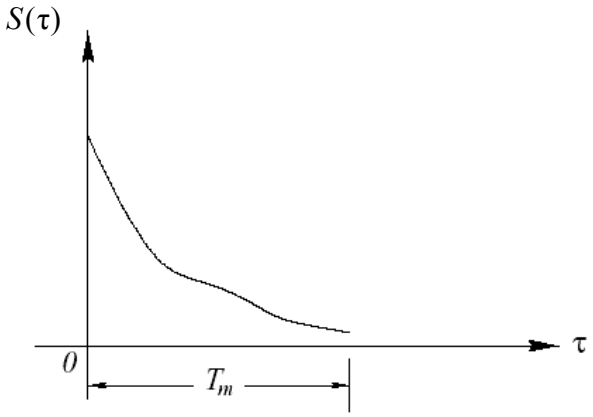

Figure 2. Multipath Intensity Profile [After Ref. 7]

However, T_m is not generally the best parameter to represent a channel, because the MIP can change significantly for channels with the same value of T_m. A more useful parameter is the root-mean-square (rms) delay spread [7], defined

$$\sigma_\tau = \sqrt{\overline{\tau^2} - \overline{\tau}^2} \tag{2.2}$$

where $\overline{\tau}$ is the mean excess delay and $\overline{\tau^2}$ is the second moment of $\overline{\tau}$. Note that a fixed relationship between B_c and σ_τ does not exist. If B_c is defined as the bandwidth over which the frequency correlation function is greater than 0.5, then an empirical rule that is often used is [8]

$$B_c \approx \frac{1}{5\sigma_\tau}. \tag{2.3}$$

If B_c is defined as the bandwidth over which the frequency correlation function is greater than 0.9, then an empirical rule that is often used is [8]

$$B_c \approx \frac{1}{50\sigma_\tau}. \tag{2.4}$$

Note that the reported values of σ_τ vary depending on the size and type of the building, with or without a clear LOS path. For small through large office buildings, the reported values of σ_τ range from 30 to 120 ns [9].

a. Frequency-Selective Fading

If the coherence bandwidth B_c is smaller than the bandwidth of the transmitted signal W, then the received signal will undergo frequency-selective fading; that is, the channel is frequency-selective if

$$B_c < W \tag{2.5}$$

which implies

$$T_m > T_s \tag{2.6}$$

since $B_c \approx 1/T_m$ and $W \approx 1/T_s$, where $1/T_s = R_s$ is the symbol rate. When frequency-selective fading occurs, the received signal is distorted since different spectral components of the signal are affected differently. The typical frequency-selective fading case is illustrated in Figure 3(a).

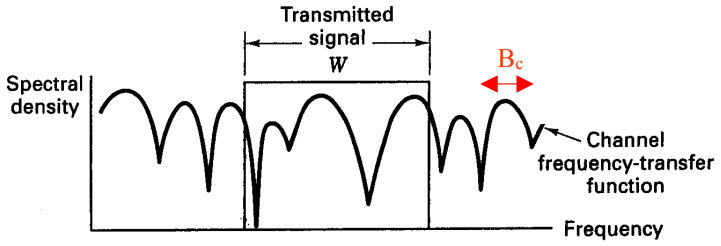

(a) ***Frequency-selective*** fading ($B_c < W$)

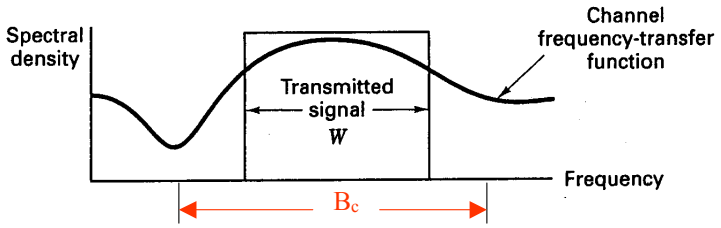

(b) ***Flat*** fading ($B_c > W$)

Figure 3. Typical frequency-selective and flat fading [After Ref. 7]

b. Flat Fading

If the channel coherence bandwidth B_c, over a bandwidth that is greater than the bandwidth of the transmitted signal, then the received signal will undergo *flat fading*; that is, the channel is *flat* if

$$B_c > W \tag{2.7}$$

or equivalently

$$T_m < T_s \ . \tag{2.8}$$

The typical flat fading case is illustrated in Figure 3(b).

2. Time-Variant Mechanism Due To Motion

Due to the motion of either the transmitter or the receiver, the time variance causes the transmitted signal to undergo either *fast fading* or *slow fading*. There are two parameters used to describe the time-variant nature of the channel: *Doppler spread* and *coherence time*.

The Doppler spread B_d is defined as the range of frequencies over which the received Doppler spectrum is essentially non-zero. When a pure sinusoidal tone of frequency f_c is transmitted over a multipath channel, the received signal spectrum will have components in the range $f_c - f_d$ to $f_c + f_d$, where f_d is the Doppler shift given by [8]

$$f_d = \frac{v}{\lambda} \cdot \sin\theta \tag{2.9}$$

where v is the relative velocity of the transmitter with respect to the receiver, λ is the signal wavelength, and θ is the spatial angle between the direction of motion of the receiver and the direction of arrival of the signal. The value of f_d depends on whether the transmitter and receiver are moving toward or away from each other.

Coherence time T_c is a statistical measure of the time duration over which the channel is essentially invariant. In other words, coherence time is the time duration over which two received signals have a strong potential for amplitude correlation. Note that the coherence time and the Doppler spread are reciprocally related as [8]

$$T_c \approx \frac{1}{B_d} . \tag{2.10}$$

a. Fast Fading

Fast fading describes a condition where the coherence time of the channel is less than the transmitted symbol period; that is,

$$T_c < T_s \tag{2.11}$$

or equivalently

$$B_d > W \tag{2.12}$$

since $T_c \approx 1/B_d$ and $W \approx 1/T_s$, where $1/T_s = R_s$ is the symbol rate. In a fast fading channel, the channel impulse response changes rapidly during the time each symbol is transmitted, distorting the shape of the baseband signal. In practice, fast fading only occurs for very low data rate transmission.

b. Slow Fading

Opposite to fast fading, slow fading describes a condition where the coherence time of the channel is greater than the transmitted symbol period. In other words, the channel changes at a rate much slower than the baseband signal rate; that is,

$$T_c > T_s \tag{2.13}$$

or equivalently

$$B_d < W . \tag{2.14}$$

3. Summary of Small Scale Fading

From Equations (2.5) through (2.8) and Equations (2.11) through (2.14), four types of the small scale fading can be characterized as shown in Figure 4, where B_c is coherence bandwidth, W is baseband signal bandwidth, T_m is the maximum excess delay, T_s is symbol time, T_c is the coherence time, and B_d is the Doppler spread.

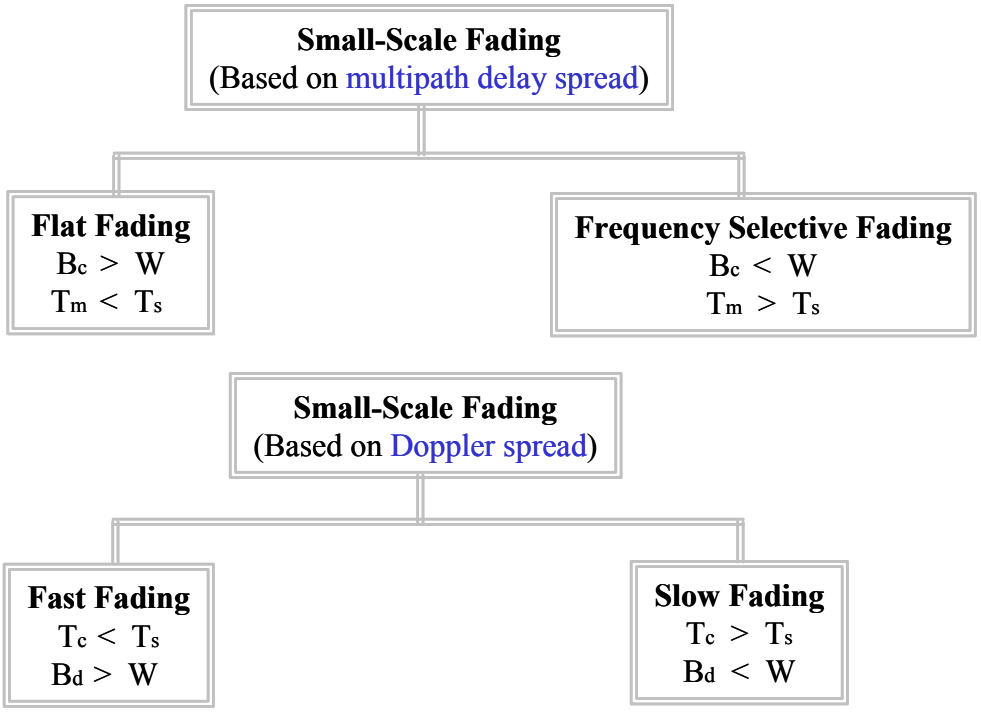

Figure 4. Types of the small scale fading [After Ref. 8]

C. DISTRIBUTION OF PATH AMPLITUDES

In a multipath environment, the received signal amplitude is modeled as a random variable. Typical models are the Rayleigh, Ricean, and Nakagami-m distributions. In this thesis, two widely used models for fading channels, the Rayleigh and Ricean fading channel model, are assumed.

1. Rayleigh Fading

A well-accepted model for small-scale rapid amplitude fluctuations is the Rayleigh model, which is used when there is no line-of-sight (LOS) between transmitter and receiver and all of the received signal power is due to multipath. For Rayleigh fading channels, the received amplitude is modeled as a Rayleigh random variable with the probability density function (pdf) [10]

$$f_{A_c}(a_c) = \frac{a_c}{\sigma^2}\exp\left(\frac{-a_c^{\,2}}{2\sigma^2}\right), \qquad a_c \geq 0 \tag{2.15}$$

where $2\sigma^2$ represents the received diffuse, or non-LOS, signal power.

2. Ricean Fading

The Ricean model is used when there is a LOS between transmitter and receiver but a substantial portion of the received signal power is also due to multipath. Note that when there is a LOS but none of the received signal power is due to multipath, the channel is non-fading. For Ricean fading channels, the received amplitude is modeled as a Ricean random variable with pdf [10]

$$f_{A_c}(a_c) = \frac{a_c}{\sigma^2}\exp\left(\frac{-\left(a_c^{\,2}+\alpha^2\right)}{2\sigma^2}\right)\mathrm{I}_0\left(\frac{\alpha \cdot a_c}{\sigma^2}\right), \qquad a_c \geq 0 \tag{2.16}$$

where $\mathrm{I}_0(\cdot)$ is the zeroth-order modified Bessel function of the first kind, α^2 is the received direct, or LOS signal power, and $2\sigma^2$ is the non-LOS signal power. The average received signal power for a Ricean fading channel is

$$\overline{S^2(t)} = \overline{a_c^{\,2}} = \alpha^2 + 2\sigma^2 \ . \tag{2.17}$$

Note that when $\alpha \to 0$, the Ricean probability density function for a_c reduces to the Rayleigh probability density function since $I_0(0) = 1$, and the average received signal power reduces to $2\sigma^2$. The Rayleigh and Ricean probability density function are illustrated in Figure 5, where the *Ricean low SNR* curve is plotted with $\alpha = 2$ and $\sigma^2 = 1$,

Ricean medium SNR curve is plotted with $\alpha = 4$ and $\sigma^2 = 1$, and *Ricean high SNR* curve is plotted with $\alpha = 8$ and $\sigma^2 = 1$.

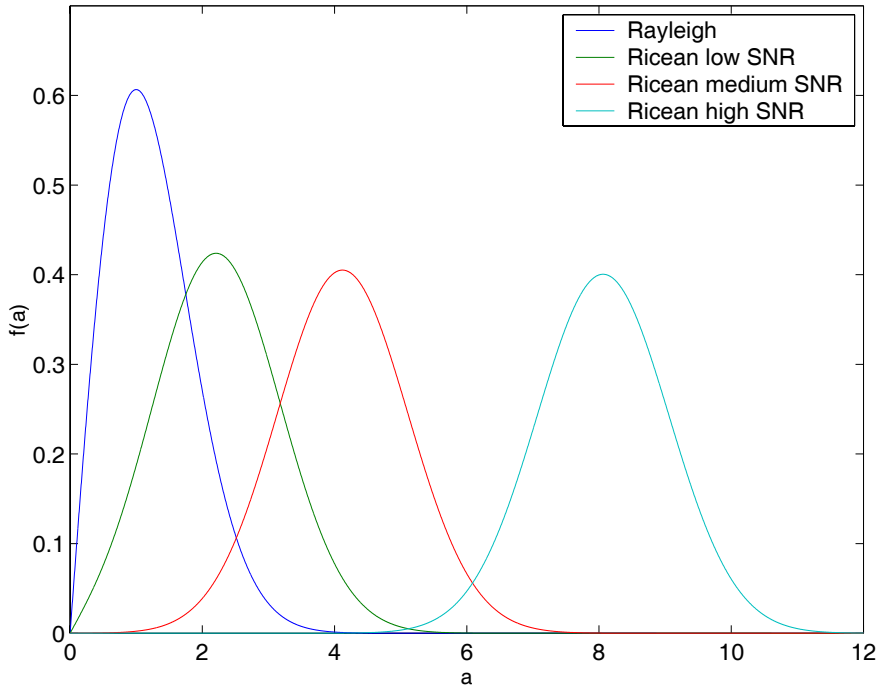

Figure 5. Rayleigh and Ricean probability density function [After Ref.10]

D. SUMMARY OF MULTIPATH FADING CHANNELS

In this chapter, we discussed multipath fading and introduced different types of small scale fading channels: *frequency-selective* fading, *flat* fading, *fast* fading, and *slow* fading. Multipath fading can cause inter-symbol interference (ISI), where the received signal consists of multiple versions of the transmitted waveforms. There are several ways to minimize ISI, and OFDM is one of the antidotes. In the next chapter, we explain why OFDM is robust over *frequency-selective* fading channels.

THIS PAGE INTENTIONALLY LEFT BLANK

III. OFDM BASED *IEEE 802.11a* STANDARD

A. *IEEE 802.11a* BACKGROUND

IEEE 802.11a was adopted as a WLAN standard in September 1999. Misleading by its name, many readers naturally think of *802.11a* as the first *IEEE* PHY standard for WLANs. Actually, the first *IEEE* standard adopted for WLANs was approved in June 1997 and specifies the medium access control (MAC) and three physical layers (PHY): *frequency hopping spread spectrum* (*802.11* FHSS), *direct sequence spread spectrum* (*802.11* DSSS) and *diffuse infrared* (*802.11* IR). The 802.11 IR standard operates at baseband and the *802.11* FHSS and *802.11* DSSS standards operate in the 2.4 GHz band. In terms of data rates, *802.11* DSSS originally supported both 1 Mbps and 2 Mbps, while the other two support 1 Mbps with 2 Mbps optional. With the growing demand for higher bit rates, a high-data-rate DSSS proposal, *802.11b*, was selected for standardization in July 1998, and extends the data rate to 11 Mbps. While developing *802.11b*, *802.11a* was also being developed. The development was motivated by the U.S. Federal Communications Commission (FCC), which released 300 MHz of spectrum in the 5.2 GHz band in January 1997. The rate-dependent parameters of *802.11a*, which utilizes BPSK, QPSK, 16-QAM, and 64-QAM as sub-carrier modulation schemes in combination with rate $1/2$, $2/3$, and $3/4$ convolutional codes to obtain a variable data bit rate from 6 up to 54 Mbps are listed in Table 1.

Data rate (Mbits/s)	Modulation	Coding rate (R)	Coded bits per subcarrier (N_{BPSC})	Coded bits per OFDM symbol (N_{CBPS})	Data bits per OFDM symbol (N_{DBPS})
6	BPSK	1/2	1	48	24
9	BPSK	3/4	1	48	36
12	QPSK	1/2	2	96	48
18	QPSK	3/4	2	96	72
24	16-QAM	1/2	4	192	96
36	16-QAM	3/4	4	192	144
48	64-QAM	2/3	6	288	192
54	64-QAM	3/4	6	288	216

Table 1. OFDM rate-dependent parameters [From Ref. 5]

B. WHY OFDM?

Recall from Chapter II that a channel is referred to as *frequency-selective* if the coherence bandwidth B_c is less than the signal bandwidth W. When this happens, the received signals are distorted and overlapped in time causing ISI and degrade system performance. There are several ways to minimize ISI. One is to reduce the symbol rate, but then the data rate is also reduced. Another technique is to utilize equalizers, but equalization is processor intensive. Finally, the effects of a frequency-selective channel can be mitigated by OFDM, and OFDM has none of the drawbacks of the previous techniques.

OFDM is a special case of multi-carrier transmission, where a high-bit-rate data stream is split into a number of low-bit-rate data streams that are transmitted simultaneously over a number of sub-carriers. For the *IEEE 802.11a* standard, there are 48 data sub-carriers; hence, the symbol rate for one sub-carrier is $R_{SC} = R_S/48$. Thus, the band-width for each sub-carrier is reduced by a factor of 48 as compared with the band-width the signal requires when only a single carrier frequency is used. As a result, $B_C \gg W_{SC} = W/48$, and the channel for each sub-carrier will be *flat*, or *frequency-nonselective*, which reduces ISI and avoids multipath in frequency-selective channels.

C. OFDM FUNDAMENTALS

In addition to its OFDM's ability to avoid ISI while achieving high data rates, OFDM has other benefits, such as robustness to RF interference and high spectral efficiency. In what follows, we discuss several fundamental OFDM concepts.

1. Single/Multi-Carrier Modulation

Single carrier modulation uses a single carrier frequency to transmit all data symbols sequentially. Compared to multi-carrier modulation, single-carrier modulation has several advantages. For example, it avoids excessive peak-to-average power ratio problems, and it is much less sensitive to frequency offsets and phase noise. The main disadvantage of single carrier modulation is that it is susceptible to multipath fading or

interference because it uses only one carrier frequency. If the multipath distortion or interference causes the frequency response to have a null at the carrier frequency, then the entire link experiences severe performance degradation.

Unlike single-carrier modulation, multi-carrier modulation uses multiple sub-carriers to transmit data in parallel. For example, OFDM-based *IEEE 802.11a* utilizes 48 sub-carries to transmit data. Given the same multipath distortion or interference as that of single-carrier modulation, only a small portion of the sub-carriers in the OFDM system is distorted, not the entire system. Therefore, the use of the multi-carrier OFDM can reduce RF interference and multipath distortion.

2. FDM/OFDM

Multi-carrier transmission is nothing more than a parallel data system. For other parallel data systems, such as frequency-division multiplexing (FDM) techniques, each sub-carrier is modulated with spectrally separate symbols to avoid inter-carrier interference (ICI), or cross-talk, from adjacent sub-carriers; however, this complete separation in spectrum leads to waste of the available bandwidth.

Unlike FDM, OFDM uses orthogonal overlapped sub-channels. The difference between FDM and OFDM is illustrated in Figure 6. As shown in Figure 6, orthogonal OFDM saves almost 50 percent of the available bandwidth compared to FDM.

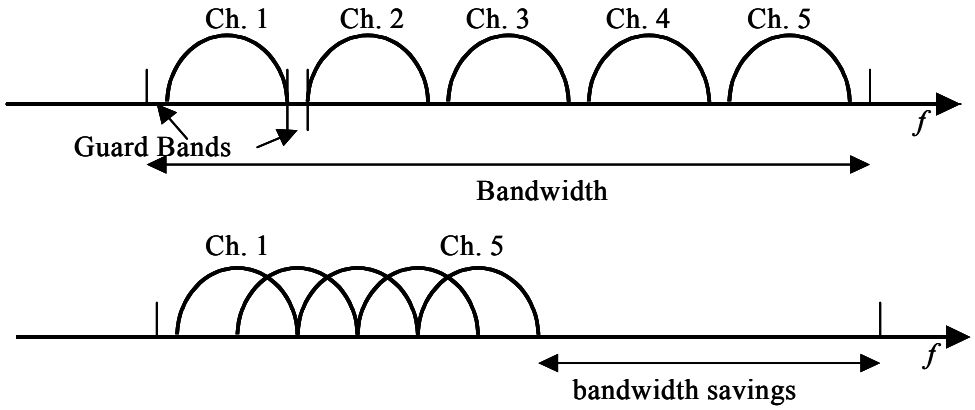

Figure 6. Sub-channel overlapping technique for FDM and OFDM [From Ref. 4]

3. Orthogonality

The reason that sub-channels can overlap with OFDM without causing ICI is that the individual cub-carriers are orthogonal. In mathematics, two vectors perpendicular to each other are orthogonal and their *dot product* is equal to zero. In communications, orthogonality means two signals are uncorrelated, or independent, over one symbol duration. In OFDM, orthogonality prevents the sub-channel demodulators from seeing frequencies other than their own, which is achieved by precisely selecting the sub-carrier spacing such that each sub-carrier is located on all the other sub-carriers' spectra zero crossing points. When sampling at the sub-carrier frequencies, the sub-carriers will not interfere each other (as shown in Figure 7). Note that for better observation, the orthogonal spectrum of an OFDM signal with four sub-carriers only is shown in Figure 7.

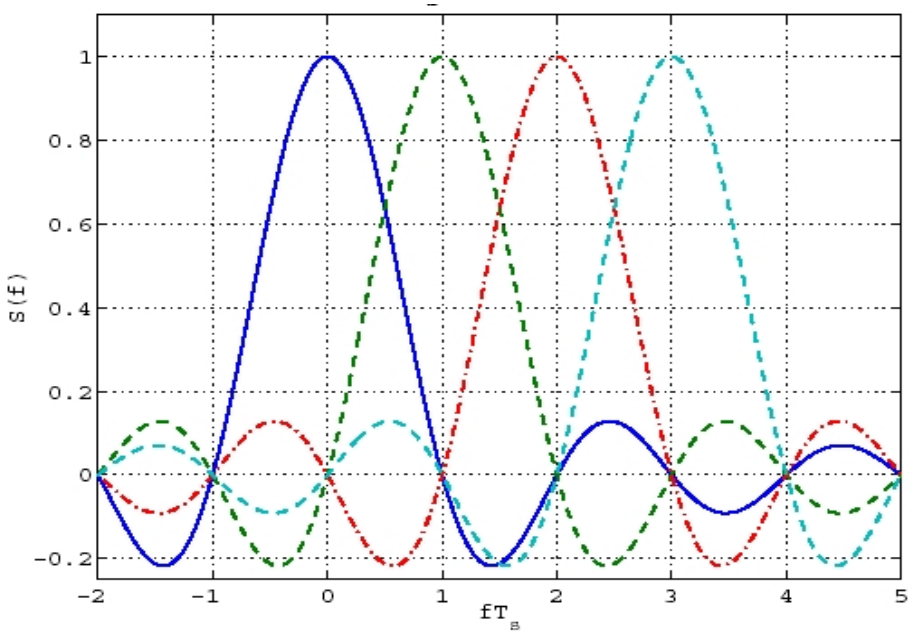

Figure 7. OFDM orthogonal spectrum with 4 sub-carriers [From Ref. 11]

D. OFDM BASED *802.11a* PARAMETERS

So far, we have explained why OFDM has the ability to combat multipath fading while achieving high data rates. We have also discussed several important concepts that

make OFDM robust in RF interference and maintain high spectral efficiency. In this section, we investigate the details of the OFDM based *IEEE 802.11a* standard. The major parameters of the OFDM PHY are listed in Table 2.

Information data rate	**6, 9, 12, 18, 24, 36, 48 and 54 Mbit/s (6, 12 and 24 Mbit/s are mandatory)**
Modulation	BPSK OFDM QPSK OFDM 16-QAM OFDM 64-QAM OFDM
Error correcting code	K = 7 (64 states) convolutional code
Coding rate	1/2, 2/3, 3/4
Number of subcarriers	52
OFDM symbol duration	4.0 μs
Guard interval	0.8 μs[a] (T_{GI})
Occupied bandwidth	16.6 MHz

Table 2. Major Parameters of the *802.11a* PHY [From Ref. 5]

1. Guard Interval

The most important parameter in *802.11a* PHY is the *guard interval* T_{GI}, because it determines not only the choice of the other parameters, but also the effectiveness of combating ISI. In order to eliminate ISI, the T_{GI} should be much larger than the expected multipath delay spread. From [9], the reported values of rms delay spread can be up to 200 ns for a large office building and up to 300 ns for various factory environments. As we can see in Table 2, the *guard interval* T_{GI} for each OFDM symbol is 0.8 μs, which is much greater than 300 ns.

2. OFDM Symbol Duration and Sub-Carrier Spacing

As mentioned above, the T_{GI} should be chosen much larger than the expected multipath delay spread in order to combat ISI; however, the T_{GI} cannot be chosen too large, either. When T_{GI} increases, the OFDM effective symbol duration decreases and

data rates drop. To limit the relative amount of power and time spent on the guard interval, the total symbol duration chosen in *802.11a* is 4 microseconds. This in turn determines the sub-carrier spacing of 312.5 kHz, which is the inverse of the symbol duration minus the guard time.

3. Number of Sub-Carriers

In addition to the 48 data sub-carriers, each OFDM symbol has an additional four pilot sub-carriers, which provide a reference to minimize frequency and phase shifts of the signal during transmission. Therefore, there are a total of 52 sub-carriers for each OFDM symbol.

4. Error Correcting Code and Coding Rate

To correct for sub-carriers in deep fades, *802.11a* applies FEC coding across the sub-carriers with variable code rates. Convolutional coding is used with industry standard rate $1/2$, constraint length 7 encoded with generator polynomials (133, 171). The convolutional encoder is shown in Figure 8. Higher coding rates of $2/3$ and $3/4$ are obtained by puncturing the rate $1/2$ code. The rate $1/2$ code is used with BPSK, QPSK, and 16-QAM to give rates of 6, 12, and 24 Mbps, respectively. The rate $2/3$ code is used with 64-QAM only to obtain a data rate of 48 Mbps. The rate $3/4$ code is used with BPSK, QPSK, 16-QAM, and 64-QAM to give rates of 9, 18, 36, and 54 Mbps, respectively.

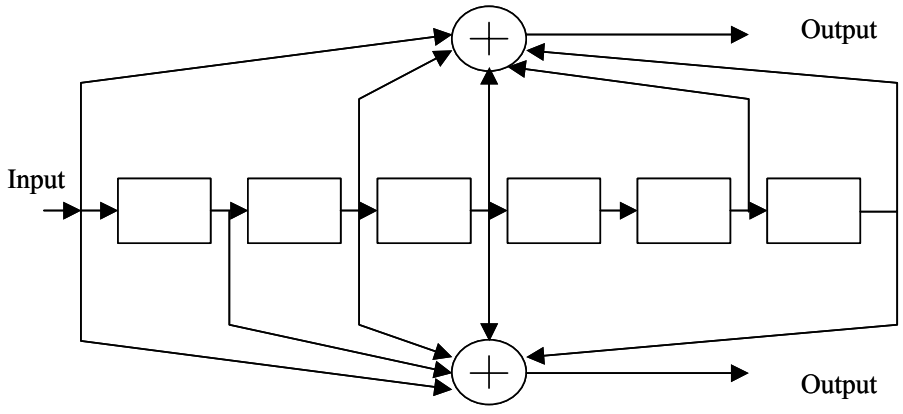

Figure 8. Convolutional Encoder with constraint length $v = 7$ [From Ref. 5]

E. OFDM SIGNAL PROCESSING

This section gives a general description of how the *IEEE 802.11a* PHY is implemented. The *IEEE 802.11a* PHY transmitter and receiver block diagram is shown in Figure 9 [5].

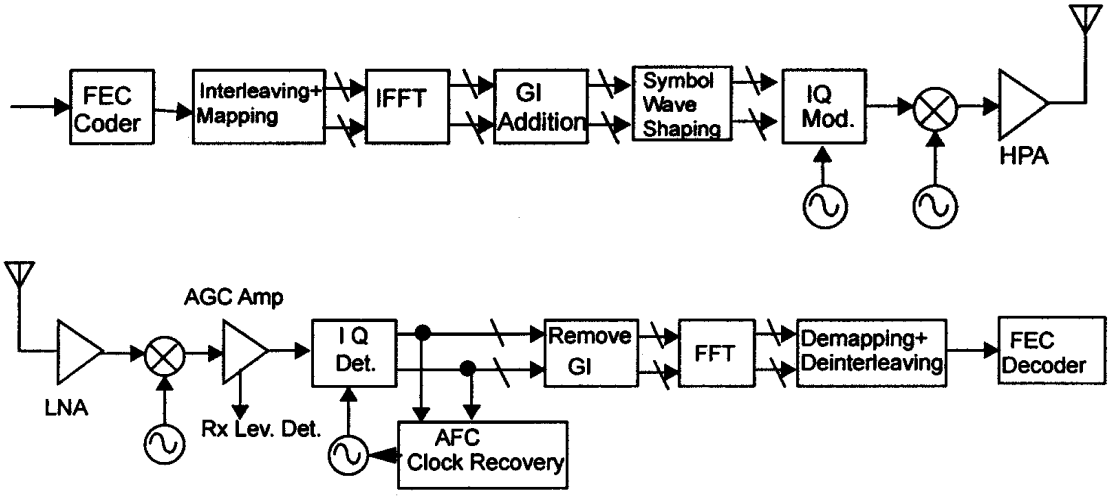

Figure 9. OFDM PHY transceiver block diagram [From Ref. 5]

In the transmitter, the serial binary input data are encoded by a rate $1/2$ constraint length 7, convolutional encoder. The code rate can be increased to $2/3$ or $3/4$ by puncturing the coded output bits. The coded output bits are next interleaved and mapped. Interleaving is a technique for handling burst errors. The interleaver randomizes burst errors and the convolutional decoder can easily correct random errors. After interleaving, the coded binary data are converted into PSK or QAM symbols by mapping onto respective constellation points. The constellations for BPSK, QPSK, 16QAM, and 64QAM are all shown in Figure 10.

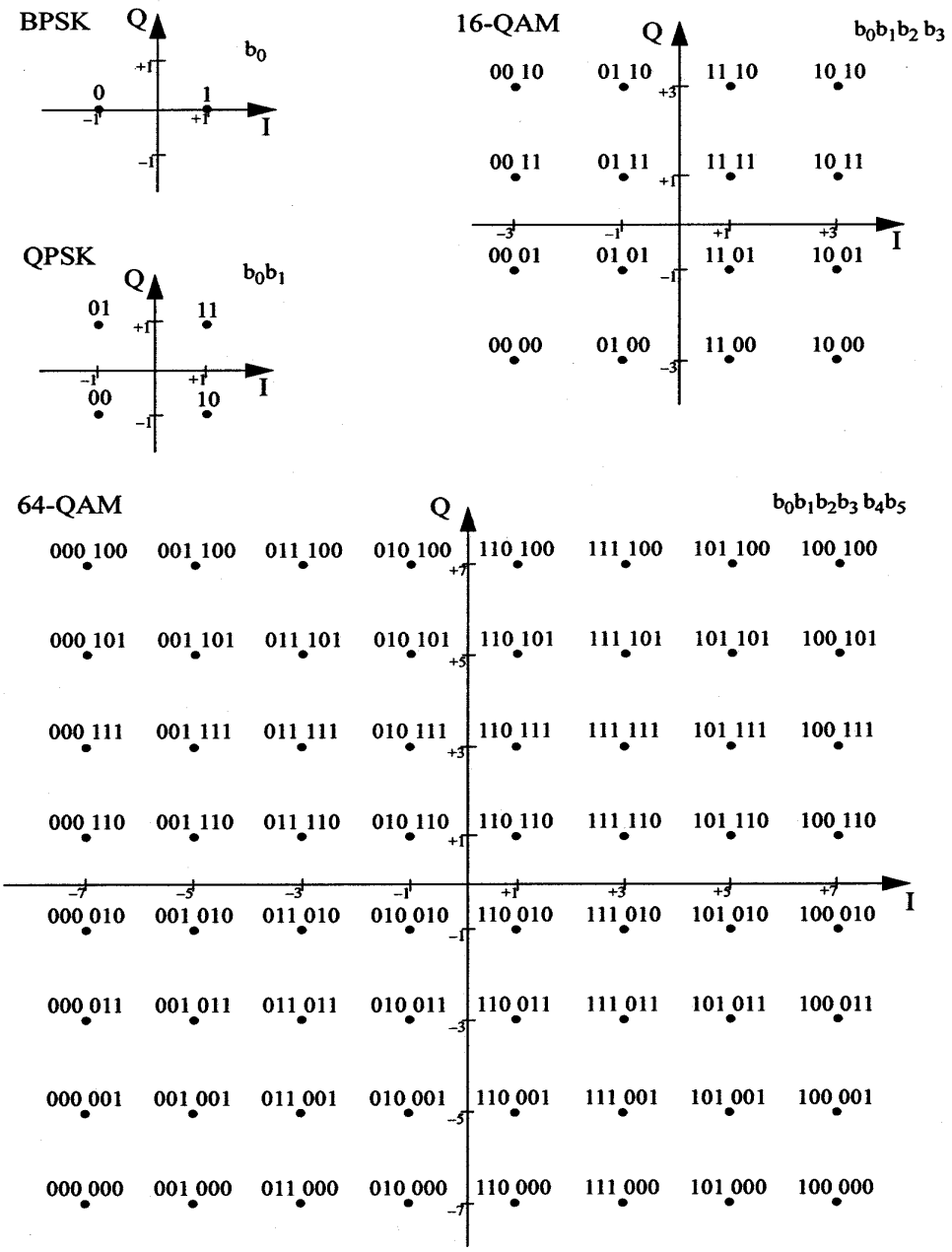

Figure 10. Constellation for BPSK, QPSK, 16QAM, and 64QAM [From Ref. 5]

In order to facilitate coherent reception, 4 pilot tones are added to each 48 data symbols to make one OFDM symbol. Each OFDM symbol is, after serial-to-parallel conversion, modulated onto 52 sub-carriers by applying an inverse fast Fourier transform (IFFT). To make the system immune to multipath fading, a cyclic extension is added to

the guard interval. As discussed earlier, a key parameter in the OFDM system is the 800 ns guard time, which is much longer than the maximum reported rms delay spread, 300 ns, in [9]. Since the guard interval is longer than the delay spread, ISI is eliminated; however, it is shown in [12] that this guard interval has to be a cyclic extension of the OFDM symbol in order to maintain orthogoanlity. Three sub-carriers in one OFDM symbol duration with no cyclic extension added in the guard time was illustrated in Figure 11. As we can see, there is not an integer number of cycles for each sub-carrier over the OFDM symbol duration, thus there will be cross-talk, or ICI, among sub-carriers in the frequency domain.

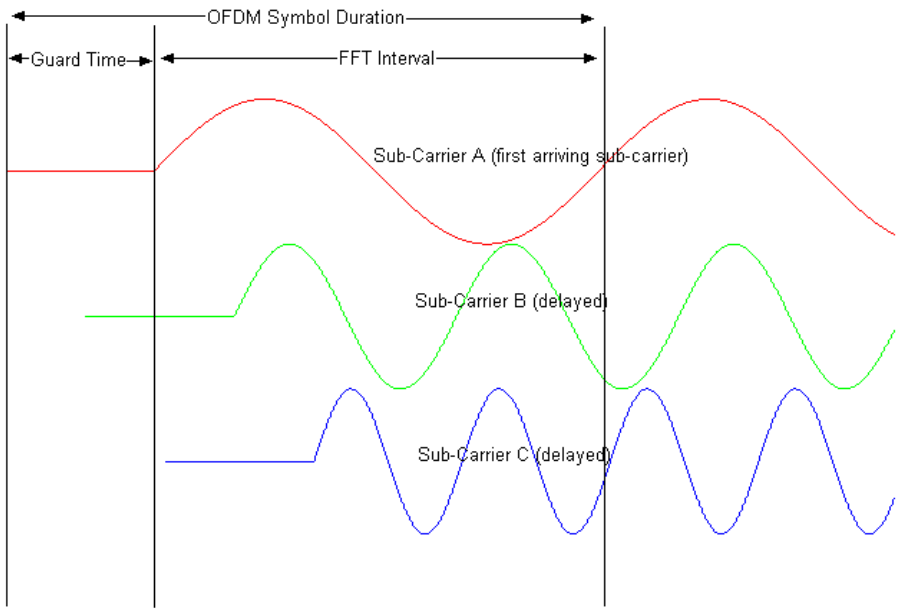

Figure 11. Effect of no cyclic extension in the guard interval [From Ref.4]

On the contrary, by adding the cyclic extension in the guard time, each sub-carrier will have an integer number of cycles over the OFDM symbol duration, and there will be no cross-talk among sub-carriers. This is shown in Figure 12.

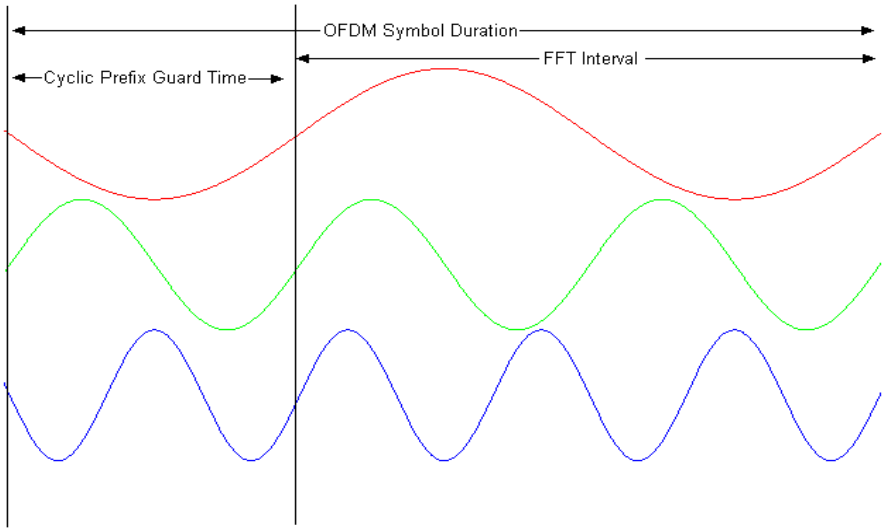

Figure 12. Effect of adding cyclic extension in the guard interval [From Ref. 4]

After adding the cyclic extension, windowing is applied to smooth the transition region between symbols and to narrow the output spectrum. Further, the symbols are modulated onto sine and cosine carriers and are up-converted to the 5-GHz band, then amplified and transmitted through the antenna.

Most of the processes done in the transmitter are reversed in the receiver, except for adding a low noise amplifier (LNA) and automatic gain control (AGC). The LNA minimizes the effective system noise temperature of the receiver. The AGC estimates the power of the received pilot tone, and controls the power of the received signal.

Now that we have examined multipath fading, the *IEEE 802.11a* standard, and OFDM, we are ready to investigate the performance of the *IEEE 802.11a* WLAN standard over frequency-selective, slow, Ricean fading channels in the following chapters.

IV. PERFORMANCE WITHOUT FEC CODING

This chapter examines the performance of uncoded OFDM transmitted over Ricean fading channels. The analysis begins with the sub-carrier modulation schemes utilized in the *IEEE 802.11a* standard: BPSK, QPSK, 16QAM, and 64QAM. The overall OFDM modulation scheme is then analyzed. In this chapter, analytic expressions for the performance of all sub-carrier modulation schemes used in the *IEEE 802.11a* standard are derived.

A. PERFORMANCE IN AWGN

1. BPSK/QPSK Modulation

As mentioned above, the performances of all four sub-carrier modulation schemes used in the *IEEE 802.11a* standard are derived in this chapter. Actually, only two expressions are required, one for BPSK and one for square QAM, since QPSK and BPSK have the same probability of bit error [7]

$$P_b = Q\left(\sqrt{\frac{2E_b}{N_0}}\right) \tag{4.1}$$

where E_b/N_0 is the ratio of average energy per bit-to-noise power spectral density. Note that $E_b = A_c^2 \cdot T_b$, where A_c^2 is the received signal power and T_b is the bit duration. The symbol $Q(\cdot)$ is the Q-function, defined as

$$Q(z) = \frac{1}{\sqrt{2\pi}} \int_z^\infty \exp\left(\frac{-\lambda^2}{2}\right) d\lambda \tag{4.2}$$

which can be approximated as

$$Q(z) \approx \frac{1}{\sqrt{2\pi} \cdot z} \exp\left(\frac{-z^2}{2}\right) \qquad \text{for } z \geq 2\,. \tag{4.3}$$

2. QAM Modulation with a Square Constellation

In terms of a set signal constellations as shown in Figure 13, MQAM can be categorized as either rectangular QAM or square QAM. For example, in Figure 13 M=8 (blue line) is rectangular QAM and M=16 (red line) is square QAM. Of course, the square QAM can be considered a special case of rectangular QAM.

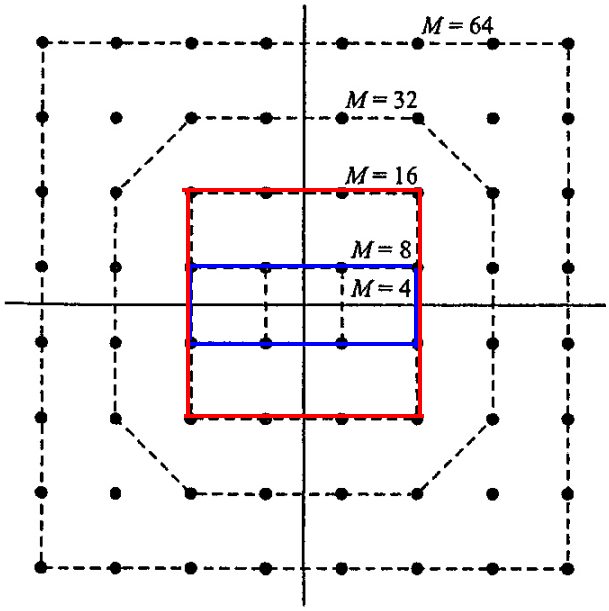

Figure 13. MQAM signal constellation [After Ref. 13]

Rectangular QAM can be thought of as a M_i - PAM signal on the in-phase (I) signal component and a M_q - PAM signal on the quadrature (Q) signal component where $M = M_i \times M_q$; therefore, the probability of symbol error for rectangular QAM can be expressed as

$$\begin{aligned} P_s &= P_r\left(\text{error on } I \bigcup \text{error on } Q\right) \\ &= P_{s_i} \bigcup P_{s_q} \\ &= P_{s_i} + P_{s_q} - P_{s_i} \bigcap P_{s_q} \ . \end{aligned} \tag{4.4}$$

Since the I and Q components can be modeled as independent random processes, Equation (4.4) can be rewritten as

$$P_s = P_{s_i} + P_{s_q} - P_{s_i} P_{s_q} \tag{4.5}$$

where P_{s_i} and P_{s_q} are the probability of symbol error for M_i - PAM and M_q - PAM, respectively.

For a square QAM, $M_i = M_q$, $P_{s_i} = P_{s_q}$, and $M = M_i^2$, thus Equation (4.5) can be rewritten as

$$P_s = 2P_{s_i} - P_{s_i}^2 \ . \tag{4.6}$$

The probability of symbol error for M_i - PAM is given by [13]

$$\begin{aligned} P_{s_i} &= \frac{2\left(M_i - 1\right)}{M_i} Q\left(\sqrt{\frac{\left(6\log_2 M_i\right)E_b}{\left(M_i^2 - 1\right)N_0}}\right) \\ &= \frac{2\left(\sqrt{M} - 1\right)}{\sqrt{M}} Q\left(\sqrt{\frac{3qE_b}{\left(M-1\right)N_0}}\right) \end{aligned} \tag{4.7}$$

where $q = \log_2\left(M\right)$ is the number of bits per symbol. For example, $q = 4$ implies 16QAM, and $q = 6$ implies 64QAM. Substituting Equation (4.7) into Equation (4.6), we obtain the probability of symbol error for square QAM as

$$P_s = 4\left(1 - \frac{1}{\sqrt{M}}\right) Q\left(\sqrt{\frac{3qE_b}{\left(M-1\right)N_0}}\right) \cdot \left[1 - \left(1 - \frac{1}{\sqrt{M}}\right) Q\left(\sqrt{\frac{3qE_b}{\left(M-1\right)N_0}}\right)\right]. \tag{4.8}$$

The probability of bit error P_b is now obtained by dividing Equation (4.8) by q to obtain

$$P_b \approx \frac{4\left(1 - \frac{1}{\sqrt{M}}\right)}{q} Q\left(\sqrt{\frac{3qE_b}{\left(M-1\right)N_0}}\right) \cdot \left[1 - \left(1 - \frac{1}{\sqrt{M}}\right) Q\left(\sqrt{\frac{3qE_b}{\left(M-1\right)N_0}}\right)\right] \tag{4.9}$$

since P_s and P_b are related as $P_b \approx P_s / q$. Note that for square QAM, $q \geq 4$. With Equation (4.1) and (4.9), we plot performance of BPSK/QPSK, 16QAM and 64QAM in AWGN versus E_b / N_0 as shown in Figure 14. As expected, the performance of BPSK/-

QPSK is superior to the performance of 16QAM, and the performance of 16QAM is superior to that of 64QAM.

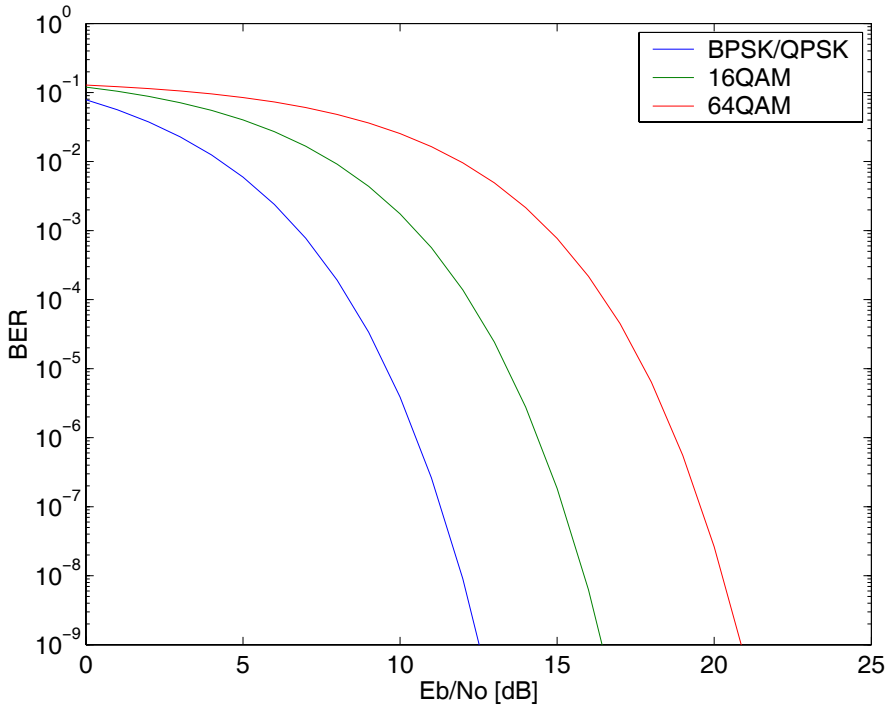

Figure 14. Performance of BPSK/QPSK, 16QAM and 64QAM in AWGN

B. PERFORMANCE IN RICEAN FADING CHANNELS

The probability of bit error of all sub-carrier modulation formats we have considered are functions of $E_b = A_c^2 \cdot T_b$, where A_c is simply modeled as a constant parameter. In fading channels, the received signal amplitude fluctuates and can no longer be modeled as a parameter but must be modeled as a random variable a_c. Consequently, $E_b = a_c^2 \cdot T_b$ is also a random variable; therefore, Equation (4.1) and Equation (4.9) are now conditional probabilities $P_b(a_c)$. In this case, we need to obtain the *average* probability of bit error for all sub-carrier modulations.

1. BPSK/QPSK Modulation

The probability of bit error for BPSK/QPSK in AWGN is given by Equation (4.1). However in Ricean fading channels, Equation (4.1) is a conditional probability, which can be expressed as

$$P_b(a_c) = Q\left(\sqrt{\frac{2a_c{}^2 T_b}{N_0}}\right). \tag{4.10}$$

In order to obtain the *average* probability of bit error, we need to find the expected value of $P_b(a_c)$; that is,

$$P_b = \int_0^\infty P_b(a_c) \cdot f_{A_c}(a_c)\, da_c \tag{4.11}$$

where $f_{A_c}(a_c)$ is the Ricean pdf given by Equation (2.7), rewritten here as

$$f_{A_c}(a_c) = \frac{a_c}{\sigma^2} \exp\left(\frac{-\left(a_c{}^2 + \alpha^2\right)}{2\sigma^2}\right) \mathrm{I}_0\left(\frac{\alpha \cdot a_c}{\sigma^2}\right), \qquad a_c \geq 0\,. \tag{4.12}$$

If we define

$$\gamma_\mathrm{b} = \frac{E_b}{N_0} = \frac{a_c{}^2 T_b}{N_0}\,, \tag{4.13}$$

then

$$a_c = \sqrt{\frac{\gamma_\mathrm{b} N_0}{T_b}} = \sqrt{\gamma_\mathrm{b} \sigma_0{}^2} \tag{4.14}$$

where $\sigma_0{}^2 = N_0/T_b$ is the AWGN noise power and N_0 is the noise power spectral density (PSD). Using Equation (4.13) in Equation (4.10) and applying Equation (4.3), we get

$$P_b(\gamma_\mathrm{b}) \approx \frac{1}{2\sqrt{\pi c}} \cdot \exp(-\gamma_\mathrm{b}) \tag{4.15}$$

where c is empirically obtained to give the best results for a Ricean fading channel.

Given the pdf for a_c, we find the pdf for γ_b from [14]

$$f_Y(y) = \left|\frac{dx}{dy}\right| f_X(x) . \tag{4.16}$$

Substituting Equation (4.12) into Equation (4.16), we get

$$\begin{aligned} f_{\Gamma_b}(\gamma_b) &= \left|\frac{da_c}{d\gamma_b}\right| f_{A_c}\left(a_c = \sqrt{\gamma_b \sigma_0^2}\right) \\ &= \frac{1}{\left(2\sigma^2/\sigma_0^2\right)} \exp\left[\frac{-\left(\gamma_b + \alpha^2/\sigma_0^2\right)}{2\sigma^2/\sigma_0^2}\right] I_0\left(\frac{(\alpha/\sigma_0)\sqrt{\gamma_b}}{\sigma^2/\sigma_0^2}\right), \ \gamma_b \geq 0 . \end{aligned} \tag{4.17}$$

For BPSK/QPSK with diversity over Ricean fading channels, the optimum performance is obtained by using a maximal ratio combiner (MRC) receiver. In this case, Equation (4.13) becomes

$$\gamma_b = \frac{\sum_{k=1}^{d} a_{C_K}^2}{\sigma_0^2} . \tag{4.18}$$

It can be shown that [15]

$$f_{\Gamma_b}(\gamma_b) = \frac{\gamma_b^{(d-1)/2}}{\left(d\alpha^2/\sigma_0^2\right)^{(d-1)/2}\left(2\sigma^2/\sigma_0^2\right)} \exp\left[\frac{-\left(\gamma_b + \left(d\alpha^2/\sigma_0^2\right)\right)}{2\sigma^2/\sigma_0^2}\right] I_{d-1}\left(\frac{(\alpha/\sigma_0)\sqrt{d\gamma_b}}{\sigma^2/\sigma_0^2}\right), \ \gamma_b \geq 0 \tag{4.19}$$

where d is the diversity order. Note that when $d = 1$, which is equivalent to no diversity, Equation (4.19) reduces to (4.17). Now using Equation (4.15) and (4.19), we find the average probability of bit error for BPSK/QPSK with diversity in Ricean fading as

$$\begin{aligned} P_b &= \int_0^\infty P_b(\gamma_b) \cdot f_{\Gamma_b}(\gamma_b) d\gamma_b \\ &\approx \int_0^\infty \frac{e^{-\gamma_b}}{2\sqrt{\pi c}} \cdot \frac{\gamma_b^{(d-1)/2}}{\left(d\alpha^2/\sigma_0^2\right)^{(d-1)/2}\left(2\sigma^2/\sigma_0^2\right)} \exp\left[\frac{-\left(\gamma_b + \left(d\alpha^2/\sigma_0^2\right)\right)}{2\sigma^2/\sigma_0^2}\right] I_{d-1}\left(\frac{(\alpha/\sigma_0)\sqrt{d\gamma_b}}{\sigma^2/\sigma_0^2}\right) d\gamma_b \\ &\approx \frac{e^{-d\zeta}}{2\sqrt{\pi c}\left(d\alpha^2/\sigma_0^2\right)^{(d-1)/2}\left(2\sigma^2/\sigma_0^2\right)} \int_0^\infty \gamma_b^{(d-1)/2} e^{-\left(1+\frac{1}{2\sigma^2/\sigma_0^2}\right)\gamma_b} \cdot I_{d-1}\left(\frac{(\alpha/\sigma_0)\sqrt{d\gamma_b}}{\sigma^2/\sigma_0^2}\right) d\gamma_b \end{aligned} \tag{4.20}$$

where $\zeta = \alpha^2/2\sigma^2$ is the ratio of direct-to-diffuse signal power. Note that $\zeta = 0$ corresponds to Rayleigh fading, and $\zeta \to \infty$ corresponds to no fading. To evaluate Equation (4.20), we use [16]

$$\int_0^\infty x^{m+\frac{n}{2}} \cdot e^{-vx} J_n\left(2\beta\sqrt{x}\right) dx = \frac{m!\beta^n \exp\left(-\beta^2/v\right)}{v^{m+n+1}} \Lambda_m^n\left(\beta^2/v\right) \tag{4.21}$$

where $\Lambda_m^n(\bullet)$ is the *Laguerre polynomial* and is defined as

$$\Lambda_m^n\left(\beta^2/v\right) = \sum_{p=0}^{m} \frac{(-1)^p}{p!} \binom{m+n}{m-p} \left(\frac{\beta^2}{v}\right)^p . \tag{4.22}$$

Note that

$$\Lambda_0^n(\bullet) = 1 \tag{4.23}$$

and that

$$I_n(z) = (-j)^n J_n(jz) \tag{4.24}$$

where $j = \sqrt{-1}$. Comparing the integral in Equation (4.20) to the left hand side of Equation (4.21) and using the Equation (4.23) and (4.24), we obtain

$$m = 0 \;\Rightarrow\; \Lambda_0^n(\bullet) = 1 \tag{4.25}$$

$$n = d - 1 \tag{4.26}$$

$$v = 1 + \frac{1}{2\sigma^2/\sigma_0{}^2} \tag{4.27}$$

$$\beta = \frac{j(\alpha/\sigma_0)\sqrt{d}}{2\sigma^2/\sigma_0{}^2} \;\Rightarrow\; \beta^2 = \frac{-d \cdot \alpha^2}{4\sigma^2\left(\sigma^2/\sigma_0{}^2\right)} . \tag{4.28}$$

Substituting Equation (4.25) through (4.28) into the right hand side of Equation (4.21), we can evaluate the integral in Equation (4.20) to obtain

$$P_b \approx \frac{\exp\left(-d \cdot \zeta\left(1-\frac{1}{\left(2\sigma^2/\sigma_0{}^2\right)+1}\right)\right)}{2\sqrt{\pi \cdot c}\left(\frac{2\sigma^2}{\sigma_0{}^2}+1\right)^d}. \tag{4.29}$$

If we define

$$\overline{\gamma_b} = \frac{\overline{E_b}}{N_0} = \frac{\overline{a_c{}^2} \cdot T_b}{N_0} = \frac{\overline{a_c{}^2}}{\sigma_0{}^2} \tag{4.30}$$

and substitute Equation (2.17) into Equation (4.30), then

$$\overline{\gamma_b} = \frac{\alpha^2 + 2\sigma^2}{\sigma_0{}^2} \tag{4.31}$$

where $\overline{\gamma_b}$ is the ratio of the average energy per bit-to-noise power spectral density. Since $\zeta = \alpha^2/2\sigma^2$, we can rewrite Equation (4.31) as

$$\overline{\gamma_b} = \frac{2\sigma^2}{\sigma_0{}^2}(\zeta+1) \tag{4.32}$$

which yields

$$\frac{2\sigma^2}{\sigma_0{}^2} = \frac{\overline{\gamma_b}}{(\zeta+1)}. \tag{4.33}$$

Finally, substituting Equation (4.33) into Equation (4.29), we find the analytic expression for the performance of BPSK/QPSK with diversity in Ricean fading channels in terms of $\overline{\gamma_b}$, ζ, and diversity d as

$$P_b \approx \frac{1}{2\sqrt{\pi \cdot c_1}}\left(\frac{\zeta+1}{\overline{\gamma_b}+\zeta+1}\right)^d \exp\left(\frac{-d \cdot \zeta \cdot \overline{\gamma_b}}{\overline{\gamma_b}+\zeta+1}\right). \tag{4.34}$$

Note that when $d=1$, c is replaced by c_1, where $c_1 = 1.2 + 0.1\zeta$ is empirically obtained to make Equation (4.34) an accurate approximation of the *exact* performance of BPSK/QPSK in Ricean fading channels with no diversity, which is given by

$$P_b = \int_0^{\infty} Q\left(\sqrt{2\cdot\gamma_b}\right)\cdot\frac{\exp\left(-\left(\frac{\gamma_b}{\delta}+\zeta\right)\right)}{\delta}\cdot I_0\left(2\cdot\sqrt{\frac{\zeta\cdot\gamma_b}{\delta}}\right)d\gamma_b \qquad (4.35)$$

where $\delta = 2\sigma^2/\sigma_0{}^2 = \overline{\gamma_b}/(\zeta+1)$. Results obtained with Equation (4.34) and Equation (4.35) with $\zeta = 0$ and $\zeta = 10$ are compared in Figure 15. Note that $\zeta = 0$ corresponds to Rayleigh fading. From Figure 15, we can see that the approximate expression is virtually perfect for Rayleigh fading. For Ricean fading, the approximate expression is a tight upper bound for $2\,dB < E_b/N_0 < 20\,dB$, which corresponds to the signal-to-noise ratios that are typically of the most interest.

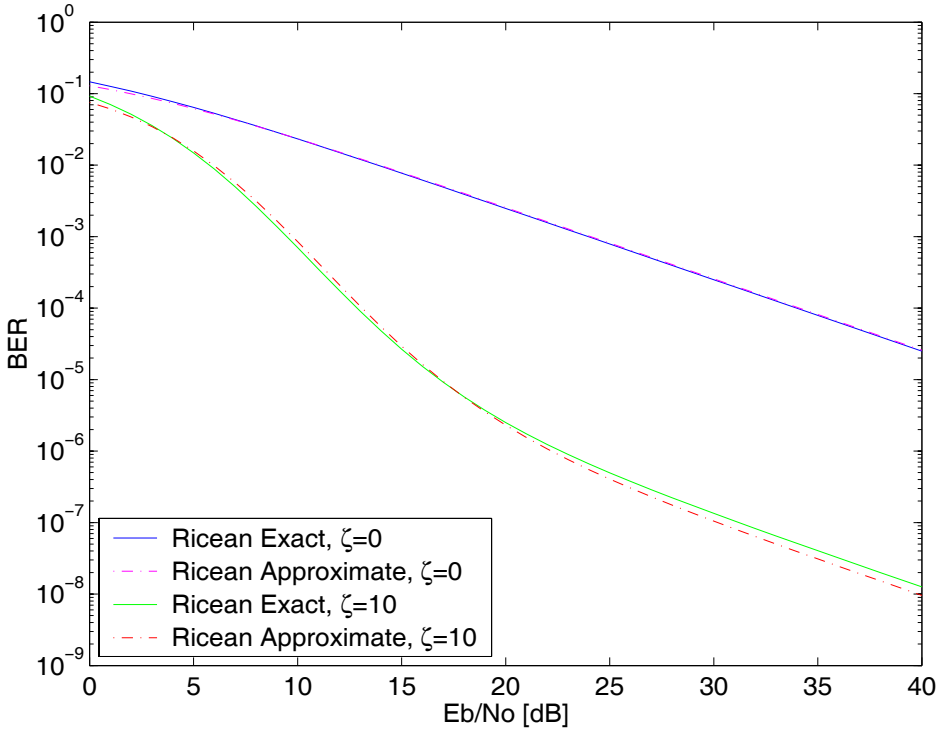

Figure 15. BPSK/QPSK performance in Ricean fading channels

In order to double check the accuracy of Equation (4.34), we set $\zeta = 0$ and $d = 1$, and compare the results obtained with the exact result for BPSK/QPSK in Rayleigh fading channels, given by [13]

$$P_b = \frac{1}{2}\left(1 - \sqrt{\frac{\overline{\gamma_b}}{1+\overline{\gamma_b}}}\right). \tag{4.36}$$

Figure 16 is a plot of Equations (4.34), (4.35) and (4.36). As we can see, the approximate analytic expression given by Equation (4.34) is very accurate for Rayleigh fading channels.

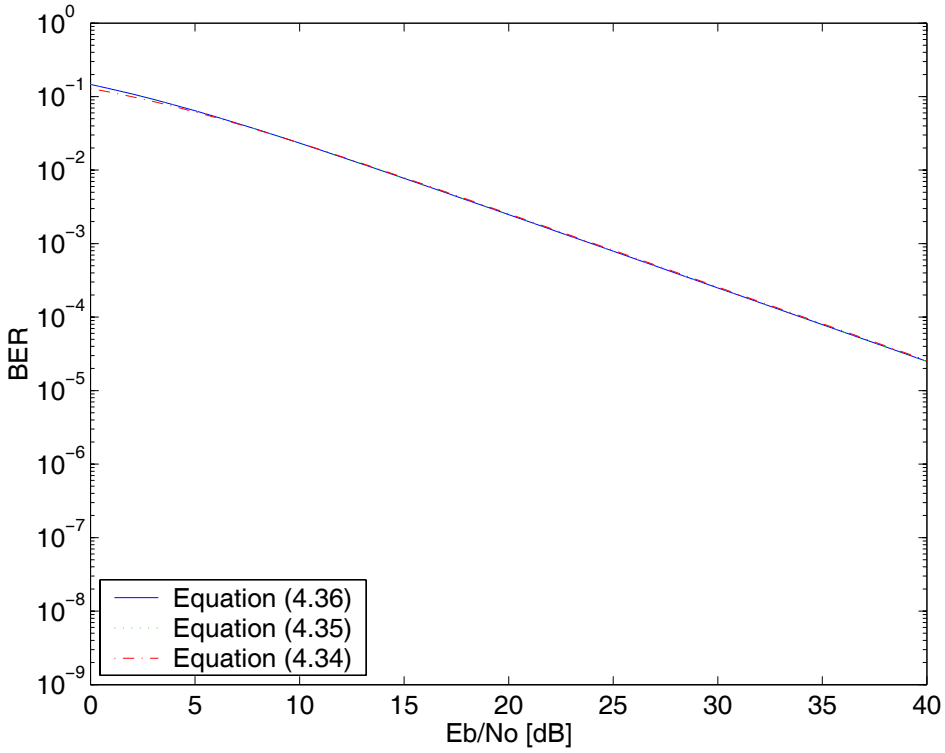

Figure 16. BPSK/QPSK performance in Rayleigh fading channels

As previously discussed, $\zeta = 0$ corresponds to Rayleigh fading. For $\zeta > 0$, the channel exhibits Ricean fading. When $\zeta \to \infty$, there is no fading. The performance of BPSK/QPSK over Ricean fading channels with ζ as a parameter in the range of $0 \le \zeta \le 10$ is plotted in Figure 17. As we can see, as ζ increases, the performance approaches that obtained with just AWGN and no fading.

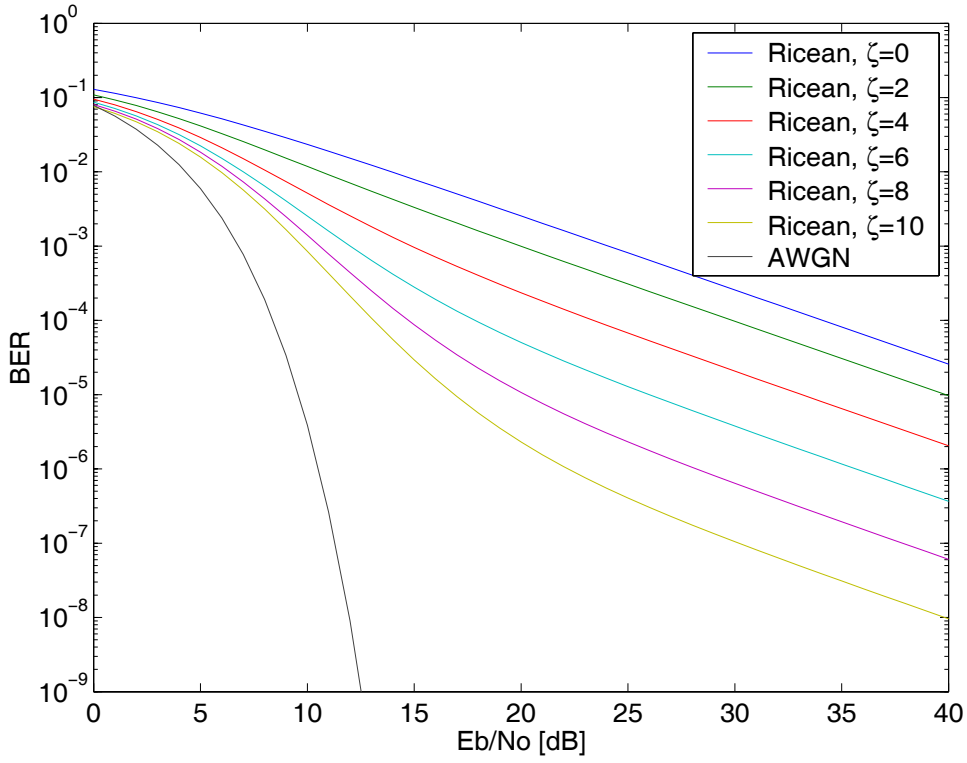

Figure 17. BPSK/QPSK performance in Ricean fading channels with $0 \le \zeta \le 10$

2. Square QAM Modulation

The derivation of an analytic expression for the performance of QAM with a square constellation in Ricean fading channels is similar to that of BPSK/QPSK, except the conditional probability of bit error for QAM with a square constellation is obtained from Equation (4.9):

$$P_b(\gamma_b) \approx \frac{4\left(1-\frac{1}{\sqrt{M}}\right)}{q} Q\left(\sqrt{\frac{3 \cdot q \cdot \gamma_b}{M-1}}\right) \cdot \left[1-\left(1-\frac{1}{\sqrt{M}}\right) Q\left(\sqrt{\frac{3 \cdot q \cdot \gamma_b}{M-1}}\right)\right] \qquad (4.37)$$

where $M = 2^q$ $\left(q = \log_2(M)\right)$ and q is the number of bits per symbol. As a result, $q = 4$ corresponds to 16 QAM, and $q = 6$ corresponds to 64QAM. Recall that $Q(\bullet)$ can be approximated by Equation (4.3); therefore, analogous to BPSK/QPSK

$$\mathrm{Q}\left(\sqrt{\frac{3\cdot q\cdot \gamma_{\mathrm{b}}}{M-1}}\right)\approx\frac{1}{\sqrt{2\pi\cdot c}}\exp\left(\frac{-3\cdot q\cdot\gamma_{\mathrm{b}}}{2(M-1)}\right) \tag{4.38}$$

where c is empirically obtained. Substituting Equation (4.38) into Equation (4.37), we obtain

$$P_b(\gamma_{\mathrm{b}})\approx\frac{4\left(1-\frac{1}{\sqrt{M}}\right)\cdot\exp\left(\frac{-3\cdot q\cdot\gamma_{\mathrm{b}}}{2(M-1)}\right)}{q\cdot\sqrt{2\pi\cdot c}}-\frac{4\left(1-\frac{1}{\sqrt{M}}\right)^2\cdot\exp\left(\frac{-3\cdot q\cdot\gamma_{\mathrm{b}}}{M-1}\right)}{2\pi\cdot c\cdot q}. \tag{4.39}$$

Now substituting Equation (4.39) and Equation (4.19) into

$$P_b=\int_0^\infty P_b(\gamma_{\mathrm{b}})\cdot f_{\Gamma_b}(\gamma_{\mathrm{b}})\,\mathrm{d}\gamma_{\mathrm{b}} \tag{4.40}$$

we find

$$\begin{aligned}P_b\approx&\frac{4\left(1-\frac{1}{\sqrt{M}}\right)e^{-\mathrm{d}\cdot\zeta}}{q\sqrt{2\pi c}\left(\frac{\mathrm{d}\alpha^2}{\sigma_0{}^2}\right)^{(d-1)/2}\left(\frac{2\sigma^2}{\sigma_0{}^2}\right)}\int_0^\infty\gamma_{\mathrm{b}}{}^{\frac{(\mathrm{d}-1)}{2}}e^{-\left(\frac{3q}{2(M-1)}+\frac{1}{2\sigma^2/\sigma_0{}^2}\right)\gamma_{\mathrm{b}}}I_{d-1}\left(\frac{(\alpha/\sigma_0)\sqrt{\mathrm{d}\gamma_{\mathrm{b}}}}{\sigma^2/\sigma_0{}^2}\right)\mathrm{d}\gamma_{\mathrm{b}}\\&-\frac{4\left(1-\frac{1}{\sqrt{M}}\right)^2e^{-\mathrm{d}\cdot\zeta}}{2\pi cq\left(\frac{\mathrm{d}\alpha^2}{\sigma_0{}^2}\right)^{(d-1)/2}\left(\frac{2\sigma^2}{\sigma_0{}^2}\right)}\int_0^\infty\gamma_{\mathrm{b}}{}^{\frac{(\mathrm{d}-1)}{2}}e^{-\left(\frac{3q}{(M-1)}+\frac{1}{2\sigma^2/\sigma_0{}^2}\right)\gamma_{\mathrm{b}}}I_{d-1}\left(\frac{(\alpha/\sigma_0)\sqrt{\mathrm{d}\gamma_{\mathrm{b}}}}{\sigma^2/\sigma_0{}^2}\right)\mathrm{d}\gamma_{\mathrm{b}}.\end{aligned} \tag{4.41}$$

In a manner similar to BPSK/QPSK, we evaluate Equation (4.41) by comparing the integrals in Equation (4.41) to the left hand side of Equation (4.21). Using Equation (4.23) and (4.24), we obtain

$$m=0\ \Rightarrow\ \Lambda_0^n(\bullet)=1, \tag{4.42}$$

$$n=d-1, \tag{4.43}$$

$$v=\frac{\left[3q/2(M-1)\right]\left(2\sigma^2/\sigma_0{}^2\right)+1}{2\sigma^2/\sigma_0{}^2}, \tag{4.44}$$

$$\beta = \frac{j\left(\alpha/\sigma_0\right)\sqrt{d}}{2\sigma^2/{\sigma_0}^2} \Rightarrow \beta^2 = \frac{-d\cdot\alpha^2}{4\sigma^2\left(\sigma^2/{\sigma_0}^2\right)}. \tag{4.45}$$

Now substituting Equations (4.42) through (4.45) into the right hand side of Equation (4.21), we can evaluate the two integrals in Equation (4.41). After some simplification, we obtain

$$P_b \approx \frac{4\left(1-\frac{1}{\sqrt{M}}\right)e^{-d\cdot\zeta\left[\frac{3q\overline{\gamma_b}}{3q\overline{\gamma_b}+2(M-1)(\zeta+1)}\right]}}{q\sqrt{2\pi c_2}\left[\frac{3q\overline{\gamma_b}+2(M-1)(\zeta+1)}{2(M-1)(\zeta+1)}\right]^d} - \frac{2\left(1-\frac{1}{\sqrt{M}}\right)^2 e^{-d\cdot\zeta\left[\frac{3q\overline{\gamma_b}}{3q\overline{\gamma_b}+(M-1)(\zeta+1)}\right]}}{\pi c_2 q\left[\frac{3q\overline{\gamma_b}+(M-1)(\zeta+1)}{(M-1)(\zeta+1)}\right]^d}. \tag{4.46}$$

For $d=1$, Equation (4.46) is an approximate analytic expression for the performance of square QAM in Ricean fading. Note that c is replaced by c_2, where $c_2 = 2.6 + 0.1\zeta$ is empirically obtained to make Equation (4.46) an accurate approximation to the *exact* performance of square QAM in Ricean fading channels given by

$$\begin{aligned} P_b = \int_0^\infty \frac{4}{q}\left(1-\frac{1}{\sqrt{M}}\right)Q\left(\sqrt{\frac{3q\gamma_b}{M-1}}\right)\left[1-\left(1-\frac{1}{\sqrt{M}}\right)Q\left(\sqrt{\frac{3q\gamma_b}{M-1}}\right)\right] \\ \times\frac{\exp\left(-\left(\frac{\gamma_b}{\delta}+\zeta\right)\right)}{\delta} I_0\left(2\sqrt{\frac{\zeta\cdot\gamma_b}{\delta}}\right)d\gamma_b \end{aligned} \tag{4.47}$$

where $\delta = 2\sigma^2/{\sigma_0}^2 = \overline{\gamma_b}/(\zeta+1)$. Results obtained with Equations (4.46) and (4.47) for 16QAM performance in Ricean fading channels with $\zeta = 0$ and $\zeta = 10$ are compared in Figure 18. The approximate expression yields very accurate results for both Rayleigh and Ricean fading. The performance of 16QAM in Ricean fading channels with ζ as a parameter in the range of $0 \le \zeta \le 10$ is plotted in Figure 19. As expected, 16QAM performance is poorer than that of BPSK/QPSK and, as ζ increases, the performance approaches that obtained with no fading.

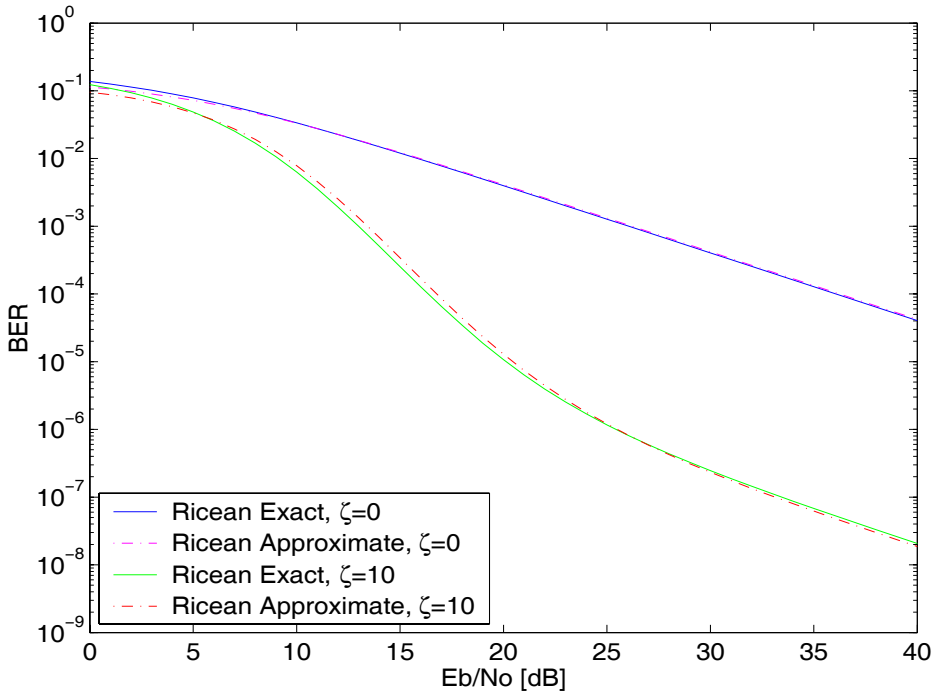

Figure 18. 16QAM performance in Ricean fading channels

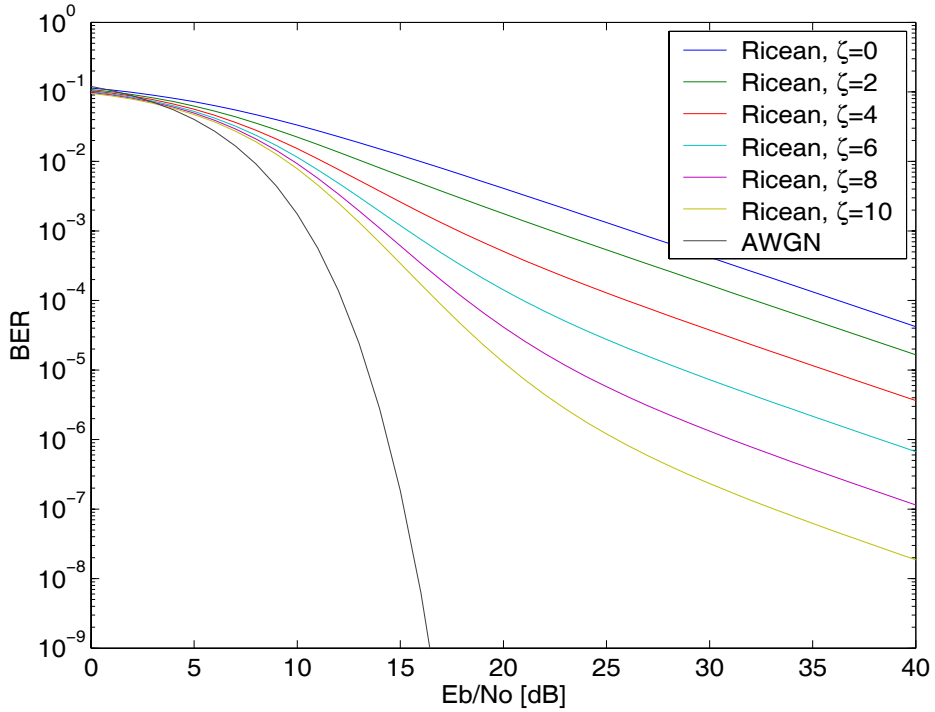

Figure 19. 16QAM performance in Ricean fading channels with $0 \le \zeta \le 10$

The performance obtained with Equations (4.46) and (4.47) for 64 QAM performances in Ricean fading channels with $\zeta = 0$ and $\zeta = 10$ is compared in Figure 20. As we can see, the approximate expression is still very accurate for $q = 6$ for both Rayleigh and Ricean fading channels.

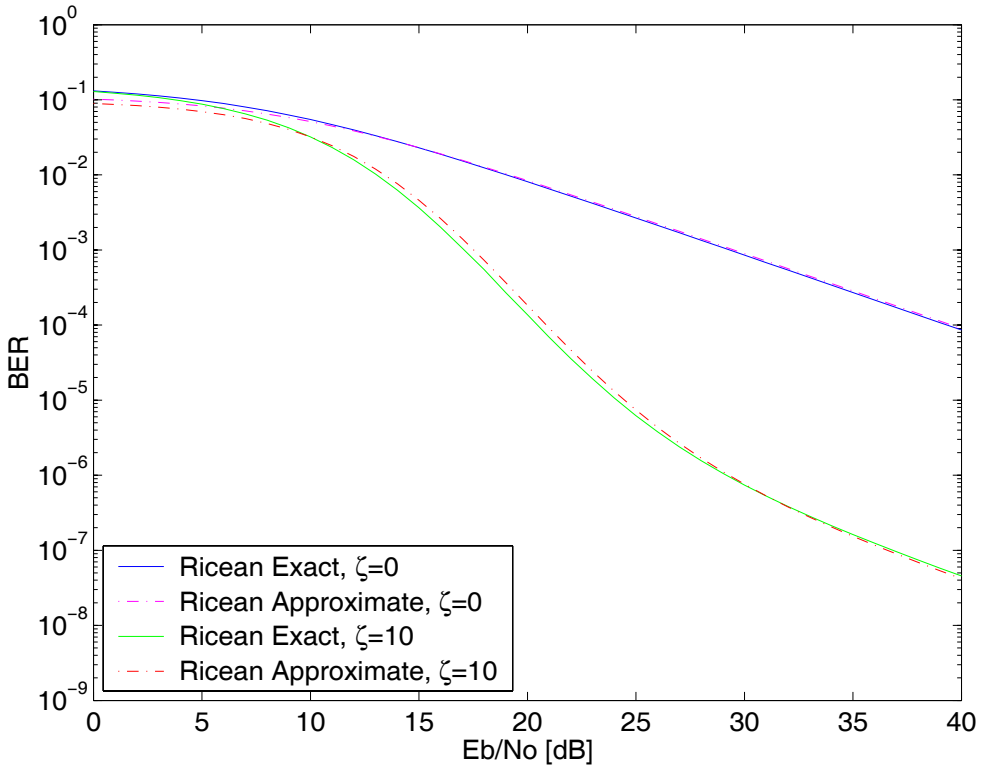

Figure 20. 64QAM performance in Ricean fading channels

The performance of 64QAM over Ricean fading channels with ζ as a parameter in the range of $0 \le \zeta \le 10$ is plotted in Figure 21. As expected, 64QAM has the poorest performance compared to BPSK/QPSK and 16QAM.

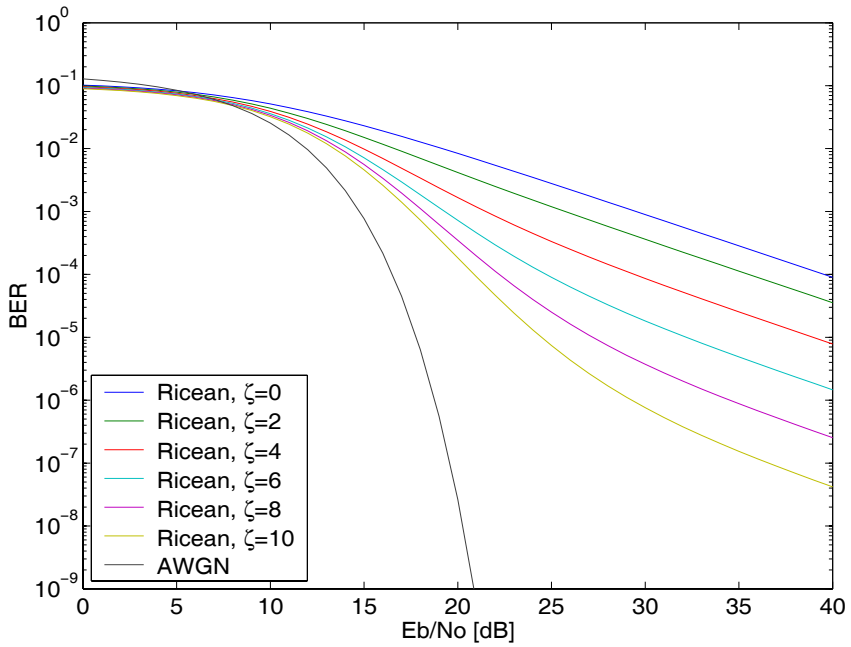

Figure 21. 64QAM performance in Ricean fading channels with $0 \le \zeta \le 10$

C. UNCODED OFDM SYSTEM PERFORMANCE

After confirming the analytic expressions for BPSK/QPSK, 16QAM, and 64QAM performance in Rayleigh and Ricean fading channels, we are ready to analyze OFDM system performance without FEC coding for the *IEEE 802.11a* standard. However, there are several issues needed to be discussed first.

First, with the *IEEE 802.11a* standard, one OFDM symbol utilizes 48 sub-carriers for data transmission, and each sub-carrier is separated by 0.3125 MHz. Ideally, if the channel coherence bandwidth is less than or equal to the sub-carrier spacing Δf_{sc}, then each sub-carrier will encounter independent fading. In this case, it is reasonable to assume that each OFDM symbol has 48 independent sub-carriers; however, this condition may not be true for all applications. Referring to Equation (2.4), if B_c is defined as the bandwidth over which the frequency correlation function is greater than 0.9, then $B_c \approx 1/50\sigma_\tau$, where σ_τ is the rms delay spread. According to [9], the reported values of σ_τ range from 30 to 120 ns for small to large office buildings. Using this range of σ_τ in

Equation (2.4), we obtain a range of values for coherence bandwidth as $0.667 \geq B_c \geq 0.167$ MHz. Note that the lower range of B_c is less than Δf_{sc}, while the upper range of B_c is approximately equivalent to $2 \cdot \Delta f_{sc}$; that is, we can assume 48 independent sub-carriers for large office buildings where $\Delta f_{sc} \geq B_c$, and 24 independent sub-carriers for small office buildings where $\Delta f_{sc} < B_c \leq 2\Delta f_{sc}$. In this thesis, both cases will be considered.

Second, we must consider that the *IEEE 802.11a* is standardized for 5-GHz band wireless LAN indoor transmission. Therefore, we model the environment as an office building, where a limited number of end-users link to LAN through the access point from different corners in the office (that is, some users may have LOS transmission, while others do not). Hence, we assume that ζ can be modeled as a uniformly distributed random variable. Moreover, the range for ζ must be carefully considered. In this thesis, we assume the reasonable range of ζ is $0 \leq \zeta \leq 10$. As discussed earlier, $\zeta = \alpha^2 / 2\sigma^2$ is the ratio of direct-to-diffuse signal power, where $\zeta = 0$ is Rayleigh fading, and $\zeta \to \infty$ is no fading. Thus, we should not choose ζ too large. Note that $\zeta = 10$ implies that the LOS path has 10 dB more signal power than the non-LOS paths. Therefore, the assumption for $0 \leq \zeta \leq 10$ seems reasonable for any regular office building, which in general will have a combination of LOS and non-LOS paths.

Lastly, this thesis uses the following approach to analyze OFDM performance: we first evaluate each sub-carrier's performance using Equation (4.34) or Equation (4.46), 48 times for the 48 independent sub-carrier case and 24 times for the 24 independent sub-carrier case. Since ζ is assumed to be uniformly distributed, its value will generally be different each time. We then average each independent sub-carrier's performance to obtain the overall OFDM system performance.

We now investigate the performance of the *IEEE 802.11a* standard without FEC coding according to the preceding assumptions. Note that the preceding assumptions will also be applied in next chapter, where the performance of the *IEEE 802.11a* standard with FEC coding is investigated.

1. BPSK/QPSK Modulated OFDM

As discussed above, to investigate BPSK/QPSK modulated OFDM performance over composite Rayleigh/Ricean fading channels, we need to evaluate Equation (4.34) either 48 or 24 times. We then average all sub-carrier's performance results to obtain the overall OFDM system performance. Note that for pure Rayleigh fading channels, there is no difference in performance between 48 and 24 independent sub-carriers since $\zeta = 0$ is constant for all sub-carriers. BPSK/QPSK modulated OFDM performance for both 48 and 24 independent sub-carriers cases over composite Rayleigh/Ricean fading channels where ζ is assumed to be a uniform random variable over the range $0 \le \zeta \le 10$ is plotted in Figure 22 for one trial.

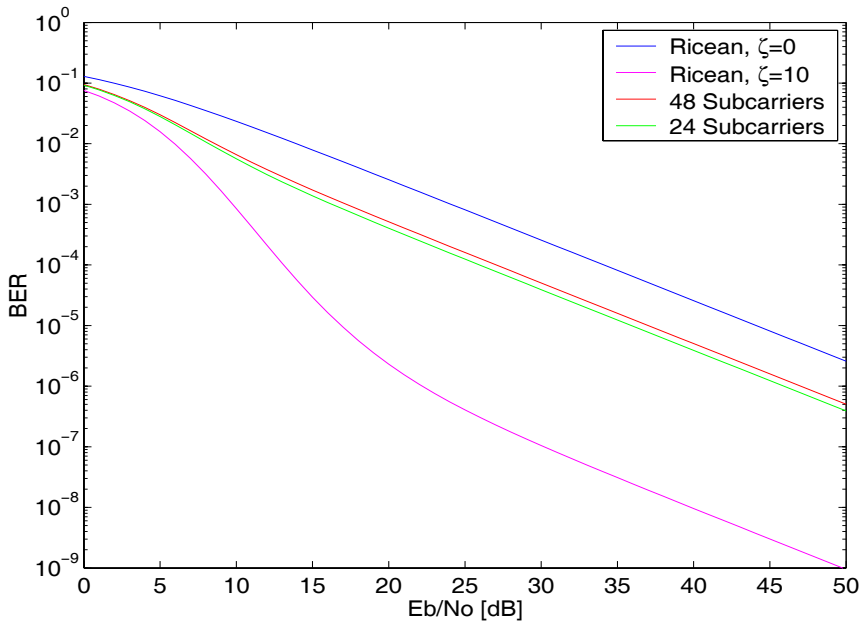

Figure 22. BPSK/QPSK modulated OFDM in composite Rayleigh/Ricean fading channels

As we can see, there is a slight performance difference between 48 and 24 independent sub-carriers at $P_b = 10^{-5}$. Actually, this difference is randomly distributed because ζ is modeled as a random variable. Therefore, an average probability of bit error is obtained by evaluating the BPSK/QPSK modulated OFDM performance for ten trials for both 48 and 24 independent sub-carriers. The minimum, maximum, and mean values

for the $\overline{\gamma_b}$ required for $P_b = 10^{-5}$ obtained with ten trials for the BPSK/QPSK modulated OFDM performance is shown in Table 3. As we can see, the difference in the mean value of $\overline{\gamma_b}$ between 48 and 24 independent sub-carrier's performance is 1.8 dB. In other words, BPSK/QPSK modulated OFDM with 24 sub-carriers has slightly better performance given the assumptions that have been made.

Uncoded BPSK/QPSK	48 sub-carriers [dB]	24 sub-carriers [dB]	Difference [dB]
Minimum	35.8	30	5.8
Maximum	38.8	37.2	1.6
Mean	37.5	35.7	1.8

Table 3. Uncoded BPSK/QPSK modulated OFDM performance statistics for $\overline{\gamma_b}$ at $P_b = 10^{-5}$

2. 16QAM and 64QAM Modulated OFDM

To investigate 16QAM and 64QAM modulated OFDM performance, we basically follow the same approach as for BPSK/QPSK. 16QAM and 64QAM modulated OFDM performance over composite Rayleigh/Ricean fading channels modeled as in the previous subsection are plotted in Figure 23 and 24, respectively. The curves are similar to those obtained for BPSK/QPSK but, as expected, with poorer performance.

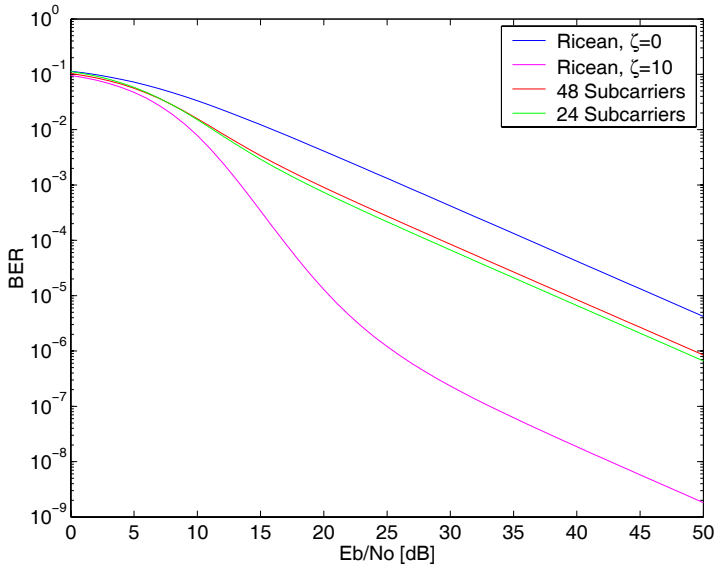

Figure 23. 16QAM modulated OFDM in composite Rayleigh/Ricean fading channels

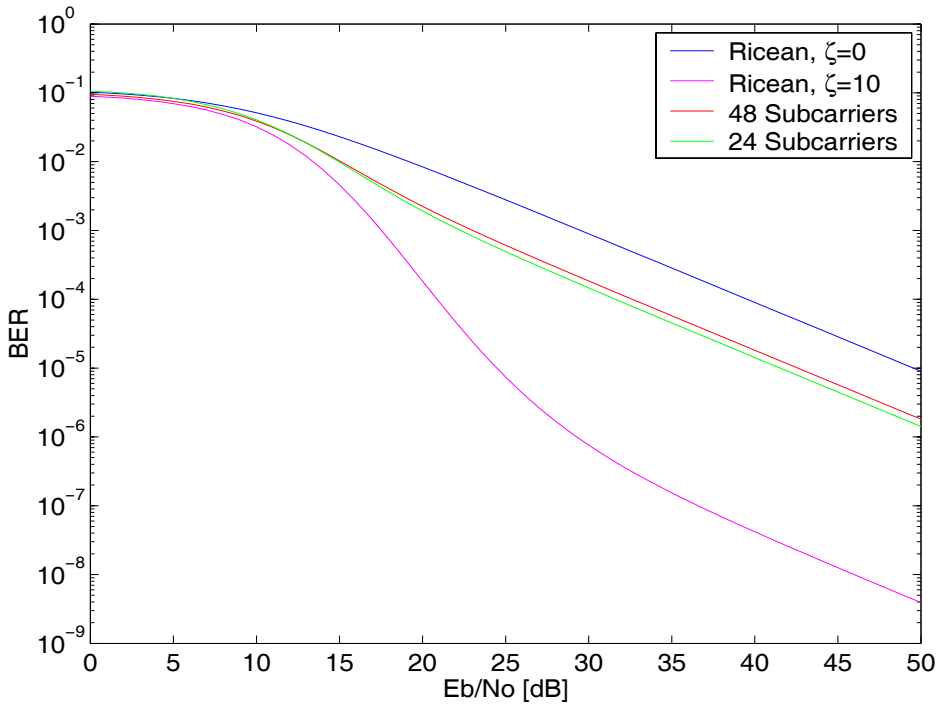

Figure 24. 64QAM modulated OFDM in composite Rayleigh/Ricean fading channels

The minimum, maximum and mean value for the $\overline{\gamma_b}$ required for $P_b = 10^{-5}$ obtained with ten trials for 16QAM and 64QAM modulated OFDM are listed in Table 4 and 5, respectively. As we can see, the difference in the mean value of $\overline{\gamma_b}$ between 48 and 24 independent sub-carrier's performance is 1.7 dB for 16QAM, and 1.6 dB for 64 QAM, almost the same as for BPSK/QPSK. However, performance degrades from BPSK/QPSK to 16QAM to 64QAM. Note that without FEC coding, performance is not acceptable regardless of modulation or the number of independent sub-carriers. The preceding results are summarized in Table 6.

Uncoded 16QAM	48 sub-carriers [dB]	24 sub-carriers [dB]	Difference [dB]
Minimum	38.1	32.4	5.7
Maximum	41	39.4	1.6
Mean	39.7	38	1.7

Table 4. Uncoded 16QAM modulated OFDM performance statistics

Uncoded 64QAM	48 sub-carriers [dB]	24 sub-carriers [dB]	Difference [dB]
Minimum	41.3	35.6	5.7
Maximum	44.2	43	1.2
Mean	42.9	41.3	1.6

Table 5. Uncoded 64QAM modulated OFDM performance statistics

Uncoded OFDM System Performance	BPSK/QPSK [dB]		16QAM [dB]		64QAM [dB]	
	48 Subc	24 Subc	48 Subc	24 Subc	48 Subc	24 Subc
Minimum	35.8	30.0	38.1	32.4	41.3	35.6
Maximum	38.8	37.2	41.0	39.4	44.2	43.0
Mean	37.5	35.7	39.7	38.0	42.9	41.3

Table 6. Overall uncoded OFDM system performance statistics

D. SUMMARY OF UNCODED OFDM PERFORMANCE

In this chapter, we derived analytic expressions, which accurately evaluate uncoded OFDM performance for either pure Rayleigh fading or for composite Rayleigh/Ricean fading channels. We also examined the assumption that we have 48 independent sub-carriers for large office buildings when $\Delta f_{sc} \geq B_c$ and 24 independent sub-carriers for small office buildings when $\Delta f_{sc} \leq B_c \leq 2\Delta f_{sc}$. Then we evaluated uncoded OFDM performance for both pure Rayleigh fading and composite Rayleigh/-Ricean fading channels. According to the results obtained, uncoded OFDM performance of composite Rayleigh/Ricean fading channels is dominated by the smaller values of ζ, which corresponds to more severe fading conditions. As expected, the performance of uncoded BPSK/QPSK modulated OFDM is better than uncoded 16QAM and 64QAM; however, even BPSK/QPSK does not yield performance acceptable for wireless communications.

THIS PAGE INTENTIONALLY LEFT BLANK

V. PERFORMANCE ANALYSIS WITH FEC CODING

As was shown in Table 6, the performance of OFDM without FEC coding over a composite Rayleigh/Ricean fading channels is not acceptable for any sub-carrier modulation specified in *IEEE 802.11a* PHY. In this chapter, we investigate the performance of *IEEE 802.11a* with FEC coding both in a pure Rayleigh fading ($\zeta = 0$) and in a composite Rayleigh/Ricean fading ($0 \le \zeta \le 10$) channel. Before the analysis, we discuss the concept of error control coding (especially FEC coding), the implementation of FEC coding, and the definition of coding gain in Section A. We then analyze *IEEE 802.11a* performance with FEC coding in Section B, where Viterbi hard decision decoding (HDD) will be implemented with BPSK/QPSK, 16QAM, and 64QAM, respectively. In Section C, we examine the performance of *IEEE 802.11a* with Viterbi soft decision decoding (SDD), but only for BPSK/QPSK due to the difficulty of analyzing the probability of bit error for SDD of a binary code transmitted with non-binary modulation.

A. ERROR CONTROL CODING

For any communication system, performance can be improved significantly by implementing error control coding. Generally, there are two error control strategies, automatic repeat request (ARQ) and forward error correcting (FEC) coding. In an ARQ system, the receiver checks for errors but does not correct them; it simply requests that the transmitter resend the data. Unlike an ARQ system, a FEC coding system does correct the data errors at the receiver. In this thesis, we do not consider ARQ systems since *IEEE 802.11a* PHY utilizes FEC coding as shown in Figure 9.

1. Forward Error Correcting (FEC) Coding

The basic idea of FEC coding is the addition of *redundancy*. This involves adding a certain number of redundant bits to the actual data bits in a particular pattern such that recovery of the actual data bits is enhanced. There are two fundamental types of FEC codes, block codes and convolutional codes. Block codes take a block of k data bits and

encode them into a codeword of length n, where $n > k$; thus, there are $n-k$ *parity bits* in the codeword, which are used to check the codeword for errors upon decoding. If there are errors, the decoder will detect and correct them. Unlike block codes, which operate in relatively large data blocks, convolutional codes operate on serial data and are generated by passing the information bit sequence through a linear finite-state shift register. There are a variety of block codes and convolutional codes. In this thesis, we do not consider block codes since *IEEE 802.11a* PHY employs convolutional codes and a convolutional encoder as shown in Figure 8. Therefore, the terms FEC coding and convolutional coding are used interchangeably in this chapter. Later, we will discuss the general concepts of convolutional coding: convolutional encoding and Viterbi decoding, but not the Viterbi algorithm. If readers are interested in the decoding algorithm, more information can be found in [7, 13, 17, 18, and 19].

a. Convolutional Encoding

Convolutional encoding is a technique to add redundancy to the data systematically. The information bits are input into shift registers and the output-encoded bits are obtained by modulo-2 addition of the input information bits and the contents of the shift registers. A general convolutional encoder can be implemented with s shift registers and m modulo-2 adders. For example, as shown in Figure 8, the *IEEE 802.11a* PHY convolutional encoder has six registers and two modulo-2 adders. The constraint length is $\nu = 7$. Note that the definition of constraint length ν is not standardized in the literature. In [17] the constraint length ν is defined as the length of the shift register, while in [18] it is defined as the length of the shift register plus one. The latter is the definition used here. Generally, a convolutional code is defined by two parameters, r and ν, where $r = k/n$ is the code rate, k is the number of information bits and n is the number of output coded bits per clock cycle, and ν is the constraint length. The typical range of values for r and ν are

$$\frac{1}{4} \le r \le \frac{7}{8} \tag{5.1}$$

and

$$2 \le \nu \le 9 \,. \tag{5.2}$$

Note that when r decreases or ν increases, the convolutional code achieves higher coding gain.

b. Viterbi Decoding

In modern, digital communication systems, convolutional encoding and Viterbi decoding have been the dominate FEC coding technique for years since Viterbi decoding algorithm is a computationally efficient and easily realizable algorithm used for the optimum decoding of convolutional codes. The Viterbi decoding algorithm utilizes the code trellis to compute the path metrics. Each state (node) in the trellis diagram is assigned a value and this value is determined from state $S = 0$ at time $t = 0$ to a particular state K at $t \ge 0$. At each state, the *best* value is chosen from the paths terminated at that state. The *best* value may be either the smallest or the largest, depending on hard or soft decision decoding and the metric chosen. The selected metric represents the survivor path and the remaining metrics represent the non-survivor paths. The survivor paths are stored, while the non-survivor paths are discarded. The Viterbi algorithm selects the single survivor path left at the end of the process as the maximum-likelihood (ML) path. Track-back of the ML path on the trellis then provides the ML decoded sequence.

As just mentioned, there are two possible ways in which to generate the branch metric for a Viterbi decoder, hard decision and soft decision. For hard decision decoding (HDD), the decoder receives a binary 0 or 1 from the demodulator output and decodes convolutional codes by using the Hamming distance as the metric. Hamming distance is obtained by choosing a path through the trellis diagram which yields a codeword that differs from the received codeword in the fewest possible places. For soft decision decoding (SDD), the decoder receives analogs outputs from the demodulator. Furthermore, the Viterbi decoding can be separated as HDD or SDD by the levels of quantization used on the received bits. A 2-level quantization corresponds to HDD, while an infinite-level quantization corresponds to the true SDD. In practice, it has been found that an 8-level quantization is almost as good as an infinite-level quantization.

2. Implementation of FEC Coding

As discussed in the section on convolutional encoding, for every k information bits input to the encoder, there will be n output coded bits where $n > k$. However, since the transmission time is the same whether coded or uncoded bits are transmitted,

$$kT_b = nT_{b_C} \tag{5.3}$$

where T_b is the actual data bit duration, T_{b_C} is the coded bit duration, and the coded bit rate is $R_{b_C} = 1/T_{b_C}$. Therefore, Equation (5.2) can be rewritten as

$$R_{b_C} = \frac{n}{k} R_b = \frac{R_b}{r} \tag{5.4}$$

where $r = k/n$ is the code rate, and $r < 1$ since $n > k$. In other words, $R_{b_C} > R_b$, which is equivalent to saying that the trade-off of using FEC coding is a sacrifice in bandwidth. In addition to the transmission time, the average transmitted power is also the same whether coded or uncoded bits are transmitted; that is,

$$P = E_b R_b = E_{b_C} R_{b_C} \tag{5.5}$$

where E_b is the average energy of actual data bit, and E_{b_C} is the average energy of coded data bit. Note that Equation (5.5) is derived from [7],

$$\frac{E_b}{N_0} = \frac{PT_b}{N_0} = \frac{P}{N_0 R_b} \tag{5.6}$$

where P is the average signal power. Thus, Equation (5.5) can be rewritten as

$$E_{b_C} = rE_b \tag{5.7}$$

since $r = R_b/R_{b_C}$, which is derived from Equation (5.4). Therefore, with Equations (5.3), (5.4), and (5.7), we can obtain the relationship between the coded and uncoded system in terms of T_b, R_b, or E_b.

3. Coding Gain

The coding gain is defined as [7]

$$G(\text{dB}) = \left(\frac{E_b}{N_0}\right)_{uncoded}(\text{dB}) - \left(\frac{E_b}{N_0}\right)_{coded}(\text{dB}) \tag{5.8}$$

Coding gain is a function of both the type of modulation and the type of FEC coding. In other words, the value of G varies with different types of modulation and/or FEC coding. For example, Figure 25 shows the coding gain of BPSK/QPSK with Viterbi HDD at a code rate $r = 1/2$ in AWGN. As we can see the coding gain is about 3 dB. Later, we will show more examples of coding gain obtained when investigating different combinations of modulation type and code rate specified in *IEEE 802.11a* PHY.

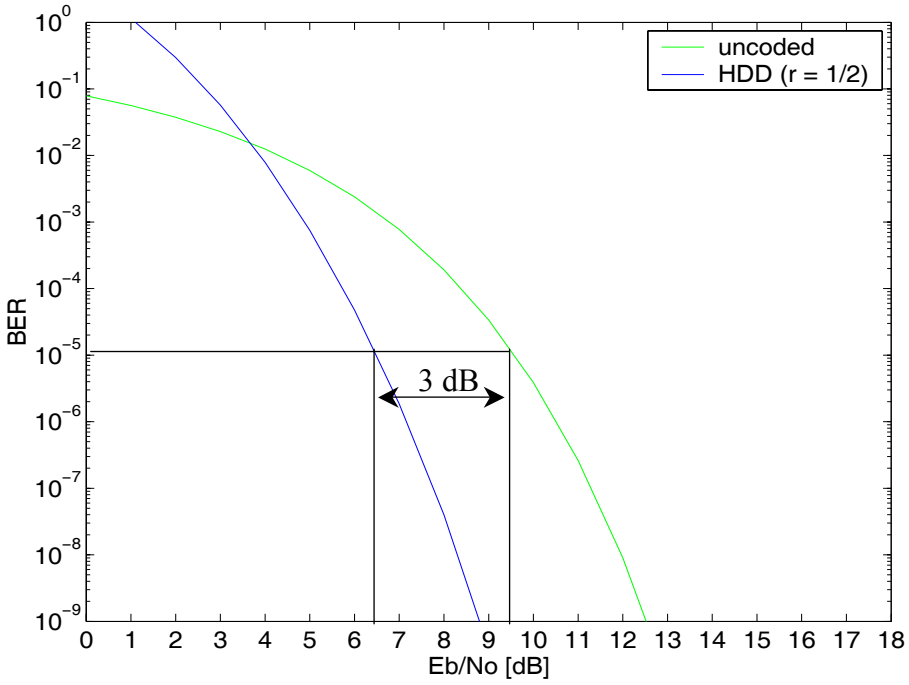

Figure 25. Coding gain of BPSK/QPSK in AWGN

B. HARD DECISION DECODING

As just discussed, for HDD the metrics in the Viterbi algorithm are the Hamming distances between the received sequence and the surviving sequences at each node of the

trellis. In this subsection, we first discuss the analytical approach by investigating the performance of BPSK/QPSK with HDD, and then examine the performance of the rest of modulations utilized in the *IEEE 802.11a* standard with HDD over Ricean fading channels.

1. BPSK/QPSK with HDD (6,9,12, and 18 Mbps)

In this section, we investigate the performance for BPSK/QPSK with HDD and a code rate $r = 1/2$ or $r = 3/4$. From Table 2, with code rate $r = 1/2$, BPSK/QPSK can support data rates of 6 and 12 Mbps, respectively. With code rate $r = 3/4$, BPSK/QPSK can support data rates of 9 and 18 Mbps, respectively.

When a rate $r = k/n$ convolutional code is employed, the probability of bit error is upper bound by [13]

$$P_b < \frac{1}{k} \sum_{d=d_{free}}^{\infty} B_d P_d \tag{5.9}$$

where d_{free} is the *free distance* of the convolutional code, B_d is the total number of information bit ones on all weight d paths, P_d is the probability of selecting a weight d output sequence as the transmitted code sequence, and k is the number of information bits per clock cycle. The quantities B_d and d_{free} are parameters of the convolutional code and P_d is determined by the type of modulation, the channel, and whether hard or soft decision decoding is used.

For a given constraint length and code rate, the values of B_d can be found in [17]. The values of B_d for the constraint length $\nu = 7$ and different code rate r specified in the *IEEE 802.11a* PHY are listed in Table 7.

Rate	d_{free}	$B_{d_{free}}$	$B_{d_{free}+1}$	$B_{d_{free}+2}$	$B_{d_{free}+3}$	$B_{d_{free}+4}$
1/2	10	36	0	211	0	1404
2/3	6	1	81	402	1487	6793
3/4	5	21	252	1903	11995	72115

Table 7. Weight Structure of the Convolutional Codes [After Ref. 17]

Note that in Table 7, the weight structures are only listed from $B_{d_{free}}$ to $B_{d_{free+4}}$, because it is generally accepted that the first five terms in Equation (5.9) dominate; therefore, Equation (5.9) can be rewritten as

$$P_b < \frac{1}{k} \sum_{d=d_{free}}^{d_{free+4}} B_d P_d \ . \tag{5.10}$$

Also note that Equation (5.10) is valid for both HDD and SDD; however, P_d is different for HDD and SDD. For HDD, the algorithm uses Hamming distance as the metric. Assume that the all-zero path is transmitted. When d is odd, the all-zero path will be correctly selected if the number of errors in the received sequence is less than $(d+1)/2$; otherwise, the incorrect path will be selected. Consequently, the probability of selecting the incorrect path when d is odd is [13]

$$P_d = \sum_{i=\frac{d+1}{2}}^{d} \binom{d}{i} p^i (1-p)^{d-i} \tag{5.11}$$

where p is the probability of channel bit error. When d is even, the incorrect path is selected when the number of errors exceeds $d/2$ and, if the number of errors equals $d/2$, there is a tie between the metrics in the two paths, which may be resolved by randomly selecting one of the paths; thus, the incorrect path is chosen half the time. Consequently, the probability of selecting the incorrect path when d is even is [13]

$$P_d = \sum_{i=\frac{d+1}{2}}^{d} \binom{d}{i} p^i (1-p)^{d-i} + \frac{1}{2} \binom{d}{d/2} p^{d/2} (1-p)^{d/2} \ . \tag{5.12}$$

Now with Equation (5.10) through (5.12) and Equation (5.7), we are ready to investigate the performance of BPSK/QPSK with HDD over AWGN and Ricean fading channels. Recall that the probability of bit error for uncoded BPSK/QPSK in AWGN is given by Equation (4.1). From Equation (5.7), Equation (4.1) can be rewritten as

$$P_b = Q\left(\sqrt{2r\overline{\gamma_b}}\right) \tag{5.13}$$

where $\overline{\gamma_b} = \overline{E_b}/N_0$ is the ratio of received average energy per bit-to-noise power spectral density (which is the same as we defined in Chapter IV) and r is the code rate. Since the *IEEE 802.11a* standard utilizes OFDM, Equation (5.13) is also the probability of channel bit error for the i^{th} sub-channel for BPSK/QPSK in AWGN, rewritten as

$$p_i = Q\left(\sqrt{2r\overline{\gamma_{b_i}}}\right) \tag{5.14}$$

where $\overline{\gamma_{b_i}}$ the ratio of received average energy per bit-to-noise power spectral density on the i^{th} sub-channel. Therefore, the overall p is the average of the probability of bit error on each of the N OFDM sub-channels:

$$p = \frac{1}{N}\sum_{i=1}^{N} p_i \tag{5.15}$$

where N is assumed to be either 48 or 24 independent sub-carriers in this thesis. Note that for no channel fading (i.e., $\overline{\gamma_{b_i}} = \overline{\gamma_b}$), then $p_i = p$. Now, using Equation (5.14) in (5.11) or (5.12) and taking the result into Equation (5.10), we obtain the performance of BPSK/QPSK in AWGN with HDD, which was already shown in Figure 25. Note that comparing Equation (5.13) to Equation (4.1), the coded and uncoded system can be related as

$$\overline{\gamma_{b_c}} = r\,\overline{\gamma_b} \tag{5.16}$$

where r is the code rate. Similarly, using Equation (5.16) and Equation (4.34), we obtain the probability of channel bit error for the i^{th} sub-channel for BPSK/QPSK over Ricean fading channels as

$$p_i \approx \frac{1}{2\sqrt{\pi \cdot c_1}} \left(\frac{\zeta_i + 1}{r\,\overline{\gamma_{b_i}} + \zeta_i + 1} \right)^d \exp\left(\frac{-d\,\zeta_i\, r\,\overline{\gamma_{b_i}}}{r\,\overline{\gamma_{b_i}} + \zeta_i + 1} \right) \tag{5.17}$$

where $c_1 = 1.2 + 0.1\zeta$ is empirically obtained and $d = 1$ for HDD. Note that for either no channel fading or for all sub-channels experiencing the same fading (that is, $\zeta_i = \zeta$ and $\overline{\gamma_{b_i}} = \overline{\gamma_b}$ for all i), then $p_i = p$. Now, using Equation (5.17) in Equation (5.11) or (5.12) and taking the result into Equation (5.10), we obtain the performance of BPSK/QPSK with HDD over Ricean fading channels. In Figure 26, the performance of BPSK/QPSK with HDD ($r = 1/2$) over Ricean fading channels with ζ as a parameter in the range of $0 \le \zeta \le 10$ is plotted.

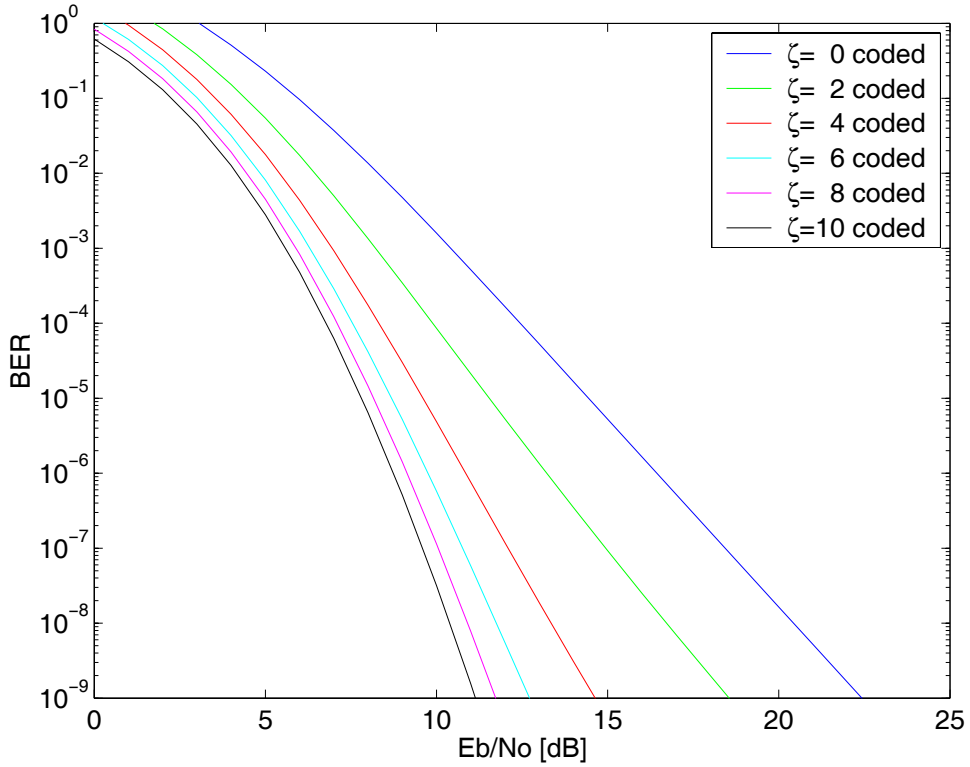

Figure 26. Performance of BPSK/QPSK with HDD ($r = 1/2$) over Ricean Fading

In order to gain some perspective on the performance improvement, in Figure 27 we compared Figure 26 with Figure 17, which is the performance of BPSK/QPSK without FEC coding. As we can see, the FEC coding provides remarkable performance improvement for Ricean fading channels.

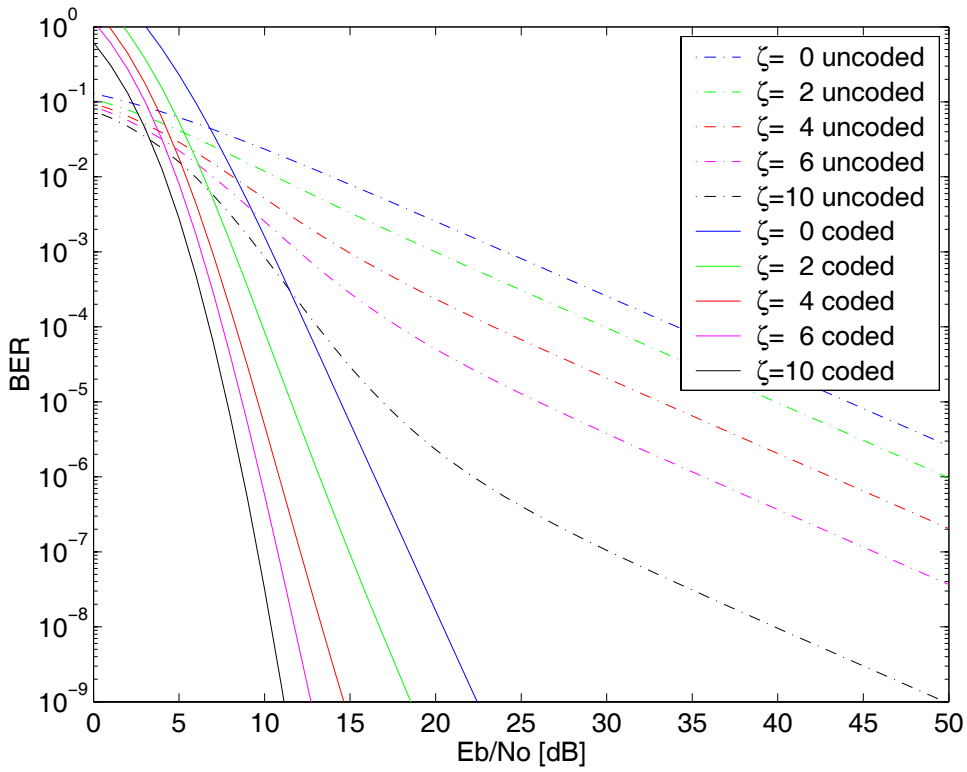

Figure 27. HDD ($r = 1/2$) versus uncoded BPSK/QPSK Performance over Ricean Fading

So far, we have only investigated the sub-carrier performance of BPSK/QPSK with HDD over Ricean fading channels. In order to examine the performance of BPSK/QPSK modulated OFDM with data rates at 6 and 12 Mbps over Ricean fading channels, we need to use Equation (5.15) with Equations (5.17), (5.11), (5.12), and (5.10) at code rate $r = 1/2$ and its corresponding weight structure shown in Table 7. Further, recall that in Chapter IV, we have shown Equation (4.34) is also valid for examining the performance of uncoded BPSK/QPSK over Rayleigh fading channels; hence, we can use Equation (5.17) to analyze the performance of BPSK/QPSK modulated OFDM over

Rayleigh fading channels. In this section we investigate the performance of BPSK/QPSK modulated OFDM both over a pure Rayleigh fading ($\zeta = 0$) channel and over a composite Rayleigh/Ricean fading ($0 \le \zeta \le 10$) channel.

As discussed in Chapter IV, for a pure Rayleigh fading channel, there is no difference in performance between 48 and 24 independent sub-carriers since $\zeta = 0$ is constant for all sub-carriers. Therefore, we do not compare the difference between 48 and 24 independent sub-carriers performances over a pure Rayleigh fading channel. In Figure 28, we compare HDD ($r = 1/2$) and uncoded BPSK/QPSK modulated OFDM performance over a pure Rayleigh fading channel. As we can see the coding gain is 30 dB and $\overline{\gamma_b}$ = 14.5 dB with HDD ($r = 1/2$) and BPSK/QPSK modulation at $P_b = 10^{-5}$.

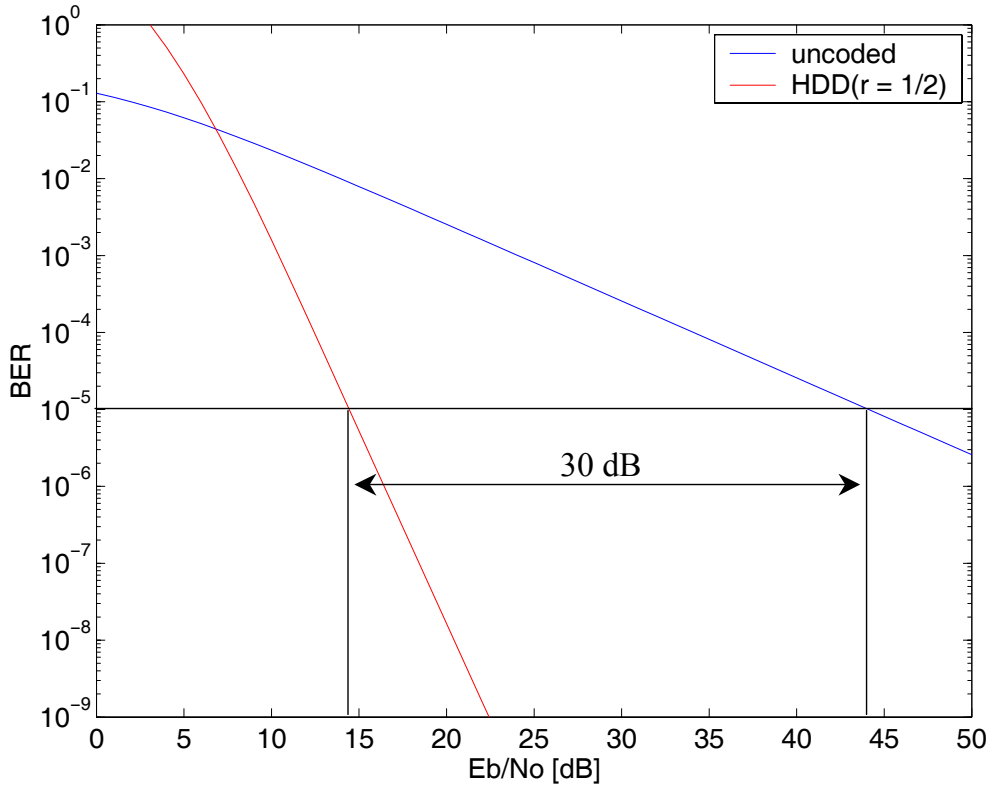

Figure 28. HDD ($r = 1/2$) versus uncoded BPSK/QPSK modulated OFDM (6 and 12 Mbps) performance over a pure Rayleigh fading channel

BPSK/QPSK modulated OFDM with HDD ($r = 1/2$) performance for both 48 and 24 independent sub-carriers cases over a composite Rayleigh/Ricean fading channel, where ζ is assumed to be a uniform random variable over the range $0 \le \zeta \le 10$, is plotted in Figure 29 for one trial.

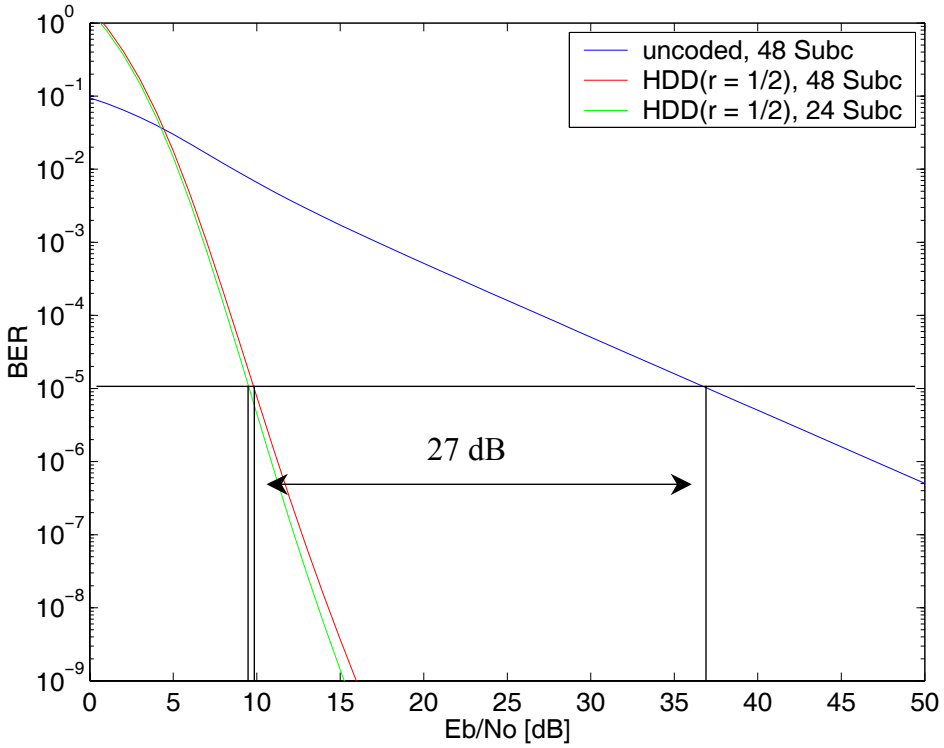

Figure 29. HDD ($r = 1/2$) versus uncoded BPSK/QPSK modulated OFDM (6 and 12 Mbps) performance over a composite Rayleigh/Ricean fading channel

As we can see, the coding gain is still remarkable, and values of $\overline{\gamma_b}$ are 9.9 and 9.3 dB for 48 and 24 independent sub-carriers at $P_b = 10^{-5}$, respectively. Actually, this difference is randomly distributed because ζ is modeled as a random variable. Therefore, as we did in Chapter IV, an average probability of bit error is obtained by evaluating the BPSK/QPSK modulated OFDM performance with HDD ($r = 1/2$) for ten trials for both 48 and 24 independent sub-carriers. The minimum, maximum, and mean value for the $\overline{\gamma_b}$ required for $P_b = 10^{-5}$ obtained with ten trials for BPSK/QPSK modulated OFDM with

HDD ($r = 1/2$) performance is shown in Table 8. As we can see, the difference in the mean value of E_b/N_0 between 48 and 24 independent sub-carrier's performance is 0.13 dB, which is much smaller than that of uncoded BPSK/QPSK modulated OFDM, which is 1.8 dB.

HDD (1/2) BPSK/QPSK	48 sub-carriers [dB]	24 sub-carriers [dB]	Difference [dB]
Minimum	9.6	9.4	0.2
Maximum	10.6	10.2	0.4
Mean	9.96	9.83	0.13

Table 8. HDD ($r = 1/2$) BPSK/QPSK modulated OFDM (6 and 12 Mbps) performance statistics for $\overline{\gamma_b}$ at $P_b = 10^{-5}$

Now, we perform the same analysis for code rate $r = 3/4$ to obtain the performance for 9-Mbps BPSK and 18-Mbps QPSK as specified in *IEEE 802.11a* WLAN standard. The results of this analysis for a single sub-carrier are given in Figure 30 for the usual range of ζ.

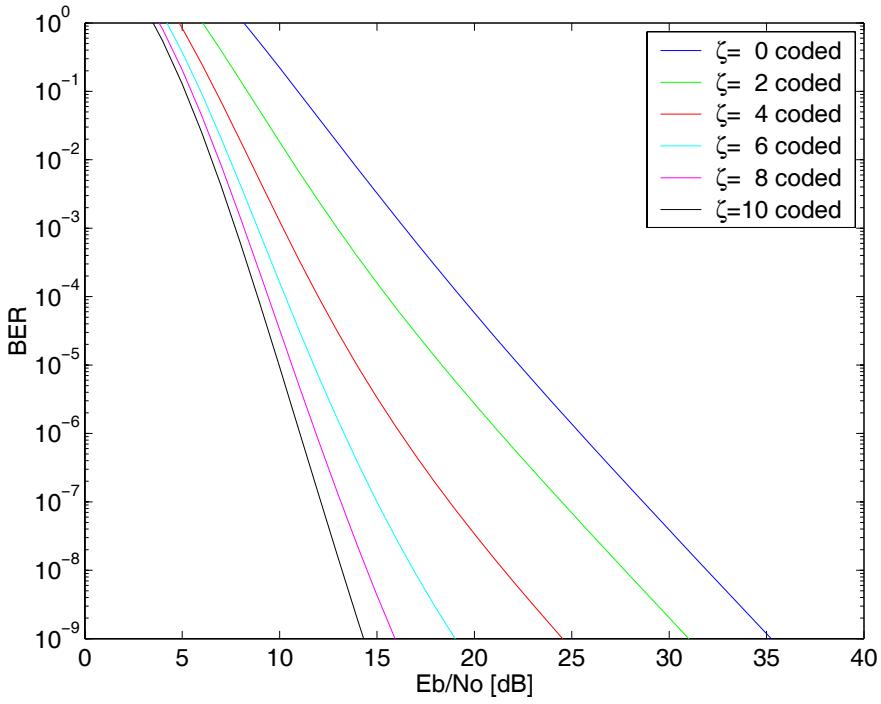

Figure 30. Performance of BPSK/QPSK with HDD ($r = 3/4$) over Ricean Fading

Comparing Figure 30 with Figure 26, we notice that the curves are shifted to the right even thought the modulation remains the same. This represents a slight degradation in performance as $r = 1/2$ is increased to $r = 3/4$. This result is as expected since the higher code rate corresponds to less redundancy added to the actual data bit stream. The advantage is higher achievable data rates for the same bandwidth. In Figure 31, we overlay the uncoded BPSK/QPSK performance onto those in Figure 30 to see the performance improvement of BPSK/QPSK when applying HDD with code rate $r = 3/4$ over Ricean fading channels.

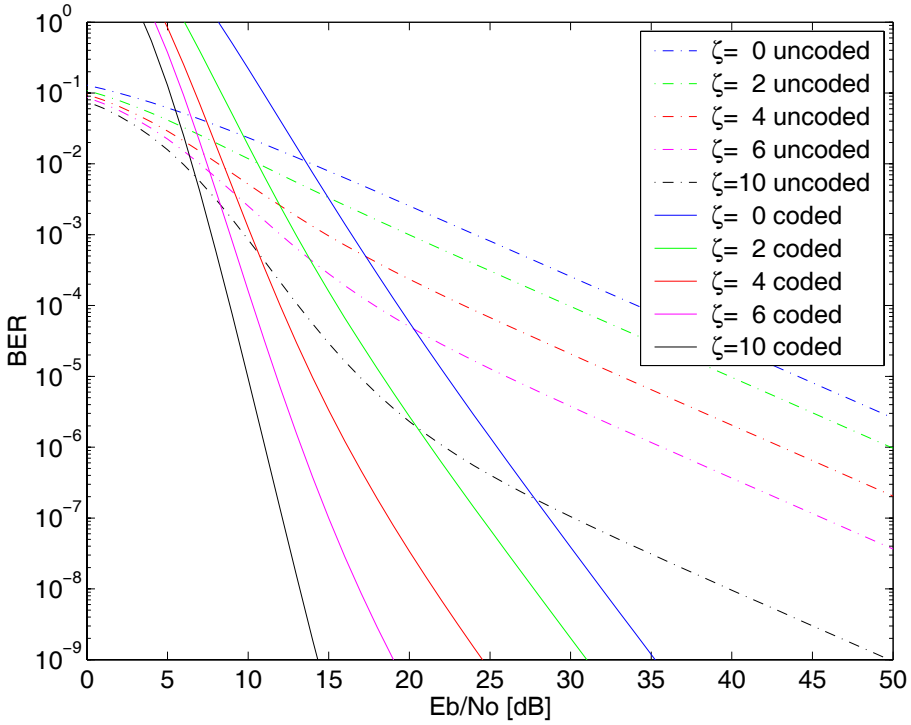

Figure 31. Uncoded versus HDD ($r = 3/4$) BPSK/QPSK Performance over Ricean Fading

As we did for $r = 1/2$, the HDD ($r = 3/4$) and uncoded BPSK/QPSK modulated OFDM performance over a pure Rayleigh Fading channel are plotted in Figure 32. As expected, the HDD ($r = 3/4$) BPSK/QPSK modulated OFDM performance curves are

shifted to the right if comparing with Figure 28. As we can see, coding gain is down to about 22 dB and $\overline{\gamma_b}$ is degrading to 22.3 dB at $P_b = 10^{-5}$.

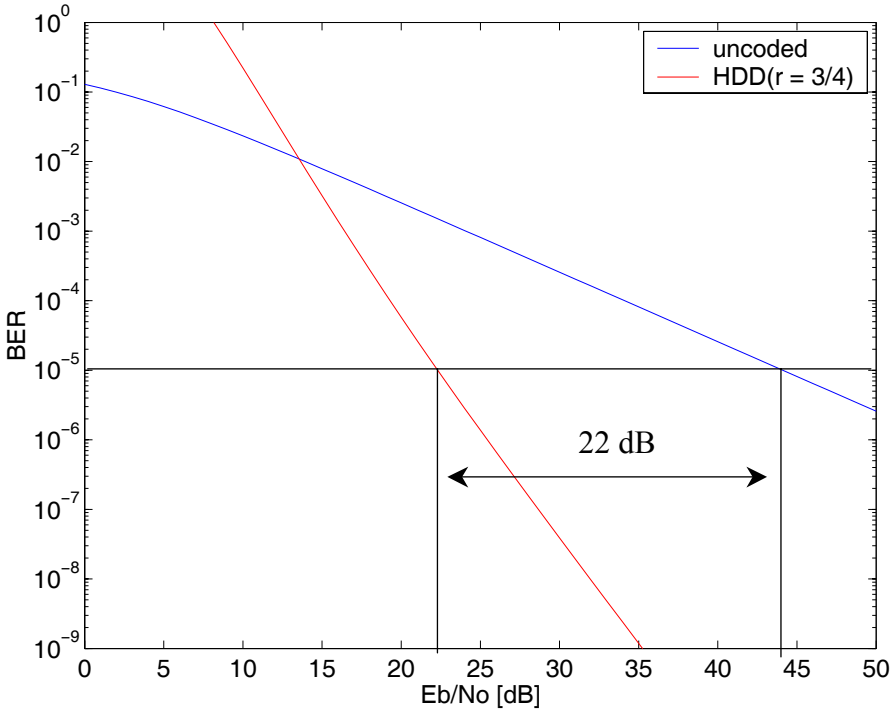

Figure 32. HDD ($r = 3/4$) versus uncoded BPSK/QPSK modulated OFDM (9 and 18 Mbps) performance over a pure Rayleigh fading channel

BPSK/QPSK modulated OFDM with HDD ($r = 3/4$) performance for both 48 and 24 independent sub-carriers cases over a composite Rayleigh/Ricean fading channel where ζ is assumed to be a uniform random variable over the range $0 \le \zeta \le 10$ is plotted in Figure 33 for one trial. As we can see, the coding gain is still remarkable and the values of $\overline{\gamma_b}$ are 15.9 and 14.9 dB for 48 and 24 independent sub-carriers, respectively, at $P_b = 10^{-5}$. Proceeding as before, we evaluate BPSK/QPSK modulated OFDM performance with HDD ($r = 3/4$) for ten trials for both 48 and 24 independent sub-carriers to obtain an average probability of bit error due to ζ is modeled as a random variable.

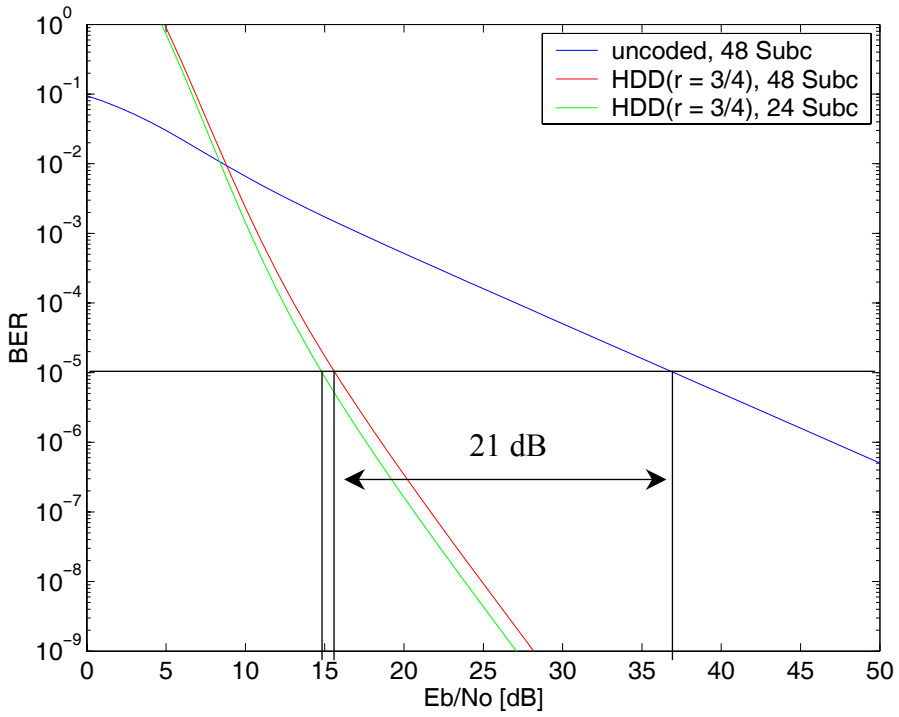

Figure 33. HDD ($r = 3/4$) versus uncoded BPSK/QPSK modulated OFDM (9 and 18 Mbps) performance over a composite Rayleigh/Ricean fading channel

The minimum, maximum, and mean value for $\overline{\gamma_b}$ required for $P_b = 10^{-5}$ obtained with ten trials for BPSK/QPSK modulated OFDM with HDD ($r = 3/4$) performance is shown in Table 9. As we can see, the difference in the mean value of $\overline{\gamma_b}$ between 48 and 24 independent sub-carriers is 0.24 dB. Here, again we see the overall performance of $r = 3/4$ code is poorer than that of $r = 1/2$ code.

HDD (3/4) BPSK/QPSK	48 sub-carriers [dB]	24 sub-carriers [dB]	Difference [dB]
Minimum	14	14.4	0.4
Maximum	16.6	17.5	0.9
Mean	15.57	15.81	0.24

Table 9. HDD ($r = 3/4$) BPSK/QPSK modulated OFDM (9 and 18 Mbps) performance statistics for $\overline{\gamma_b}$ at $P_b = 10^{-5}$

2. 16QAM with HDD (24 and 36 Mbps)

To achieve data rates of 24 and 36 Mbps for WLAN, the *IEEE 802.11a* standard utilizes 16QAM with convolutional coding at rates $r = 1/2$ and $r = 3/4$, respectively. Proceeding as for BPSK/QPSK, we first investigate the 16QAM sub-carrier performance, and then perform the analysis for 16QAM modulated OFDM both in a pure Rayleigh fading and a composite Rayleigh/Ricean fading channel. Recall from Chapter IV that uncoded square MQAM performance is inferior to that of uncoded BPSK and QPSK; therefore, we expect the performance of 16QAM with HDD will be poorer than that of BPSK/QPSK with HDD.

As is shown in Chapter IV, the probability of bit error for MQAM with a square constellation without FEC coding over Ricean fading channel is upper bounded by Equation (4.46). Analogous to the approach taken with BPSK/QPSK, using Equation (5.16) in Equation (4.46), we obtain the approximate channel bit error probability for the i^{th} sub-channel for MQAM with a square constellation as

$$p_i \approx \frac{4\left(1-\frac{1}{\sqrt{M}}\right)\cdot e^{-d\cdot\zeta_i\left[\frac{3qr\overline{\gamma_{b_i}}}{3qr\overline{\gamma_{b_i}}+2(M-1)(\zeta_i+1)}\right]}}{q\sqrt{2\pi c_2}\left[\frac{3qr\overline{\gamma_{b_i}}+2(M-1)(\zeta_i+1)}{2(M-1)(\zeta_i+1)}\right]^d} - \frac{2\left(1-\frac{1}{\sqrt{M}}\right)^2\cdot e^{-d\cdot\zeta_i\left[\frac{3qr\overline{\gamma_{b_i}}}{3qr\overline{\gamma_{b_i}}+(M-1)(\zeta_i+1)}\right]}}{\pi c_2 q\left[\frac{3qr\overline{\gamma_{b_i}}+(M-1)(\zeta_i+1)}{(M-1)(\zeta_i+1)}\right]^d} \tag{5.18}$$

where $c_2 = 2.6 + 0.1\zeta$ is empirically obtained, ζ_i is the ratio of direct-to-diffuse signal power on the i^{th} sub-channel, and $d = 1$ for HDD. Note that for either no channel fading or for all sub-channels experiencing the same fading, then $p_i = p$. Now, using Equation (5.18) with $q \geq 4$ in Equation (5.11) or (5.12) and taking the result into (5.10), we obtain the performance of square MQAM with HDD over Ricean fading channels.

In Figure 34, we plot the sub-channel performance of 16QAM ($q = 4$) with HDD ($r = 1/2$) over Ricean fading channels with ζ as a parameter in the range of $0 \le \zeta \le 10$. As expected, the performance of 16QAM is inferior to that of BPSK/QPSK as shown in Figure 26 for with the same code rate $r = 1/2$.

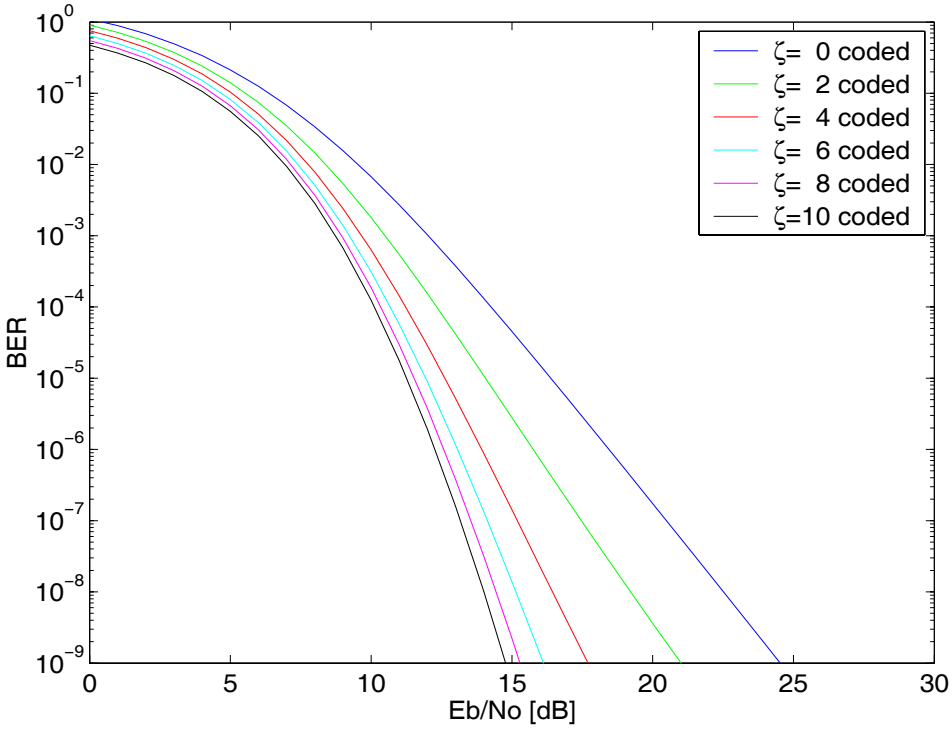

Figure 34. Performance of 16QAM with HDD ($r = 1/2$) over Ricean Fading

In order to gain some perspective on the performance improvement, in Figure 35 we compare Figure 34 with Figure 19, which is the performance of uncoded 16QAM over Ricean fading channels. As we can see, the FEC coding provides remarkable improvement over the uncoded performance.

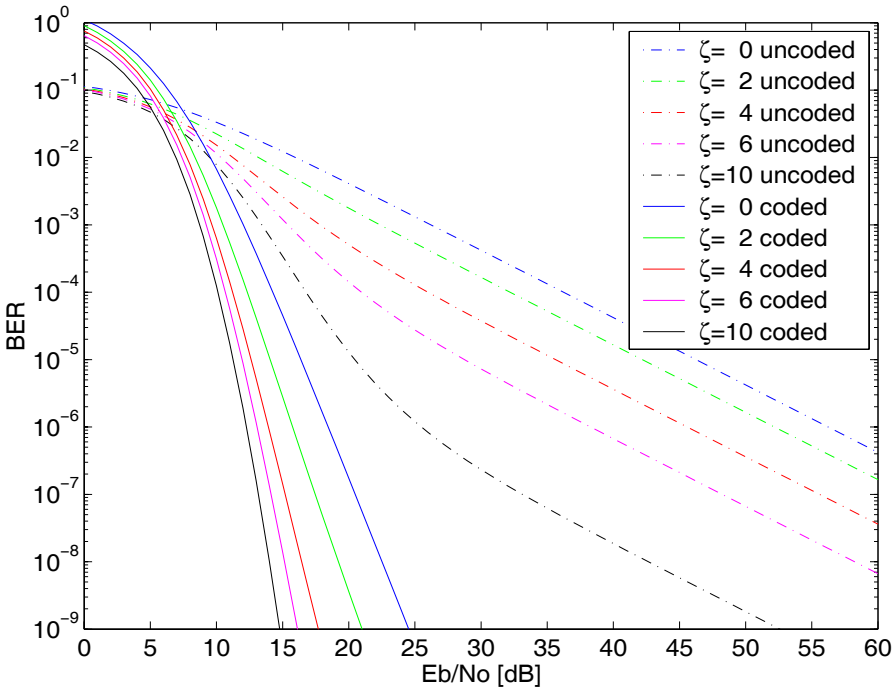

Figure 35. HDD ($r = 1/2$) versus uncoded 16QAM Performance over Ricean Fading

In order to examine the performance of 16QAM modulated OFDM with data rates at 24 Mbps over Ricean fading channels, we need to use Equation (5.15) in addition to Equations (5.18), (5.11), (5.12) in Equation (5.10) with code rate $r = 1/2$ and its corresponding weight structure shown in Table 7. Further, it is shown in Chapter IV that Equation (4.46) is also valid for the performance of uncoded 16QAM over Rayleigh fading channels. As a result, Equation (5.18) is also. In this section we investigate the performance of 16QAM modulated OFDM both over a pure Rayleigh fading ($\zeta = 0$) channel and over a composite Rayleigh/Ricean fading ($0 \le \zeta \le 10$) channel.

In Figure 36, we compare uncoded and HDD ($r = 1/2$) 16QAM modulated OFDM performance over a pure Rayleigh fading channel. As we can see, the coding gain is 30 dB and $\overline{\gamma_b}$ for HDD ($r = 1/2$) 16QAM modulated OFDM is 16.4 dB at $P_b = 10^{-5}$.

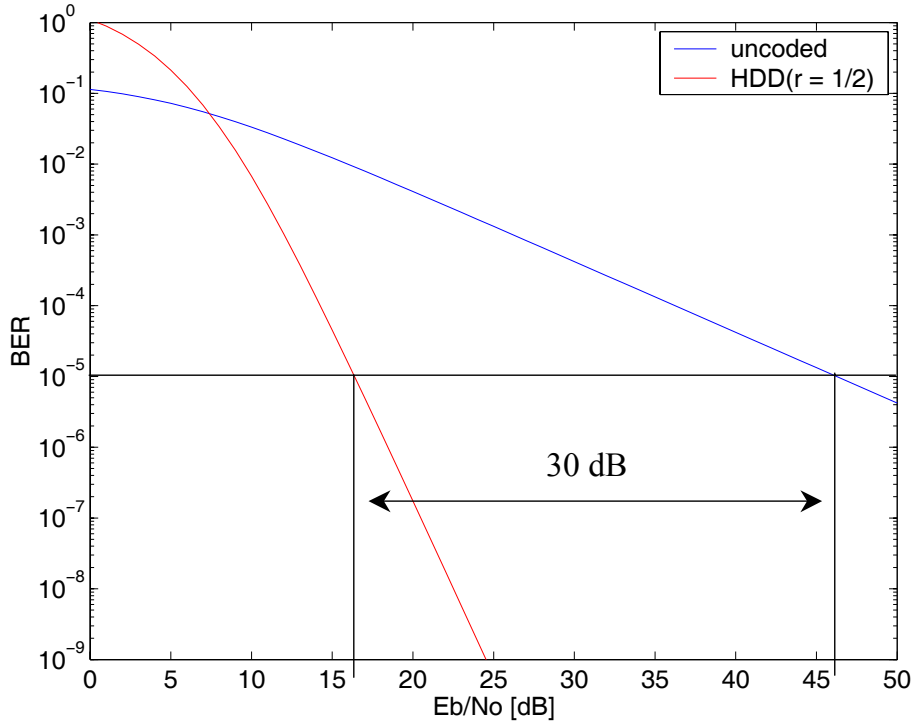

Figure 36. HDD ($r = 1/2$) versus uncoded 16QAM modulated OFDM (24 Mbps) performance over a pure Rayleigh fading channel

Performance for 16QAM modulated OFDM with HDD ($r = 1/2$) for both 48 and 24 independent sub-carriers over a composite Rayleigh/Ricean fading channel where ζ is assumed to be a uniform random variable over the range $0 \le \zeta \le 10$ is plotted in Figure 37 for one trial. As we can see, the coding gain is 27 dB, and $\overline{\gamma_b}$ for 48 and 24 independent sub-carriers at $P_b = 10^{-5}$ is 12.7 and 12.8 dB, respectively. Actually, this difference is randomly distributed because ζ is modeled as a random variable. Therefore, as we did before, an average probability of bit error is obtained by evaluating the 16QAM modulated OFDM performance with HDD ($r = 1/2$) for ten trials for both 48 and 24 independent sub-carriers.

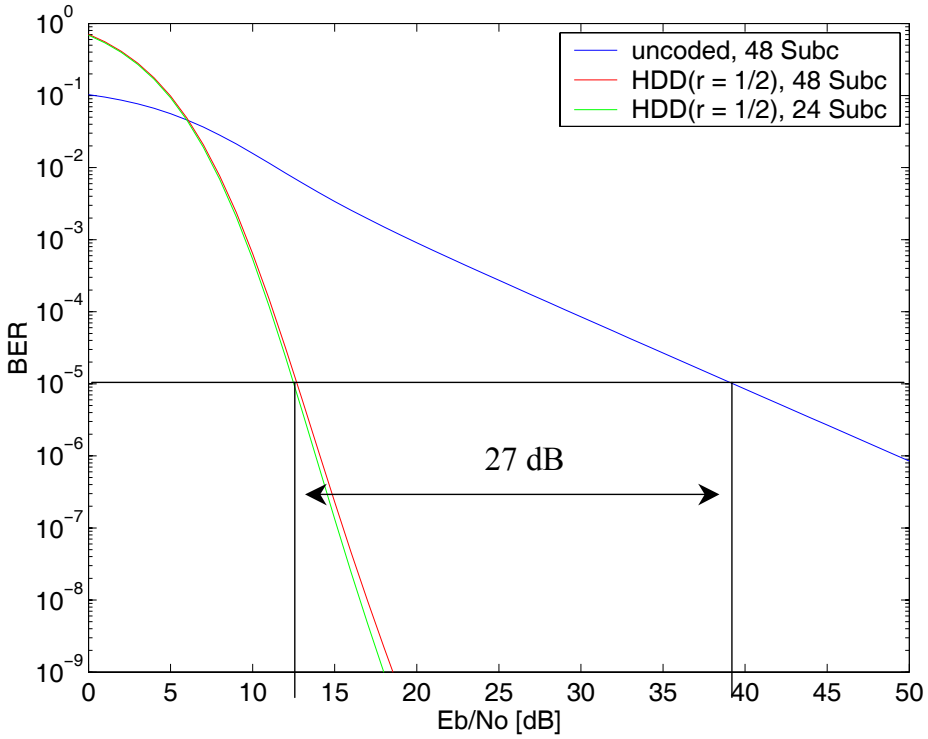

Figure 37. HDD ($r = 1/2$) versus uncoded 16QAM modulated OFDM (24 Mbps) performance over a composite Rayleigh/Ricean fading channel

The minimum, maximum, and mean value for the $\overline{\gamma_b}$ required for $P_b = 10^{-5}$ obtained with ten trials for the 16QAM modulated OFDM with HDD ($r = 1/2$) is shown in Table 10. As we can see, the mean value of $\overline{\gamma_b}$ for 48 and 24 independent sub-carriers is 12.68 and 12.91 dB, respectively. The difference is 0.23 dB, which is much smaller than 1.7 dB for uncoded 16QAM modulated OFDM.

HDD (1/2) 16QAM	48 sub-carriers [dB]	24 sub-carriers [dB]	Difference [dB]
Minimum	12.5	12.3	0.2
Maximum	13	13.5	0.5
Mean	12.68	12.91	0.23

Table 10. HDD ($r = 1/2$) 16QAM modulated OFDM (24 Mbps) performance statistics for $\overline{\gamma_b}$ at $P_b = 10^{-5}$

Likewise, the same analysis is performed for the 36 Mbps data rate with code rate $r = 3/4$. Note that the coefficients of B_d are different from those of $r = 1/2$ as shown in Table 7. The sub-channel performance of 16QAM at 36Mbps with ζ as a parameter in the range of $0 \le \zeta \le 10$ over Ricean fading channels is plotted in Figure 38.

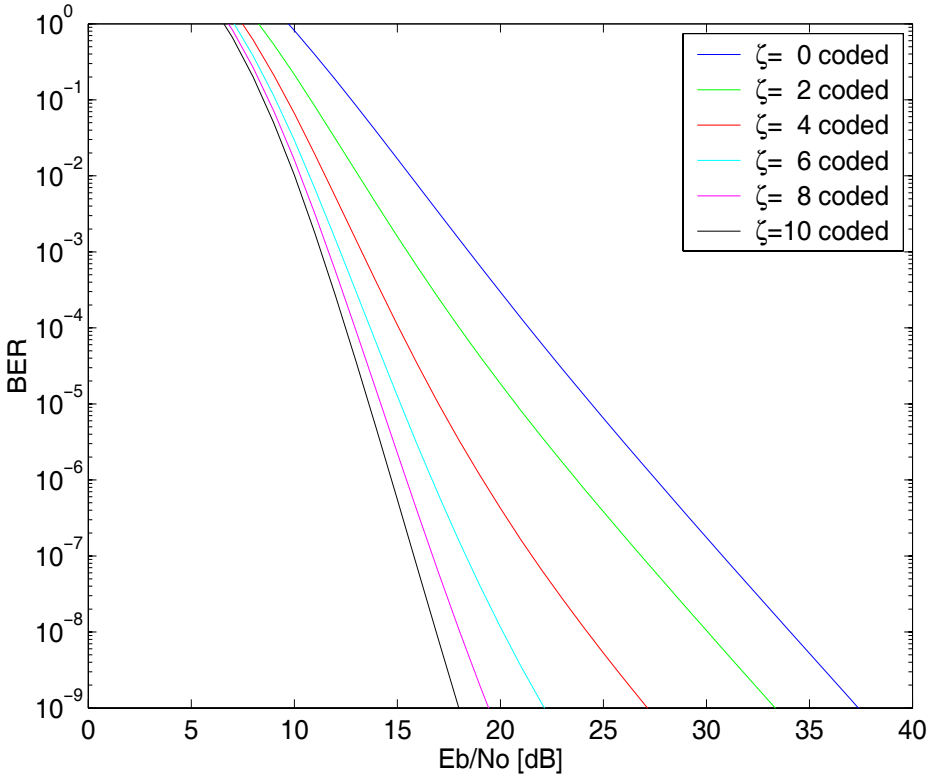

Figure 38. Performance of 16QAM with HDD ($r = 3/4$) over Ricean Fading

The performance for both uncoded and HDD ($r = 3/4$) 16QAM over Ricean fading channels is plotted in Figure 39. As before, the coding gain is remarkable and is greater for smaller values of ζ.

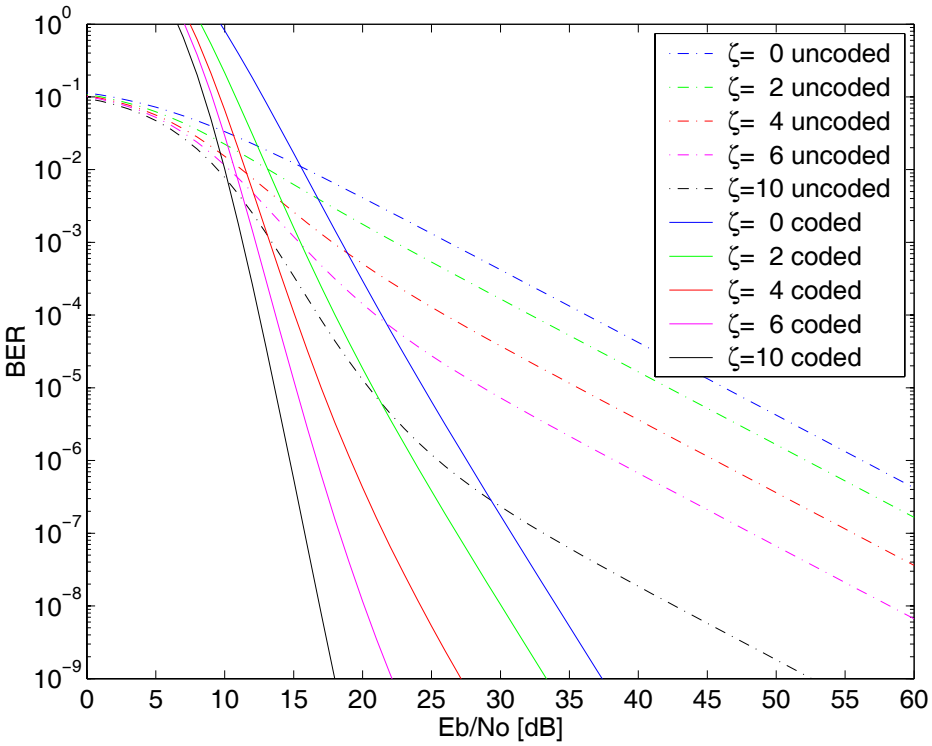

Figure 39. Uncoded versus HDD ($r = 3/4$) 16QAM Performance over Ricean Fading

In Figure 40, we plot the performance of 16QAM modulated OFDM with HDD ($r = 3/4$) over a pure Rayleigh fading channel. As we can see, the coding gain is 22 dB and $\overline{\gamma_b}$ is 24.5 dB at $P_b = 10^{-5}$. In Figure 41, we plot the performance of 16QAM modulated OFDM with HDD ($r = 3/4$) for both 48 and 24 independent sub-carriers over a composite Rayleigh/Ricean fading channel for one trial where ζ is assumed to be a uniform random variable over the range $0 \le \zeta \le 10$. As we can see, the coding gain is 21 dB, and $\overline{\gamma_b}$ for 48 and 24 independent sub-carriers at $P_b = 10^{-5}$ is 18.1 and 17.7 dB, respectively.

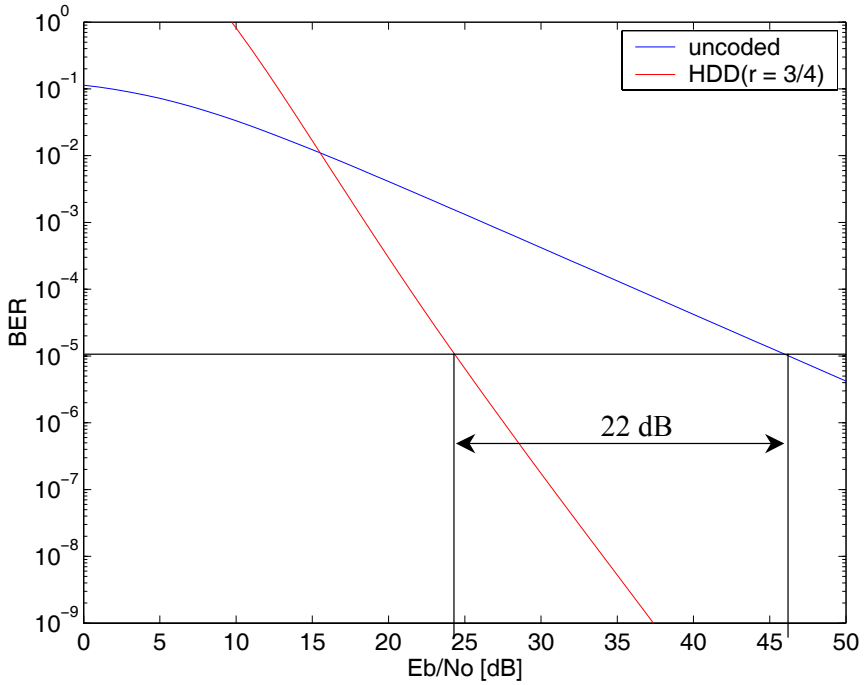

Figure 40. HDD ($r = 3/4$) versus uncoded 16QAM modulated OFDM (36 Mbps) performance over a pure Rayleigh fading channel

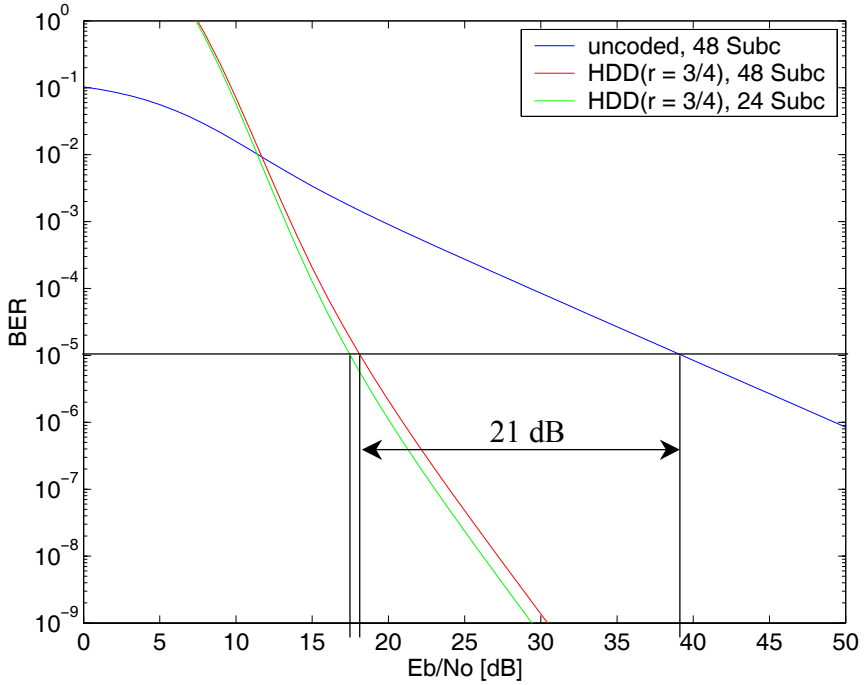

Figure 41. HDD ($r = 3/4$) versus uncoded 16QAM modulated OFDM (36 Mbps) performance over a composite Rayleigh/Ricean fading channel

As before, an average probability of bit error is obtained by evaluating the 16QAM modulated OFDM performance with HDD ($r = 3/4$) for ten trials for both 48 and 24 independent sub-carriers since ζ is modeled as a random variable. The minimum, maximum, and mean value for the $\overline{\gamma_b}$ required for $P_b = 10^{-5}$ obtained with ten trials for the 16QAM modulated OFDM with HDD ($r = 3/4$) is shown in Table 11. As we can see, the mean value of $\overline{\gamma_b}$ for 48 and 24 independent sub-carriers is 18.52 and 17.67 dB, respectively, and the difference is 0.85 dB.

HDD (3/4) 16QAM	48 sub-carriers [dB]	24 sub-carriers [dB]	Difference [dB]
Minimum	17.5	15.4	2.1
Maximum	19.3	19.1	0.2
Mean	18.52	17.67	0.85

Table 11. HDD ($r = 3/4$) 16QAM modulated OFDM (36 Mbps) performance statistics for $\overline{\gamma_b}$ at $P_b = 10^{-5}$

3. 64QAM with HDD (48 and 54 Mbps)

The analysis of 64QAM performance over Ricean fading channels proceeds in the same manner as 16QAM, except for using $q = 6$ vice $q = 4$ in Equation (5.18) and using code rate $r = 2/3$ vice $r = 1/2$ for data rates at 48 Mbps. The sub-channel performance of 64QAM at 48 Mbps with ζ as a parameter in the range of $0 \le \zeta \le 10$ over Ricean fading channels is plotted in Figure 42. As we can see, the performance curves are shifting to the right as compared to the sub-channel performance for 16QAM at 24 Mbps shown in Figure 34. In order to see the performance improvement, we overlay the uncoded and HDD ($r = 2/3$) 64QAM performance over Ricean fading channels in Figure 43. As before, the coding gain is remarkable and is greater for smaller values of ζ.

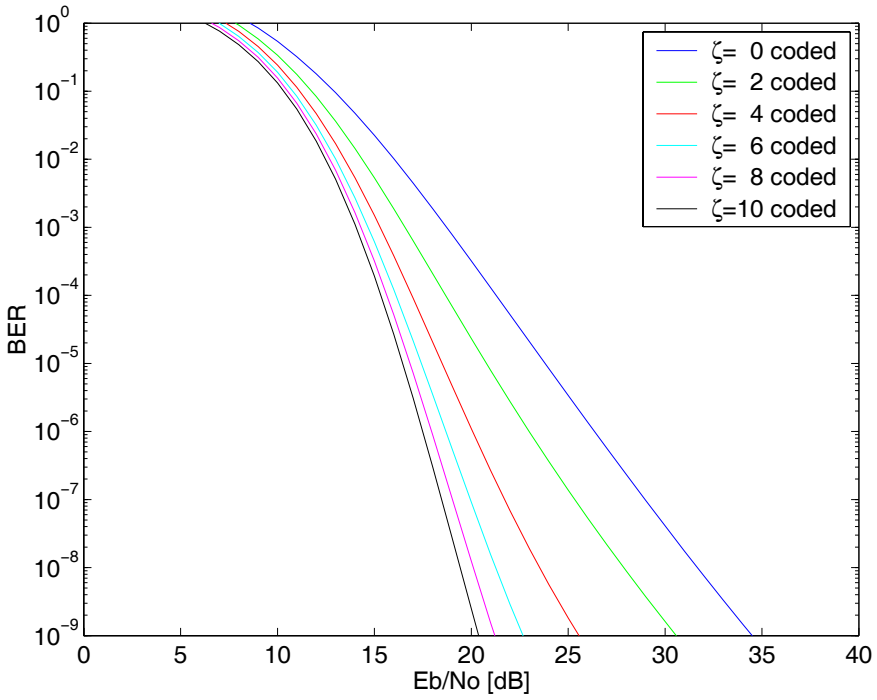

Figure 42. Performance of 64QAM with HDD ($r = 2/3$) over Ricean Fading

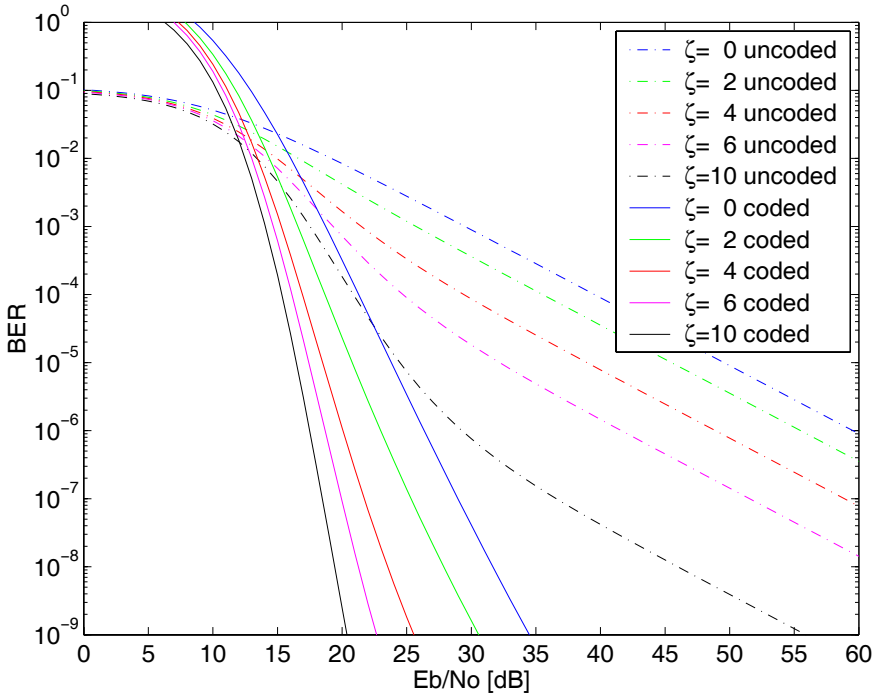

Figure 43. Uncoded versus HDD ($r = 2/3$) 64QAM Performance over Ricean Fading

In Figure 44, we plot the performance of 64QAM modulated OFDM with HDD ($r = 2/3$) over a pure Rayleigh fading channel. As we can see, the coding gain is about 26 dB and $\overline{\gamma_b}$ is 23.6 dB at $P_b = 10^{-5}$.

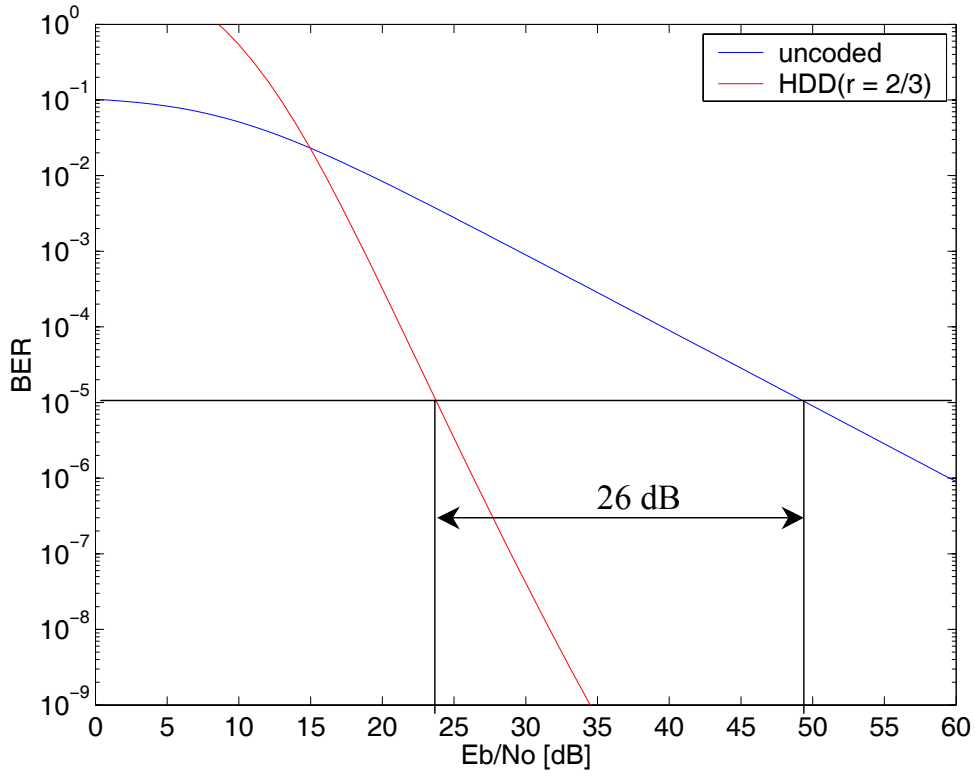

Figure 44. HDD ($r = 2/3$) versus uncoded 64QAM modulated OFDM (48 Mbps) performance over a pure Rayleigh fading channel

In Figure 45, we plot the performance of 64QAM modulated OFDM with HDD ($r = 2/3$) for both 48 and 24 independent sub-carriers over a composite Rayleigh/Ricean fading channel for one trial where ζ is assumed to be a uniform random variable over the range $0 \le \zeta \le 10$. As we can see, the coding gain is 24 dB, and $\overline{\gamma_b}$ for 48 and 24 independent sub-carriers at $P_b = 10^{-5}$ is 18.8 and 19.1 dB, respectively.

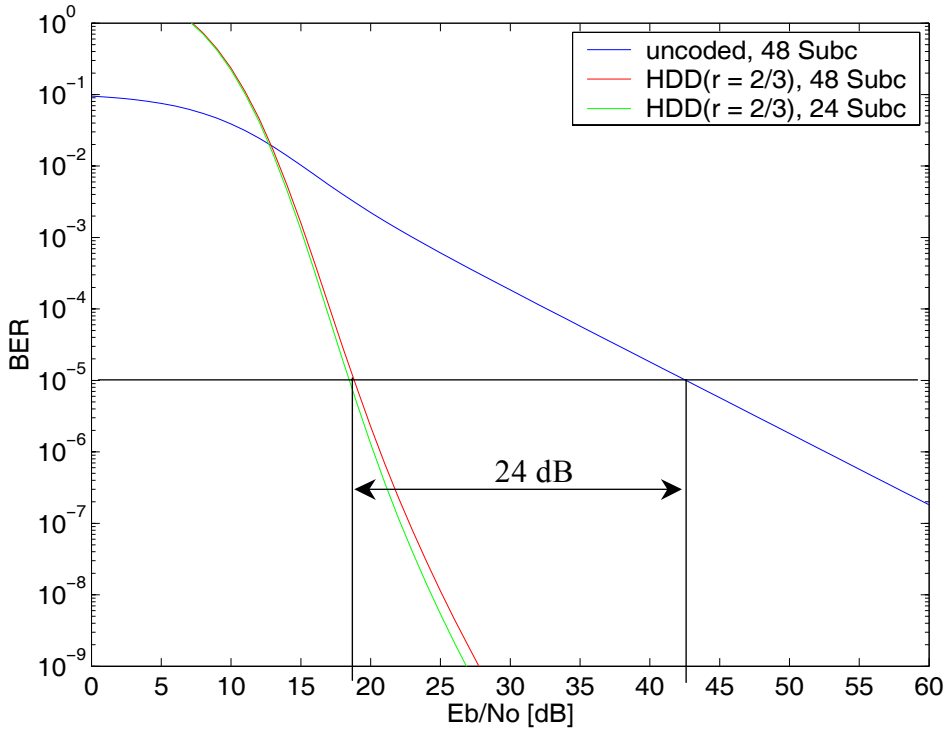

Figure 45. HDD ($r = 2/3$) versus uncoded 64QAM modulated OFDM (48 Mbps) performance over a composite Rayleigh/Ricean fading channel

As before, an average probability of bit error is obtained by evaluating the 64QAM modulated OFDM performance with HDD ($r = 2/3$) for ten trials for both 48 and 24 independent sub-carriers since ζ is modeled as a random variable. The minimum, maximum, and mean value for the $\overline{\gamma_b}$ required for $P_b = 10^{-5}$ obtained with ten trials for the 64QAM modulated OFDM with HDD ($r = 2/3$) performance is shown in Table 12. As we can see, the mean value of $\overline{\gamma_b}$ for 48 and 24 independent sub-carriers is 18.83 and 19.02 dB, respectively, and the difference is 0.19 dB.

HDD (2/3) 64QAM	48 sub-carriers [dB]	24 sub-carriers [dB]	Difference [dB]
Minimum	18.4	18.4	0
Maximum	19.4	20.1	0.7
Mean	18.83	19.02	0.19

Table 12. HDD ($r = 2/3$) 64QAM modulated OFDM (48 Mbps) performance statistics for $\overline{\gamma_b}$ at $P_b = 10^{-5}$

At this point, only the 54 Mbps data rates remains to be investigated. To achieve this data rate, *IEEE 802.11a* uses 64QAM for sub-channel modulation with convolutional coding at rate $r = 3/4$. In Figure 46, we plot the sub-channel performance of 64QAM at 54 Mbps with ζ as a parameter in the range of $0 \le \zeta \le 10$. As we can see, the performance curves are shifted to the right as compared to the sub-channel performance of 16QAM with data rates 36 Mbps shown in Figure 38.

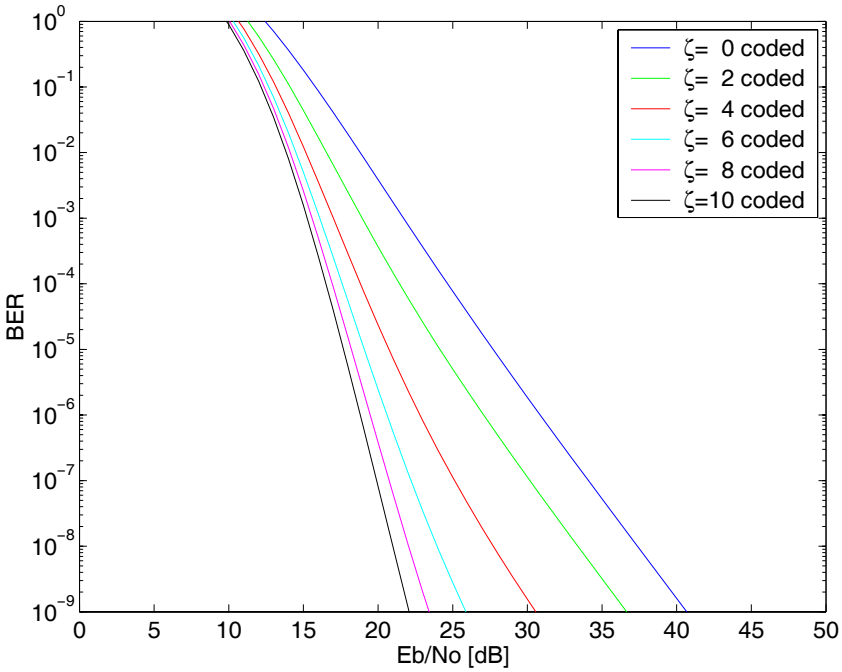

Figure 46. Performance of 64QAM with HDD ($r = 3/4$) over Ricean Fading

In order to see the performance improvement, we overlay the uncoded and HDD ($r = 3/4$) 64QAM performance curves over Ricean fading channels in Figure 47. As before, the coding gain is remarkable and is greater for smaller values of ζ. In Figure 48, we plot the performance of 64QAM modulated OFDM with HDD ($r = 3/4$) over a pure Rayleigh fading channel. As we can see, the coding gain is 22 dB and $\overline{\gamma_b}$ is 27.8 dB at $P_b = 10^{-5}$.

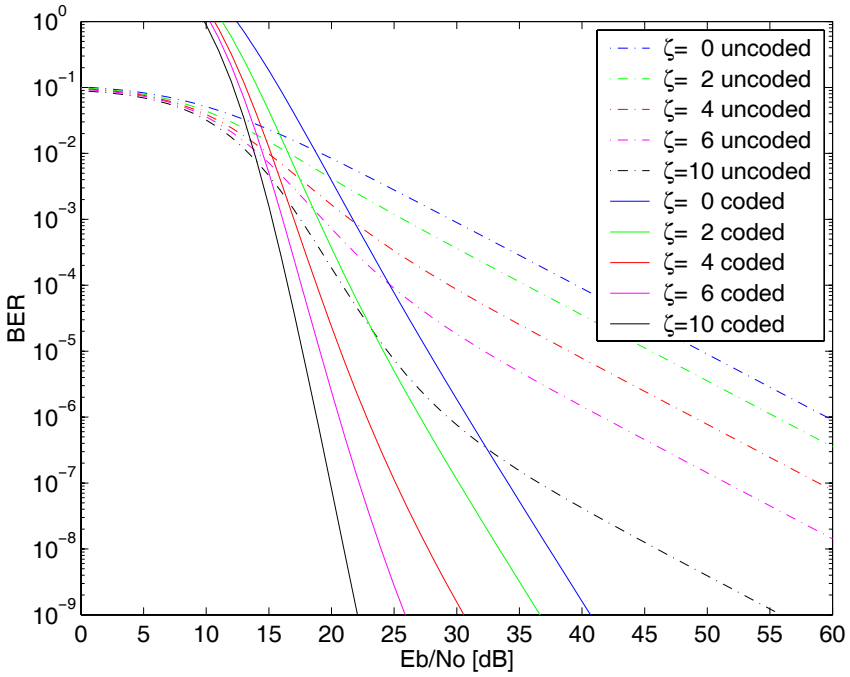

Figure 47. Uncoded versus HDD ($r = 3/4$) 64QAM Performance over Ricean Fading

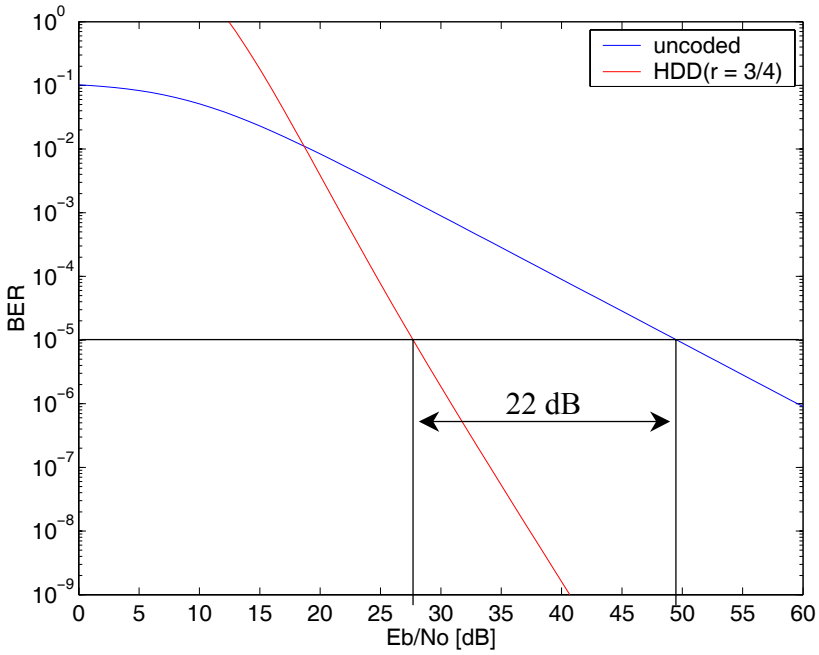

Figure 48. HDD ($r = 3/4$) versus uncoded 64QAM modulated OFDM (54 Mbps) performance over a pure Rayleigh fading channel

In Figure 49, we plot the performance of 64QAM modulated OFDM with HDD ($r = 3/4$) for both 48 and 24 independent sub-carriers over a composite Rayleigh/Ricean fading channel for one trial where ζ is assumed to be a uniform random variable over the range $0 \le \zeta \le 10$. As we can see, the coding gain is about 21 dB, and $\overline{\gamma_b}$ for 48 and 24 independent sub-carriers at $P_b = 10^{-5}$ is 21 and 21.7 dB, respectively.

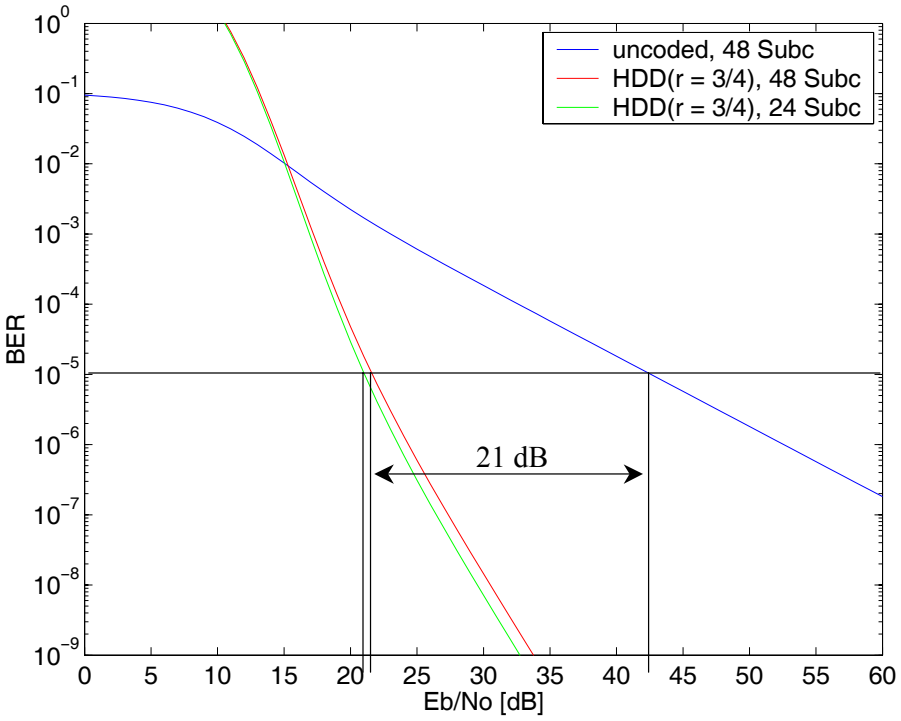

Figure 49. HDD ($r = 3/4$) versus uncoded 64QAM modulated OFDM (54 Mbps) performance over a composite Rayleigh/Ricean fading channel

As before, an average probability of bit error is obtained by evaluating the 64QAM modulated OFDM performance with HDD ($r = 3/4$) for ten trials for both 48 and 24 independent sub-carriers. The minimum, maximum, and mean value for the $\overline{\gamma_b}$ required for $P_b = 10^{-5}$ obtained with ten trials for the 64QAM modulated OFDM with

HDD ($r = 3/4$) performance is shown in Table 13. As we can see, the mean value of $\overline{\gamma_b}$ for 48 and 24 independent sub-carriers is 22.01 and 21.28 dB, respectively, and the difference is 0.73 dB.

HDD (3/4) 64QAM	48 sub-carriers [dB]	24 sub-carriers [dB]	Difference [dB]
Minimum	21.1	19.4	1.7
Maximum	22.7	22.6	0.1
Mean	22.01	21.28	0.73

Table 13. HDD ($r = 3/4$) 64QAM modulated OFDM (54 Mbps) performance statistics for $\overline{\gamma_b}$ at $P_b = 10^{-5}$

4. HDD Summary

In this section, we analyzed the *IEEE 802.11a* performance by assuming $\overline{\gamma_{b_i}} = \overline{\gamma_b}$ for all i and that either $\zeta_i = 0$ for all i (Rayleigh fading) or $0 \le \zeta_i \le 10$ where ζ_i is modeled as a uniform random variable (composite Rayleigh/Ricean fading). Furthermore, we assume the channel coherence bandwidth is such that we have $N = 48$ independent sub-channels, although very similar results are obtained if we assume $N = 24$ independent sub-channels. For the combinations of modulation type and code rate utilized by the *IEEE 802.11a* WLAN standard, the coding gain and signal-to-noise ratios required for $P_b = 10^{-5}$ in AWGN with frequency-selective, slow Rayleigh fading, and in AWGN with frequency-selective, slow composite Rayleigh/Ricean fading, all with HDD, are shown in Table 14, where the composite Rayleigh/Ricean fading results represent an average. The variation about the average generally does not exceed ± 1 dB. As expected, the signal-to-noise ratios required for a pure Rayleigh fading channel are more than for composite Rayleigh/Ricean fading, in the range of four to seven dB for $P_b = 10^{-5}$. Also as expected, for a specific modulation type, regardless of the channel conditions considered, as the code rate increases, the signal-to-noise ratio required to achieve a fixed probability of bit error increases. Moreover, the coding gains range from 21 to 30 dB.

Contrary to expectations, however, the signal-to-noise ratio required to achieve a specific P_b does not monotonically decrease with decreasing bit rate. This phenomenon is observed whether the channel is modeled as a pure Rayleigh fading channel or as a composite Rayleigh/Ricean fading channel. For example, from Table 14 we see that a larger signal-to-noise ratio is required for a bit rate of 18 Mbps than for 24 Mbps.

Data Rate (Mbps)	Modulation	Code Rate	$\zeta_i = 0$		$0 \le \zeta_i \le 10$	
			G [dB]	$\overline{\gamma_b}$ [dB]	G [dB]	$\overline{\gamma_b}$ [dB]
6	BPSK	1/2	30	**14.5**	27	**9.96**
9	BPSK	3/4	22	**22.3**	21	**15.57**
12	QPSK	1/2	30	**14.5**	27	**9.96**
18	QPSK	3/4	22	**22.3**	21	**15.57**
24	16QAM	1/2	30	**16.4**	27	**12.68**
36	16QAM	3/4	22	**24.5**	21	**18.52**
48	64QAM	2/3	26	**23.8**	24	**18.83**
54	64QAM	3/4	22	**27.8**	21	**22.01**

Table 14. Received average energy per bit-to-noise power spectral density ratio $\overline{\gamma_b}$ required for $P_b = 10^{-5}$ in AWGN with frequency-selective, slow Rayleigh fading and composite Rayleigh/Ricean fading with HDD.

C. SOFT DECISION DECODING

In the previous section, we showed that OFDM performance is improved considerably by adding convolutional encoding and Viterbi hard decision decoding. In addition to HDD, Viterbi soft decision decoding can further increase the coding gain by about 2 to 3dB in AWGN. In this section, we investigate the performance of *IEEE 802.11a* standard with Viterbi soft decision decoding, but only BPSK and QPSK will be examined due to the difficulty of analyzing the probability of bit error for SDD of a binary code transmitted with non-binary modulation.

1. BPSK/QPSK with SDD (6 and 12 Mbps)

As discussed earlier, Equation (5.10) is valid for both HDD and SDD, except the probability of selecting a weight d output sequence as the transmitted coded sequence P_d in Equation (5.10) is determined by the type of modulation, the channel, and whether HDD or SDD is used. In other words, we need to find P_d to investigate the performance of BPSK/QPSK with SDD over AWGN and Ricean fading channels. It was shown in [19] that for BPSK in AWGN with SDD, if we assume the correct path is the all-zero path, then a decoding error occurs when

$$\sum_{l=1}^{d} y_l > 0 \tag{5.19}$$

where y_l is the demodulator output, d is the number of bits that the y^{th} path differs from the correct path, and l is the index that runs over the set of d bits in which the correct path and the y^{th} path differ. If y_l is modeled as a random variable, then P_d is given by the probability that the sum of d independent random variables is greater than zero, written as

$$P_d = P_r\left(\sum_{l=1}^{d} y_l > 0\right) \tag{5.20}$$

which is equivalent to the probability of bit error for a coherent binary signaling scheme with d^{th} order diversity [19]; thus, for BPSK in AWGN with SDD, P_d can be expressed as

$$P_d = Q\left(\sqrt{\frac{2\,d\,r\,\overline{E_b}}{N_0}}\right) \tag{5.21}$$

where d is the diversity order and r is the code rate. Equation (5.21) can be rewritten as

$$P_d = Q\left(\sqrt{2\,d\,r\,\overline{\gamma_b}}\right) \tag{5.22}$$

where $\overline{\gamma_b} = \overline{E_b}/N_0$ is the ratio of received average energy per bit-to-noise power spectral density. Substituting Equation (5.22) into Equation (5.10) with the same code rate and

weight structure used in HDD, we obtain the performance of BPSK/QPSK with SDD with AWGN. In Figure 50, we show the comparative performance of uncoded, HDD, and SDD BPSK/QPSK with AWGN. As expected, SDD improves performance by about 2.5 dB over HDD in AWGN.

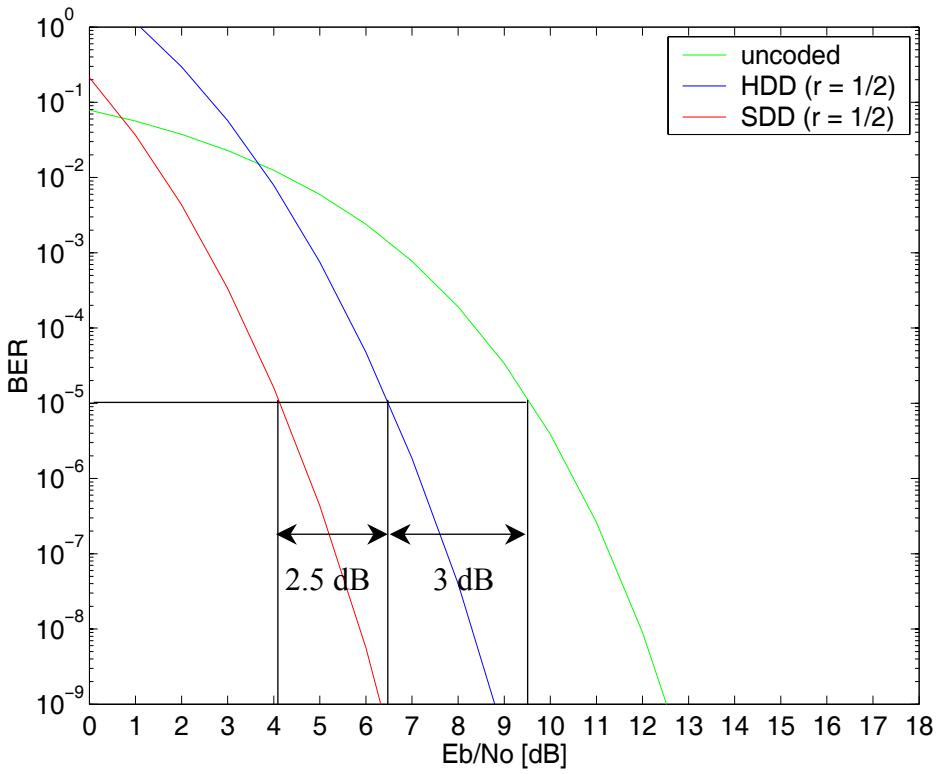

Figure 50. Uncoded, HDD, and SDD BPSK/QPSK performances with AWGN

For BPSK/QPSK with SDD over Ricean fading channels, P_d is conditioned on received signal amplitude a_c, thus we obtain the average P_d from

$$P_d = \int_0^\infty P_d(a_c) f_{A_c}(a_c) da_c = \int_0^\infty P_d(\gamma_b) f_{\Gamma_b}(\gamma_b) d\gamma_b \tag{5.23}$$

We have already solved Equation (5.23) as in Equation (4.34), since we use Equation (4.19) instead of (4.17) to solve Equation (4.20). Therefore, for BPSK/QPSK with SDD

over Ricean fading channels, P_d can be expressed as

$$P_d \approx \frac{1}{2\sqrt{\pi \cdot c_1}} \left(\frac{\zeta_i + 1}{r\,\overline{\gamma_{b_i}} + \zeta_i + 1} \right)^d \exp\left(\frac{-d\,\zeta_i\, r\,\overline{\gamma_{b_i}}}{r\,\overline{\gamma_{b_i}} + \zeta_i + 1} \right) \tag{5.24}$$

where $c_1 = 1.2 + 0.1\zeta$ is empirically obtained, ζ_i is the ratio of direct-to-diffuse signal power on the i^{th} sub-channel, d is the number of bits which are different from the correct path, r is the code rate, and $\overline{\gamma_{b_i}}$ the ratio of received average energy per bit-to-noise power spectral density on the i^{th} sub-channel. Substituting Equation (5.24) into Equation (5.10) with code rate $r = 1/2$ and its corresponding weight structure shown in Table 7, we obtain the performance of BPSK/QPSK with SDD at data rates 6 and 12 Mbps over Ricean fading channels. These results are plotted in Figure 51 with ζ as a parameter in the range of $0 \le \zeta \le 10$.

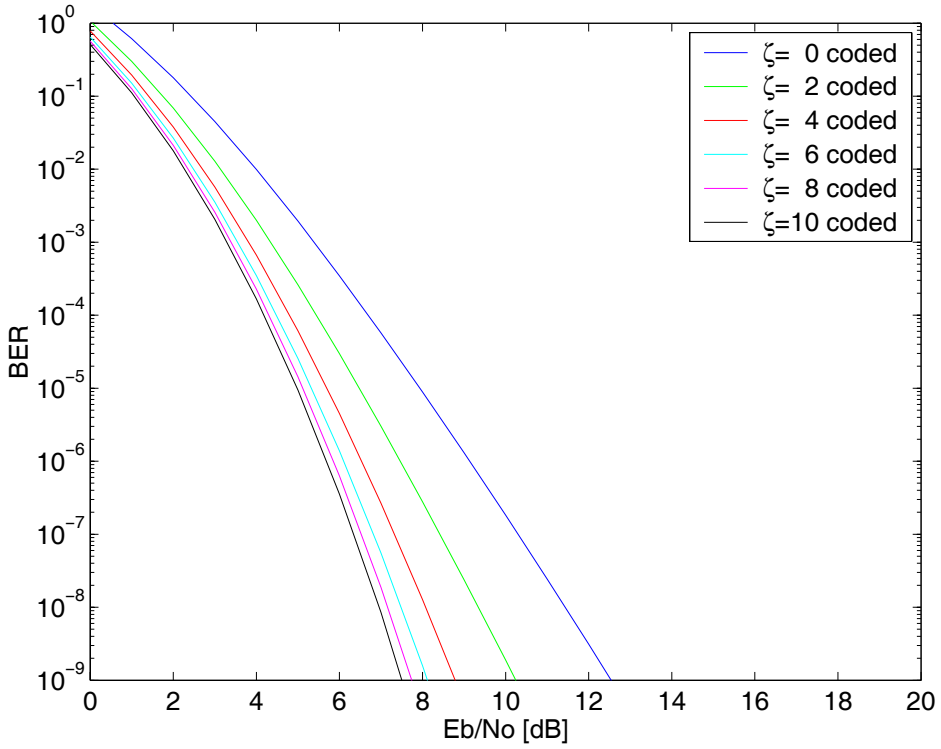

Figure 51. Performance of BPSK/QPSK with SDD ($r = 1/2$) over Ricean Fading

In Figure 52, we overlay Figure 51 with Figure 26, which is the performance of BPSK/QPSK with HDD ($r = 1/2$) over Ricean Fading. As we can see, the SDD improves the sub-channel BPSK/QPSK performance by about 3 to 6 dB at $P_b = 10^{-5}$ in the range of $0 \le \zeta \le 10$ over HDD in Ricean fading channels.

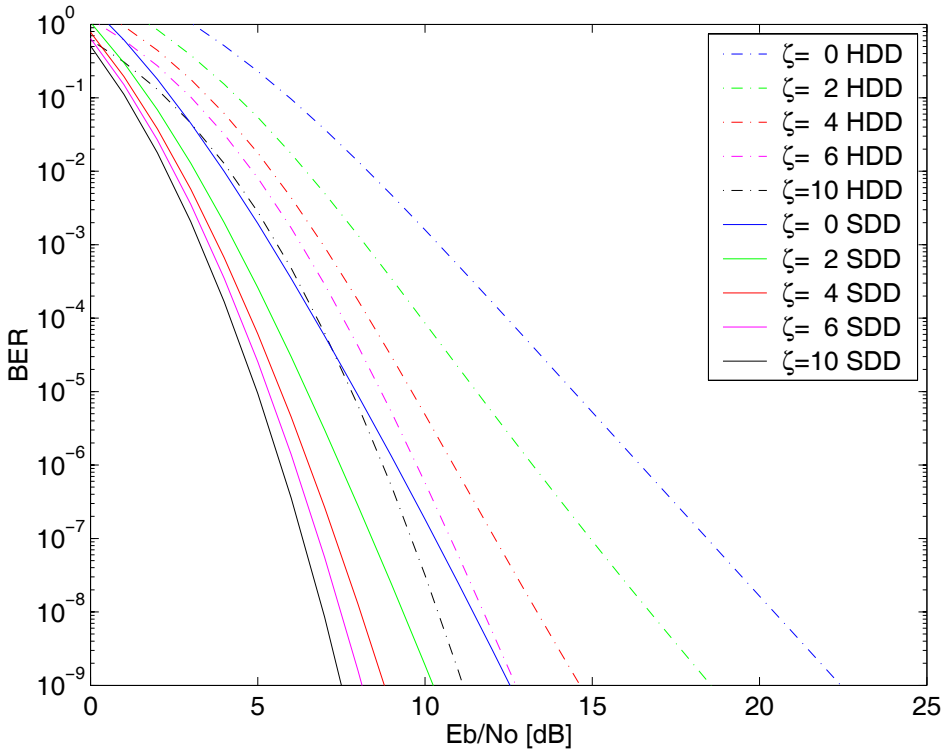

Figure 52. SDD versus HDD ($r = 1/2$) BPSK/QPSK Performance over Ricean Fading

As before, after examining sub-channel performance, we investigate the performance of BPSK/QPSK modulated OFDM with SDD over Ricean fading channels. In Figure 53, we overlay SDD and HDD performance, both with $r = 1/2$ code, for BPSK/QPSK modulated OFDM for both 48 and 24 independent sub-carriers over a composite Rayleigh/Ricean fading channel for one trial, where ζ is assumed to be a uniform random variable over the range $0 \le \zeta \le 10$. As we can see, SDD improves performance by about 3.3 dB over HDD, and $\overline{\gamma_b}$ for 48 and 24 independent sub-carriers at $P_b = 10^{-5}$ is 6.8 and 6.6 dB, respectively.

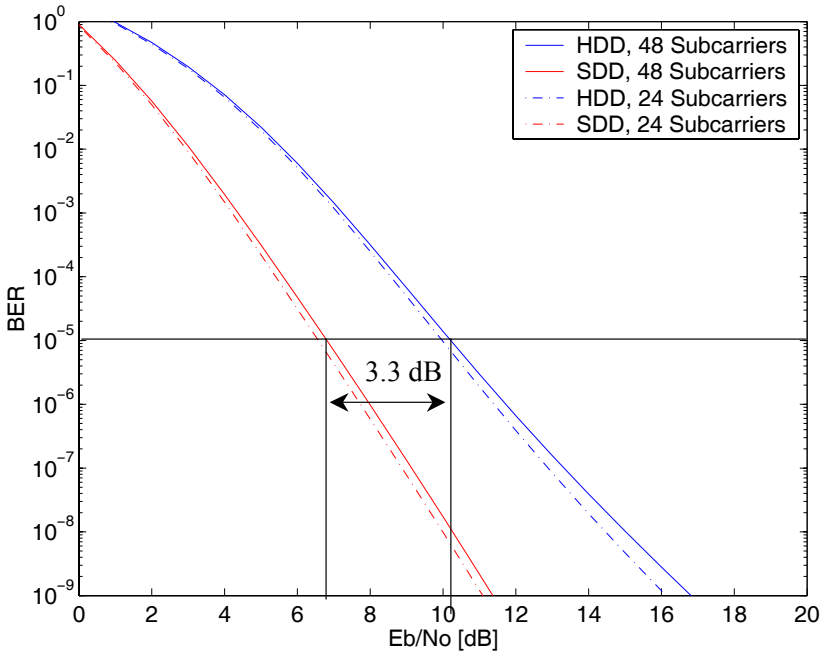

Figure 53. SDD versus HDD ($r = 1/2$) BPSK/QPSK modulated OFDM (6 and 12 Mbps) performance over a composite Rayleigh/Ricean fading channel

As before, an average probability of bit error is obtained by evaluating BPSK/QPSK modulated OFDM performance with SDD ($r = 1/2$) for ten trials for both 48 and 24 independent sub-carriers. The minimum, maximum, and mean value for the $\overline{\gamma_b}$ required for $P_b = 10^{-5}$ obtained with ten trials for BPSK/QPSK modulated OFDM with SDD ($r = 1/2$) performance is shown in Table 15. As we can see, the mean value of $\overline{\gamma_b}$ for 48 and 24 independent sub-carriers is 6.61 dB; that is, there is no difference in performance whether we have 48 or 24 independent sub-carriers in this case.

SDD (1/2) BPSK/QPSK	48 sub-carriers [dB]	24 sub-carriers [dB]	Difference [dB]
Minimum	6.4	6.2	0.2
Maximum	6.9	6.9	0
Mean	6.61	6.61	0

Table 15. SDD ($r = 1/2$) BPSK/QPSK modulated OFDM (6 and 12 Mbps) performance statistics for $\overline{\gamma_b}$ at $P_b = 10^{-5}$

By way of summarizing the results for BPSK/QPSK modulated OFDM at 6 and 12 Mbps data rates with convolutional code rate $r = 1/2$, we overlay the performance curves for SDD, HDD, and uncoded BPSK/QPSK modulated OFDM over a composite Rayleigh/Ricean fading channel in Figure 54. As we can see, $\overline{\gamma_b}$ for SDD, HDD, and uncoded BPSK/QPSK modulated OFDM at $P_b = 10^{-5}$ is 6.8, 9.9, and 37 dB, respectively. The over all coding gain achieved by the use of SDD is about 30 dB.

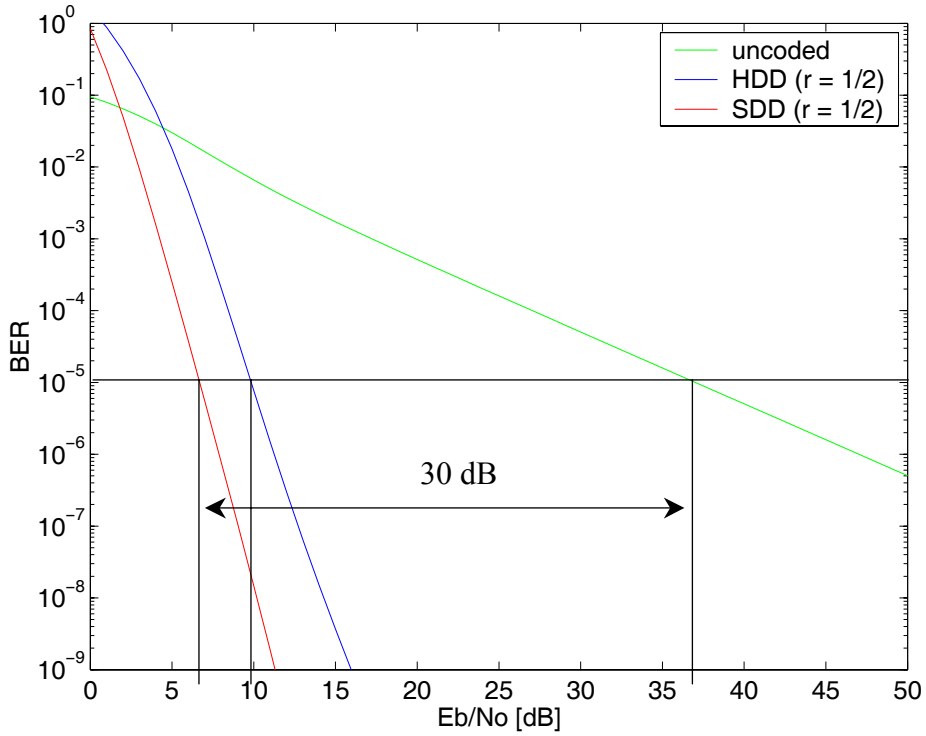

Figure 54. SDD, HDD, and uncoded BPSK/QPSK modulated OFDM performance over a composite Rayleigh/Ricean fading channel

2. BPSK/QPSK with SDD (9 and 18 Mbps)

We now perform the same analysis for code rate $r = 3/4$ to obtain the performance curves for 9 Mbps BPSK modulated OFDM and 18 Mbps QPSK modulated OFDM as specified in *IEEE 802.11a* WLAN standard. The results of this analysis for a single sub-carrier are given in Figure 55 for the usual range of ζ. As expected, the

performance curves are slightly poorer than those obtained in Figure 51 due to the higher code rate used.

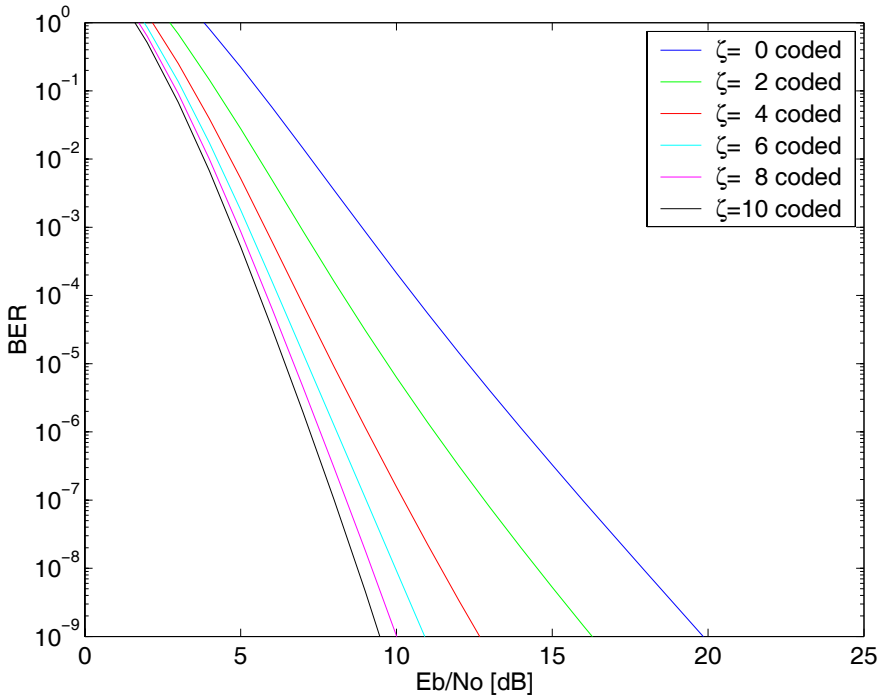

Figure 55. Performance of BPSK/QPSK with SDD ($r = 3/4$) over Ricean Fading

In Figure 56, we overlay Figure 55 with Figure 30, which is the performance of BPSK/QPSK with HDD ($r = 3/4$) over a Ricean fading channel. As we can see, SDD improves the sub-channel BPSK/QPSK performance by about 3.5 to 12 dB over HDD in Ricean fading channels. In Figure 57, we overlay SDD and HDD ($r = 3/4$) performance of BPSK/QPSK modulated OFDM for both 48 and 24 independent sub-carriers over a composite Rayleigh/Ricean fading channel for one trial where ζ is assumed to be a uniform random variable over the range $0 \le \zeta \le 10$.

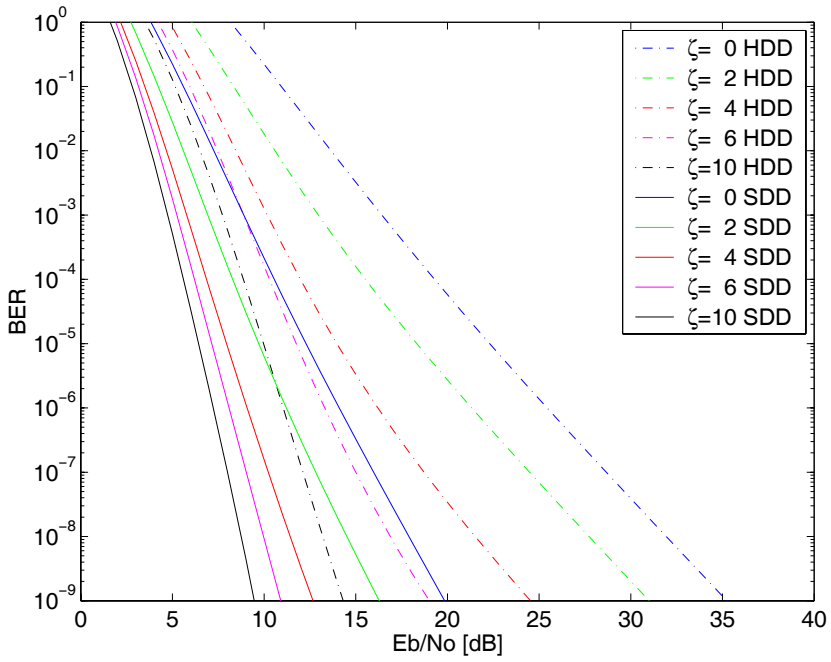

Figure 56. SDD versus HDD ($r = 3/4$) BPSK/QPSK Performance over Ricean Fading

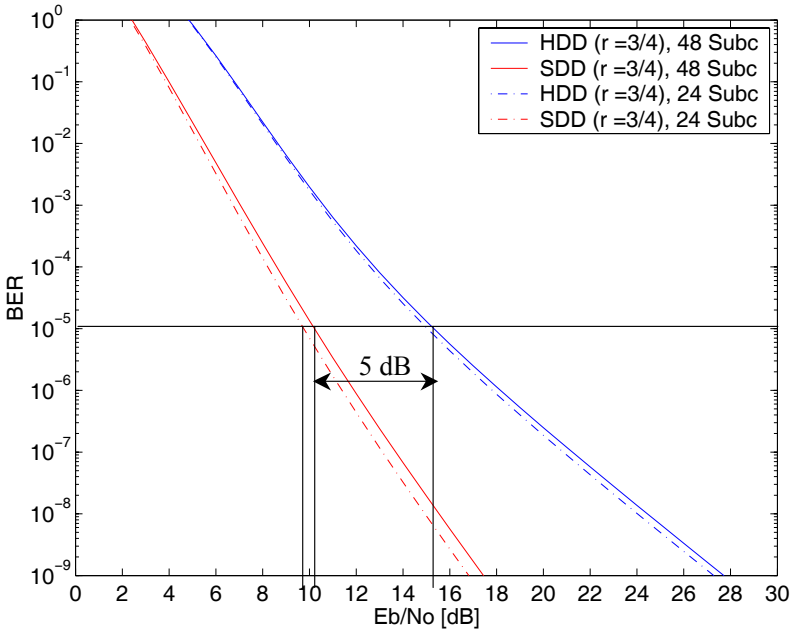

Figure 57. SDD versus HDD ($r = 3/4$) BPSK/QPSK modulated OFDM (9 and 18 Mbps) performance over a composite Rayleigh/Ricean fading channel

As we can see, SDD improves performance by about 5 dB over HDD, and $\overline{\gamma_b}$ for 48 and 24 independent sub-carriers at $P_b = 10^{-5}$ is 10.2 and 9.8 dB, respectively. As before, an average probability of bit error is obtained by evaluating BPSK/QPSK modulated OFDM performance with SDD ($r = 3/4$) for ten trials for both 48 and 24 independent sub-carriers. The minimum, maximum, and mean value for the $\overline{\gamma_b}$ required for $P_b = 10^{-5}$ obtained with ten trials for BPSK/QPSK modulated OFDM with SDD ($r = 3/4$) is shown in Table 16. As we can see, the mean value of $\overline{\gamma_b}$ for 48 and 24 independent sub-carriers is 10.34 and 10.12 dB, respectively; that is, the difference is 0.22 dB, which is slightly greater than that of BPSK/QPSK modulated OFDM with SDD at $r = 1/2$.

SDD (3/4) BPSK/QPSK	48 sub-carriers [dB]	24 sub-carriers [dB]	Difference [dB]
Minimum	9.8	9.5	0.3
Maximum	10.8	10.4	0.4
Mean	10.34	10.12	0.22

Table 16. SDD ($r = 3/4$) BPSK/QPSK modulated OFDM (9 and 18 Mbps) performance statistics for $\overline{\gamma_b}$ at $P_b = 10^{-5}$

By way of summarizing the results for BPSK/QPSK modulated OFDM at 9 and 18 Mbps data rates with convolutional code rate $r = 3/4$, we overlay the performance curves for SDD, HDD, and uncoded BPSK/QPSK modulated OFDM over a composite Rayleigh/Ricean fading channel in Figure 58. As we can see, $\overline{\gamma_b}$ for SDD, HDD, and uncoded BPSK/QPSK modulated OFDM at $P_b = 10^{-5}$ is 10.5, 15.7, and 37 dB, respectively. The overall coding gain achieved by the use of SDD is about 26.5 dB.

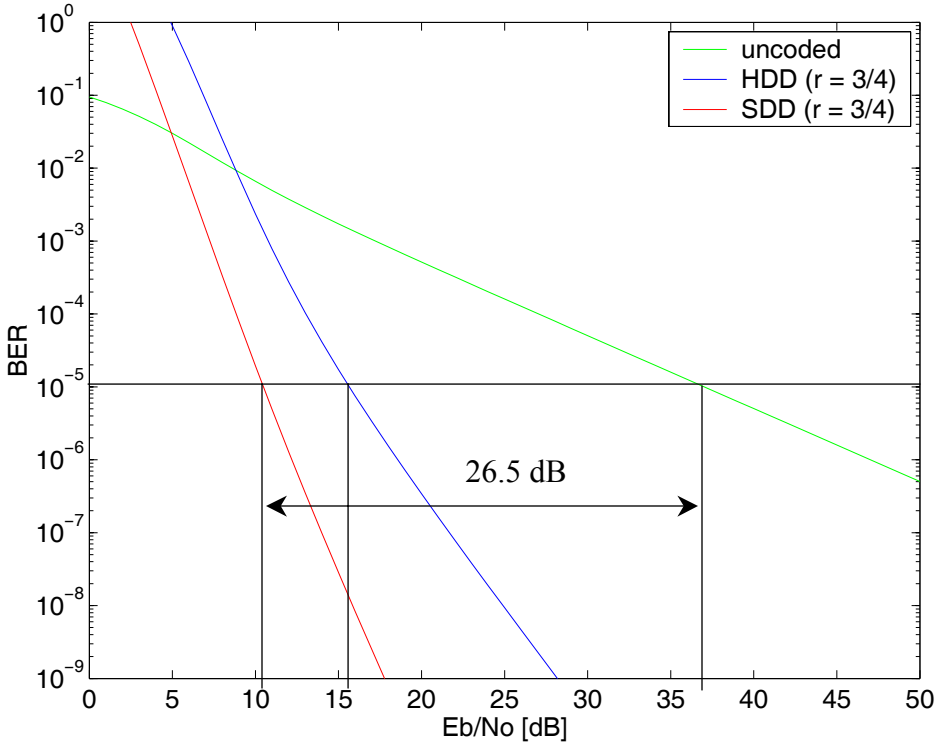

Figure 58. SDD, HDD, and uncoded BPSK/QPSK modulated OFDM performance over a composite Rayleigh/Ricean fading channel

3. SDD summary

As expected, Viterbi soft decision decoding further increases the coding gain. For BPSK/QPSK with code rate $r = 1/2$, SDD improves performance by about 2.5 dB over HDD in AWGN, and by about 3.3 dB over a composite Rayleigh/Ricean fading channel. For BPSK/QPSK with code rate $r = 3/4$, SDD improves performance by about 5.5 dB over HDD in a composite Rayleigh/Ricean fading channel.

THIS PAGE INTENTIONALLY LEFT BLANK

VI. CONCLUSION

A. FINDINGS

There are several findings that result from the analysis of the *IEEE 802.11a* WLAN standard over frequency-selective, slow, Ricean fading channels.

First, for the performance without FEC coding, OFDM performance is dominated by the smaller values of ζ, which corresponds to more severe fading conditions. As expected, the performance of uncoded BPSK/QPSK modulated OFDM is better than uncoded 16QAM and 64QAM; however, even BPSK/QPSK does not yield performance acceptable for wireless communications.

Second, for the performance with convolutional coding and Viterbi HDD, the signal-to-noise ratios required for a pure Rayleigh fading channel are larger than for composite Rayleigh/Ricean fading. Also, as expected for a specific modulation type, regardless of the channel conditions considered, as the code rate increases, the signal-to-noise ratio required to achieve a fixed probability of bit error increases. Contrary to expectations, however, the signal-to-noise ratio required to achieve a specific P_b does not monotonically decrease with decreasing bit rate. This phenomenon is observed whether the channel is modeled as a pure Rayleigh fading channel or as a composite Rayleigh/-Ricean fading channel. This phenomenon raises a question as to the utility of some of the bit rate configurations adopted for *IEEE 802.11a* WLAN standard.

Third, for the performance with convolutional coding and Viterbi SDD, for BPSK/QPSK with code rate $r = 1/2$, SDD improves performance by about 2.5 dB over HDD in AWGN, and by about 3.3 dB over a composite Rayleigh/Ricean fading channel. For BPSK/QPSK with code rate $r = 3/4$, SDD improves performance by about 5.5 dB over HDD in a composite Rayleigh/Ricean fading channel.

Fourth, in this thesis we assume the channel coherence bandwidth is such that we have either $N = 48$ or $N = 24$ independent sub-carriers. Without FEC coding, the difference in the mean value of E_b/N_0 between 48 and 24 independent sub-carrier for $P_b = 10^{-5}$ is around 1.7 dB, ranges from 0.13 through 0.85 dB for HDD, and ranges from

0 to 0.22 dB for SDD; that is, the difference in performance between 48 and 24 independent sub-carriers decreases as more powerful coding technique are used.

B. RECOMMENDATIONS FOR FURTHER RESEARCH

There are two primary areas in which follow-on research is recommended. First, in this thesis, we analyzed the performance of the *IEEE 802.11a* WLAN standard over a frequency-selective, slow, Ricean fading channels using both Viterbi hard decision decoding (HDD) and Viterbi soft decision decoding (SDD). Due to the difficulty of analyzing the probability of bit error for SDD of a binary code transmitted with non-binary modulation, we did not investigate the performance of 16 and 64QAM modulation with SDD. An approximate approach, however, to analyze MQAM performance with SDD [20] is a natural outgrowth of this thesis. Second, like other wireless communications systems, WLANs are vulnerable to either hostile jamming or exploitation by unintended recipients; therefore, the performance of *IEEE 802.11a* WLAN standard over fading channels with different types of jamming, for example, barrage jamming, pulsed jamming, or tone jamming, is also an interesting topic for further research.

C. CLOSING COMMENTS

As *IEEE 802.11a* products began shipping months ago, more and more companies and schools have been taking advantage of *IEEE 802.11a'*s superior performance; therefore, an analysis such as this thesis may prove beneficial to those designing or employing the OFDM based *IEEE 802.11a* WLAN standard.

In addition to its well-known ability to combat ISI, OFDM is also becoming very popular for high-speed transmission. In January 2002, the *IEEE* again adopted OFDM in the newest *802.11* standard for WLANs, *IEEE 802.11g*, which extends *802.11b*'s data rates to 54 Mbps within the 2.4 GHz band. Clearly, OFDM will gain broad-based acceptance as a signaling technique in the future.

LIST OF REFERENCES

1. Wan L. & Dubey, V.K., "Bit Error Probability of OFDM System Over Frequency-nonselective Fast Rayleigh Fading Channels*," IEEE Electronics Letters*, Volume: 36, Issue: 15 July. 2000. pp. 1306-07.

2. Wan L. & Dubey, V.K., "BER Performance of OFDM System Over Frequency-nonselective Fast Ricean Fading Channels," *IEEE Communications Letters*, Volume: 5, Issue: 1 Jan. 2001. pp. 19-21.

3. David A. Wiegandt & Carl R. Nassar, " High-Performance 802.11a Wireless LAN via Carrier-Interferometry Orthogonal Frequency Division Multiplexing at 5 GHz," *IEEE Global Telecommunications Conference, 2001*, Volume: 6, pp. 3579-3582.

4. Patrick, A. Count, "Performance Analysis of OFDM in Frequency-selective, Slowly Fading Nakagami Channels," Master's thesis, Naval Postgraduate School, Monterey, CA, 2001.

5. Institute of Electrical and Electronics Engineers, 802.11a, *Wireless LAN Medium Access Control (MAC) and Physical Layer (PHY) Specifications: High-Speed Physical Layer Extension in the 5 GHz Band*, 16 September 1999.

6. Alan Triggs, Notes for Wireless, Cellular & Personal Telecommunications, Lecture 7, Southern Methodist University, Fall 2001.

7. Sklar, B., *Digital Communications: Fundamental and Applications*, 2nd ed. Prentice Hall, Upper Saddle River, NJ, 2001.

8. Theodore S. Rappaport, *Wireless Communications Principles and Practice*, 2nd ed. Prentice Hall, Upper Saddle River, NJ, 2002.

9. Homayoun Hashemi, "The Indoor Radio Propagation Channel", *Proceedings of the IEEE*, Vol. 81, No.7, July 1993.

10. Ralph D. Hippenstiel, *Detection Theory Applications and Digital Signal Processing*, CRC Press, Boca Raton, FL, 2002.

11. S. Ben Slimane, Notes for Advanced Communication Theory, Royal Institute of Technology, March 2002.

12. Van Nee, R. & Prasad R., *OFDM for Wireless Multimedia Communications*, Artech House, Norwood, MA, 2000.

13. Proakis, J.G., *Digital Communications*, 4th ed., McGraw Hill, New York, NY, 2001.

14. Leon-Garcia, A., *Probability and Random Processes for Electrical Engineering*, 2nd ed. Reading, MA, 1994.

15. Robertson, Clark, Notes for EC4550 (Digital Communications), Naval Postgraduate School, Monterey, CA, 2001 (unpublished).

16. Gradshteyn, I.S. & Ryzhik, I.M., *Tables of Integrals, Series, and Products*, pp. 721, Academic Press, New York, NY, 1980.

17. Clark, G.C., Jr. & Cain, J.B., *Error-Correction Coding for Digital Communications*, Plenum Press, New York, NY, 1981.

18. Wicker, S.B., *Error Control Systems for Digital Communication and Storage*, Prentice Hall, Upper Saddle River, NJ, 1995.

19. Robertson, Clark, Notes for EC4580 (Coding and Information), Naval Postgraduate School, Monterey, CA, 2001 (unpublished).

20. May, T. Rohling, H., and Engels, V., "Performance Analysis of Viterbi Decoding for 64-DAPSK and 64-QAM Modulated OFDM Signals," *IEEE Transactions on Communications*, Vol. 46, No. 2, pp.182-190, Feb 1998.

INITIAL DISTRIBUTION LIST

1. Defense Technical Information Center
   Ft. Belvoir, Virginia

2. Dudley Knox Library
   Naval Postgraduate School
   Monterey, California

3. Chairman, Code EC
   Department of Electrical and Computer Engineering
   Naval Postgraduate School
   Monterey, California

4. Professor R. Clark Robertson, Code EC/RC
   Department of Electrical and Computer Engineering
   Naval Postgraduate School
   Monterey, California

5. Professor Roberto Cristi, Code EC/CX
   Department of Electrical and Computer Engineering
   Naval Postgraduate School
   Monterey, California